PREPARATION OF A SOURCE MODEL FOR THE EASTERN MARMARA
REGION ALONG THE NORTH ANATOLIAN FAULT SEGMENTS AND
PROBABILISTIC SEISMIC HAZARD ASSESSMENT OF DÜZCE PROVINCE

A THESIS SUBMITTED TO
THE GRADUATE SCHOOL OF NATURAL AND APPLIED SCIENCES
OF
MIDDLE EAST TECHNICAL UNIVERSITY

BY

SELİM CAMBAZOĞLU

IN PARTIAL FULFILLMENT OF THE REQUIREMENTS
FOR
THE DEGREE OF MASTER OF SCIENCE
IN
GEOLOGICAL ENGINEERING

FEBRUARY 2012

Approval of the thesis:

PREPARATION OF A SOURCE MODEL FOR THE EASTERN MARMARA REGION ALONG THE NORTH ANATOLIAN FAULT SEGMENTS AND PROBABILISTIC SEISMIC HAZARD ASSESSMENT OF DÜZCE PROVINCE

submitted by **SELİM CAMBAZOĞLU** in partial fulfillment of the requirements for the degree of **Master of Science in Geological Engineering Department, Middle East Technical University** by,

Prof. Dr. Canan ÖZGEN
Dean, Graduate School of **Natural and Applied Sciences**

Prof. Dr. Erdin BOZKURT
Head of Department, **Geological Engineering**

Prof. Dr. Haluk AKGÜN
Supervisor, **Geological Engineering Dept., METU**

Examining Committee Members:

Assoc. Prof. Dr. Bora F. ROJAY
Geological Engineering Dept., METU

Prof. Dr. Haluk AKGÜN
Geological Engineering Dept., METU

Assoc. Prof. Dr. Ayşegül Askan GÜNDOĞAN
Civil Engineering Dept., METU

Prof. Dr. Erdal ÇOKÇA
Civil Engineering Dept., METU

Dr. Mustafa K. KOÇKAR
Earthquake Eng. App. and Res. Center, Gazi University

Date: 10 / 02 / 2012

I hereby declare that all information in this document has been obtained and presented in accordance with academic rules and ethical conduct. I also declare that, as required by these rules and conduct, I have fully cited and referenced all material and results that are not original to this work.

Name, Last name: Selim CAMBAZOĞLU

Signature

ABSTRACT

PREPARATION OF A SOURCE MODEL FOR THE EASTERN MARMARA REGION ALONG THE NORTH ANATOLIAN FAULT SEGMENTS AND PROBABILISTIC SEISMIC HAZARD ASSESSMENT OF DÜZCE PROVINCE

Cambazoğlu, Selim

MSc., Department of Geological Engineering

Supervisor : Prof. Dr. Haluk AKGÜN

February 2012, 154 pages

The North Anatolian Fault System is one of the most important active strike-slip fault systems in the world. The August 17, 1999 and November 12, 1999 earthquakes at Kocaeli and Düzce are the most recent devastating earthquakes. The study area lies in the Eastern Marmara Region and is bounded by the 28.55-33.75 E and 40.00-41.20 N, latitude and longitude coordinates, respectively. There are numerous studies conducted in the study area in terms of active tectonics and seismicity, however studies are scale dependent. Therefore, a comprehensive literature survey regarding active tectonics of the region was conducted and these previous studies were combined with the lineaments extracted from 10 ASTER images via principle component analysis manual extraction method. Therefore, a line seismic source model for the Eastern Marmara region was compiled mainly based on major seismic events of instrumental period. The seismicity of these line segments were compared with the instrumental period earthquake catalogue compiled by Kandilli Observatory and Earthquake Research Institute with a homogeneous magnitude scale between 1900 and 2005. Secondary event and

completeness of this catalogue was checked. The final catalogue was matched with the compiled seismic source for historical seismicity and source-scenario-segment-weight relationships were developed. This developed seismic source model was tested by a probabilistic seismic hazard assessment for Düzce city center by utilizing four different ground motion prediction equations. It was observed that Gutenberg-Richter seismicity parameter 'b' does not have significant effect over the model, however change in the segmentation model have a low but certain influence.

Keywords: Lineament extraction, seismic source modeling, probabilistic seismic hazard assessment, Eastern Marmara Region, Düzce

ÖZ

KUZEY ANADOLU FAY SİSTEMİ BOYUNCA DOĞU MARMARA BÖLGESİ İÇİN KAYNAK MODELİ HAZIRLANMASI VE DÜZCE İLİ İÇİN OLASILIKSAL SİSMİK TEHLİKE ANALİZİNİN YAPILMASI

Cambazoğlu, Selim

Yüksek Lisans, Jeoloji Mühendisliği Bölümü

Tez Yöneticisi : Prof. Dr. Haluk AKGÜN

Şubat 2012, 154 sayfa

Kuzey Anadolu Fay Sistemi dünyadaki en önemli aktif yanal atımlı fay sistemlerinden birisidir. Yakın zamanda gerçekleşen ve büyük yıkıma yol açan 17 Ağustos 1999 ve 12 Kasım 1999 Kocaeli ve Düzce depremleri de bunun en güncel kanıtıdır. Bu çalışma kapsamında incelenen bölge doğu Marmara bölgesinde, 40.00-41.20 K ve 28.55-33.75 D enlem ve boylam koordinatlarının sınırladığı alan içerisinde yer almaktadır. Çalışma alanına dair bir çok aktif tektonik harita ve bölgeyi depremsellik açısından inceleyen bir çok çalışma olmasına karşın, bu haritalar ve çalışmalar ölçeğe dayanmaktadır. Bu çalışmada bölgenin aktif tektonik haritalandırılmasına istinaden detaylı bir literature araştırması gerçekleştirilmiş ve bu geçmiş çalışmalar 10 ASTER uydu görüntüsünden temel bileşenler analizi çizgisellik çıkarımı yönteminden elde edilen çizgisellikler ile karşılaştırılarak birleştirilmiştir. Bu veri tabanına istinaden temel olarak aletsel kayıt dönemindeki yıkıcı depremler göz önünde bulundurularak Doğu Marmara bölgesi için çizgisel bir sismik kaynak modeli oluşturulmuştur. Elde edilen bu çizgisel kaynak modelin segmanlarının depremselliği Kandilli Rasathanesi ve Deprem Araştırma Enstitüsü

tarafından 1900 – 2005 yılları arasındaki aletsel dönem kayıtlarının büyüklük ölçeği olarak homojen şekilde oluşturulmuş deprem kataloğundaki kayıtlarla karşılaştırılmıştır. Bu catalog ikincil depremler ve katalog tamlığına istinaden control edilmiştir. Son olarak elde edilen katalog oluşturulmuş çizgisel sismik kaynaklar ile eşleştirilmiş ve kaynak-senaryo-segman-ağırlık ilişkisi kurulmuştur. Nihai olarak elde edilen sismik kaynak modeli, dört farklı yer hareketi tahmin ilişkisi kullanılarak Düzce şehir merkezi için bir olasılıksal sismik tehlike değerlendirmesi ile test edilmiştir. Yapılan analiz sonuçlarına göre Gutenberg-Richter depremsellik parametresi olan 'b' değerinin analiz sonuçlarına kaydadeğer etkisinin olmadığı, ancak segmantasyon modelindeki değişikliklerin sonuçlarda az da olsa etki yarattığı görülmüştür.

Anahtar Kelimeler: Çizgisellik çıkarımı, sismik kaynak modeli, olasılıksal sismik tehlike analizi, Doğu Marmara Bölgesi, Düzce

To my family

ACKNOWLEDGMENTS

There are many people who have contributed to me either morally or scientifically throughout this work. Here I would like to acknowledge my gratitude for them, and apologize in advance, if I have forgotten anyone.

I am thankful to all my instructors who have supported me through my thesis studies, but I especially grateful for the guidance and support of my supervisor Prof. Dr. Haluk AKGÜN.

I would like to thank the examining committee, Assoc. Prof. Bora ROJAY, Assoc. Prof. Ayşegül ASKAN GÜNDOĞAN and Prof. Erdal ÇOKÇA for their valuable contributions.

I would like to thank Dr. Mustafa Kerem KOÇKAR for his support, encouragement, advices and contribution to this work with his suggestions.

I would like to thank Gözde YAL and Kıvanç YÜCEL for their assistance, moral support and friendship during my studies.

I would like to thank Dr. Zeynep GÜLERCE and Soner OCAK for their collaboration during this study, and to Mustafa KAYA, Evrim SOPACI and Kıvanç OKALP for their support.

This thesis was supported by Middle East Technical University, Scientific Research Projects no. BAP- 03-03-2009-01 and thus I would like to thank Prof. Dr. Yener ÖZKAN for allowing met o be a part of it.

I would like to express my gratitude to Dr. (to be) Arif Mert EKER, who got me into this and somehow managed to help me out from the beginning of this work to the end, and will probably help me further down the road. I am grateful for his scientific brainstorming, advice, assistance and most importantly his friendship. He has always been there for me when I needed him, supported me and encouraged me to think one step ahead, and think larger and bigger.

And most importantly, I am grateful to my family; İpek, Gencer and Kemal CAMBAZOĞLU along with my aunt Dilek ÖNAY for always being there for me, and always supporting my decisions.

TABLE OF CONTENTS

LIST OF TABLES

TABLES

LIST OF FIGURES

CHAPTER 1

INTRODUCTION

1.1 Purpose and Scope

The North Anatolian Fault System is one of the most important strike slip fault system in the World. The westward propagating seismic activity starting from the 1939 Erzincan earthquake and most recently including the 1999 Kocaeli and Düzce earthquakes have caused more than ten destructive earthquakes and more than 50,000 casualties during this period (Barka, 1996; MTA, 2003a; MTA, 2003b).

Although there are numerous studies in the literature that have both investigated the kinematics and structure of the system, and the individual events; these studies include fault delineation maps which does not match with each other in many cases as each scientist have determined his/her own fault model or the scale of the studies show variations. In addition, utilization of these fault maps is not always spatially accurate due to scale problems along with the difficulties of digitalization of these source maps into a Geographic Information Systems (GIS) environment. These difficulties include the problems with the accuracy of georeferencing, scale and quality (resolution) of the source map.

Due to these reasons, this study focuses on the determination of a source model for the study region via interpretation of satellite images (Advanced Spaceborne

Thermal Emission and Reflection Radiometer-ASTER), determination of lineaments from these images and correlation of the created lineament map with the literature in order to determine the active fault mechanism in the region. Interpretation of lineaments from a total of 10 ASTER scenes was carried out with the manual extraction method following processing of each individual scene with Principal Component Analysis (PCA). This methodology was determined by investigating different manual or automatic extraction methods such as utilization of LINE module of Geomatica Software, LINDENS Software and LESSA code for automatic extraction, and filtering operations, color composites and spectral ratio and Principal Components Analysis (PCA) for manual lineament extraction. The PCA method was determined to be a more accurate and useful method when compared with other methods. The details of this selection are given in Chapter 3 – Image Processing.

Following the lineament extraction, as remote sensing analysis is not sufficient by itself to label a fault as 'active', the constructed line database was correlated with the literature. During this stage, the spatial locations of the extracted lineaments was kept stable while their extents were redefined according to the detailed fault segmentation studies in literature. Thus, a database including the active fault segments which are considered to be accurate in terms of spatial location was acquired (see Chapter 4 for details). These determined fault segments were grouped according to the past events and source zones for earthquake activity, and then ultimately seismic hazard assessment was performed.

Determination of fault geometry and seismic source zones is an essential part of a seismic hazard assessment. Following this determination, inclusion of an earthquake database allows to define the activity and recurrence rate of these zones. For this study, the database encompassing 1900-2005 events from KOERI (Kandilli Observatory and Earthquake Research Institute) with magnitude > 4 was

utilized. Another important parameter for seismic hazard assessment is the determination of ground motion prediction equations to be utilized. Different ground motion prediction equations were investigated for this study and their sensitivity with the source model was compared. Thus, seismic hazard assessment was performed according to these three parameters.

1.2 Study Area

The study area lies in the Eastern Marmara and Western Black Sea region bounded by coordinates 28.55 latitude – 41.20 longitude from northwest and 33.75 latitude – 40.00 longitude from southeast and covers an area of approximately 37.000 km², and lies in UTM Zones 35N and 36N (Figure 1). This area includes the 17 August 1999 Kocaeli, 12 November 1999 Düzce, 22 July 1967 Mudurnu, 26 May 1957 Abant, 1 February 1944 Bolu-Gerede and 20 June 1943 Hendek earthquakes which have caused significant economic and life losses (Ambraseys and Zatopek, 1968; Ambraseys, 1970; Barka, 1996; MTA, 2003a; MTA, 2003b). A list of earthquakes during instrumental period (1900-2005) with magnitudes (M_w) higher than 6 within the study area in accordance with the earthquake catalogue compiled by Kandilli Observatory and Earthquake Research Center (KOERI, 2007) given below (Table 1 and Figure 2)
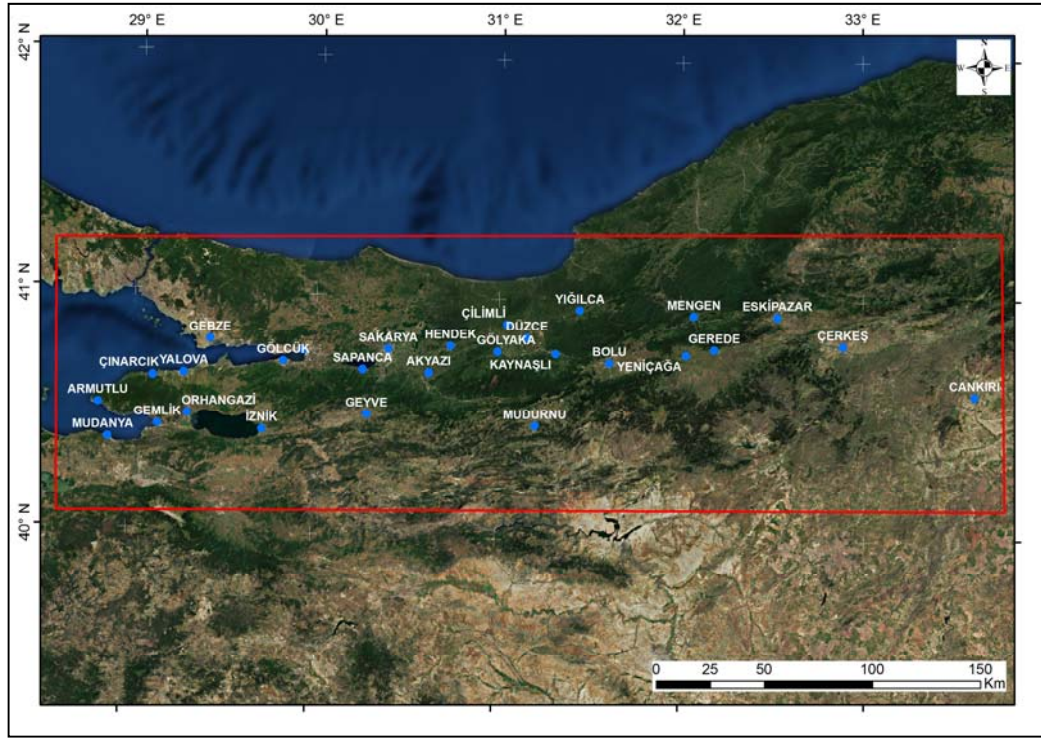
Figure 1. Location map of the study area.

Table 1. Large Earthquakes ($M_w \geq 6.0$) within the study area.

Location	Day	Month	Year	Latitude	Longitude	Depth	M_w
Kocaeli	17	8	1999	40.76	29.95	17	**7.4**
Düzce	12	11	1999	40.81	31.19	10	**7.2**
Bolu-Gerede	1	2	1944	41.41	32.69	10	**6.8**
Abant	26	5	1957	40.67	31.00	10	**6.7**
Kurşunlu	13	8	1951	40.88	32.87	10	**6.6**
Hendek-Adapazarı	20	6	1943	40.85	30.51	10	**6.4**
Yalova	18	9	1963	40.77	29.12	40	**6.2**
Mudurnu	22	7	1967	40.67	30.69	33	**6.2**
Kurşunlu	7	9	1953	41.09	33.01	40	**6.0**

4
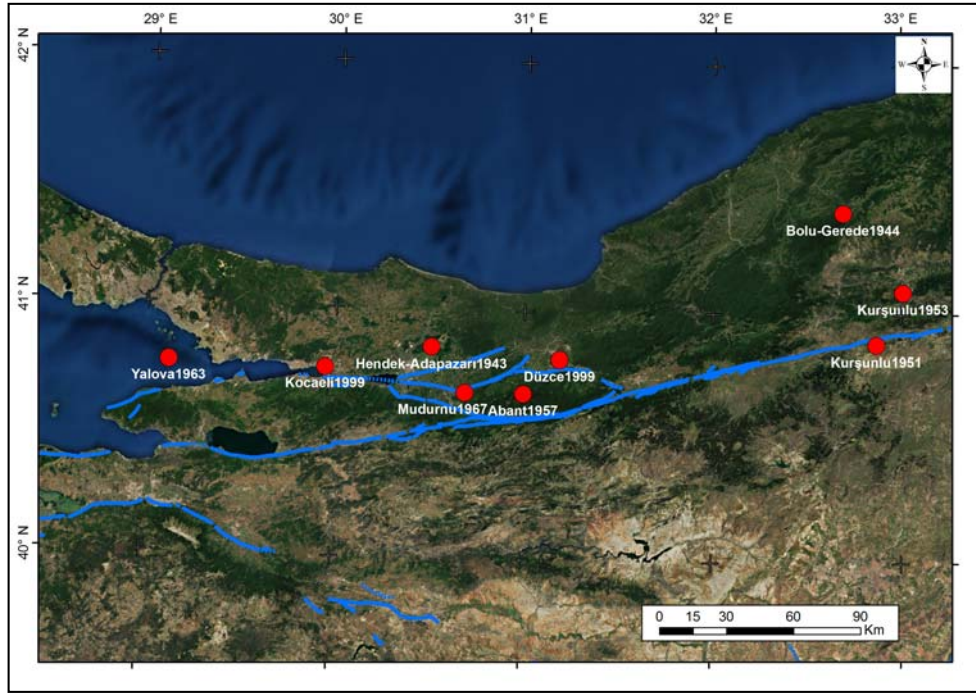
Figure 2. Large Earthquakes (red circles) within the study area and Active Faults
(blue lines, reproduced from Şaroğlu et al., 1992)

The Study area can be generally divided into two in terms of geological
formations, namely Plio-Quaternary Basin fill deposits and Pre-Pliocene rock
formations. Plio-Quaternary Basins within the study area are Gölcük-İzmit,
Sakarya-Adapazarı, İznik, Pamukova, Düzce, Bolu and Yeniçağa basins (Figure
3). These deposits constitutes basin fill, alluvial deposits, fluvial fillings, river bed
and flood plain sedimentary deposits with thicknesses generally exceeding 100 m
and up to 260 m in the Düzce basin according to geophysical data (Emre et al.,
1998; MTA and AU, 1999; METU and MTA, 1999).
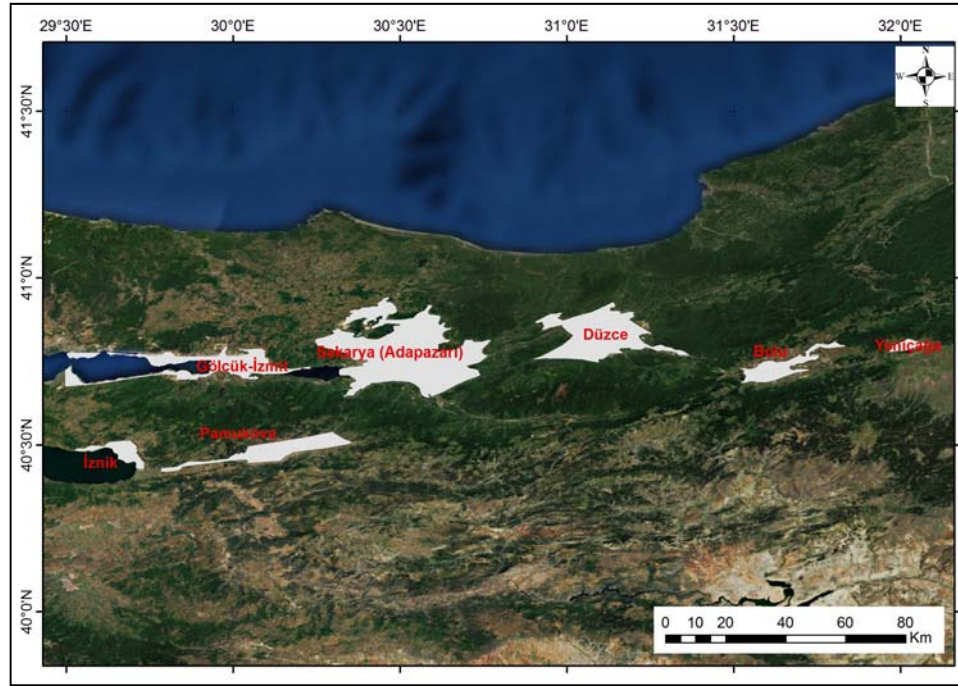
Figure 3. Major basins within the study area (Reproduced from METU and MTA, 1999)

As for Düzce basin, the younger sedimentary units (Q) filling the Düzce basin can be observed to consist completely of a clastic composition with gravel-sand-silt and clay depositions regardless of their depositional environment. These deposits can also be observed within lacustrine and alluvial environments as well as rarely talus deposits at the basin boundaries (MTA and AU, 1999). For the general purpose of this study, the lithological distribution can be re-classified as Plio-Quaternary soft deposits and Pre-Pliocene rock formations. Therefore, the area can be roughly divided into two in terms of geological lithologies (Figure 4; grey colored area is Plio-Quaternary and yellow colored area is Pre-Pliocene).
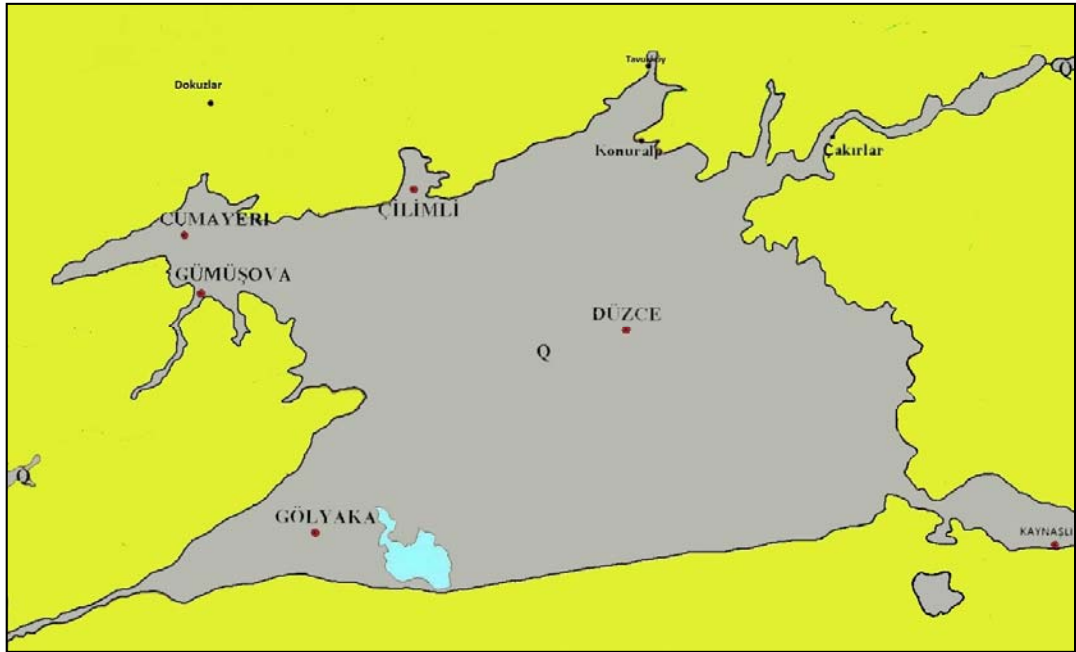
Figure 4. Generalized Geology of the Düzce Region (Modified from MTA and AU, 1999)

CHAPTER 2

SEISMO-TECTONIC

The North Anatolian Fault (NAF) System is one of the most important strike-slip fault systems in the world (Şengör, 1979; McKenzie, 1972; Barka ve Kadinsky-Cade, 1988; Barka, 1992). The NAF is a right lateral strike slip continental transform (Ketin, 1948; McKenzie, 1972). Starting with the 1939 Erzincan earthquake, a westward propagating trend has been observed in destructive earthquakes on the fault zone, namely the 1939, 1942, 1943, 1944, 1957, 1967 and finally the August and November 1999 Earthquakes (Barka, 1996; Stein et al., 1997, Barka et al., 2002; Reilinger, 2006). This propagation was clearly shown with geological studies as well as with GPS measurements (McClusky et al., 2000; Meade et al., 2002; Reilinger et al., 2006). The length of the NAF is reported to be between 1200 and 1600 km (Şengör, 1979; Barka, 1992; Şengör et al., 2004) starting from the Karlıova, following a roughly east-west trend through north Anatolia as a single strand until Mudurnu Valley. From this point the fault splays into three strands in the Marmara and the Northern Aegean regions (Barka, 1992). The NAF forms a 80 km to 100 km wide zone at northwest Anatolia (Barka and Kadinsky-Cade, 1988; Barka, 1992; 1996) where the study area lies.

Although the fault system has been studied starting from the end of the first part of the last century (i.e. Ketin, 1948), there are different fault segmentation interpretations by different researchers. However, following the two destructive earthquakes (i.e., the August 17, 1999 Kocaeli and the November 7, 1999 Düzce

earthquakes); the fault system and especially the western half was studied intensely due to the destruction of the last two events and the anticipated future westward propagation to İstanbul (population of about 15 million) (MTA, 2003; Şengör et al., 2004). The major and destructive earthquakes in the region resulted in distinct surface ruptures and definite segmentation from these designated ruptures led to the development of a model. Therefore, fault segmentation and distinction was carried out according to the information gathered from literature (e.g., Barka, 1992; Ayhan et al., 2002; Barka et al., 2002). These major events can be listed from the most recent to the past as the 1999 Düzce (Mw=7.2), 1999 Kocaeli (Mw=7.4), 1967 Mudurnu (Ms=7.1), 1957 Bolu-Abant (Ms=7.0) and the resulting surface ruptures, and hence, segments, were depicted from these events (Ambrasays and Zatopek, 1969; Ambraseys, 1970; Barka and Kadinsky-Cade, 1988; Palyvos et al., 1997; Barka et al., 2002; Akyüz et al., 2002, Kondo et al., 2005).

The most recent destructive earthquakes, namely the 1999 Kocaeli and the 1999 Düzce earthquakes, have caused surface ruptures with a length of 145 km and 40 km, respectively, leading to a total surface rupture of 185 km (Barka et al., 2002; Akyüz et al., 2002). The fault segments discriminated from the 145 km long surface rupture of the Kocaeli earthquake have been investigated in four sections as Hersek, Karamürsel-Gölcük, İzmit-Sapanca Gölü, Sapanca-Akyazı-Karadere segments from west to east (Barka et al., 2002). The earthquake is considered to have originated from the İzmit-Sapanca segment (Sapanca segment in Harris et al., 2002) and step over normal faults present between Karamürsel-Gölcük and İzmit-Sapanca Lake have constituted a continuous mechanical link in between (Harris et al., 2002). Along with these, the exact location of the 1943 Hendek earthquake has not been accurately determined in the literature and it is discussed that it may be associated with the Karadere segment (Harris et al., 2002); hence, in this study, primarily, a separate segment (identified as the 1943, Hendek segment) has been

included in the seismic model. Another segmentation set in the study area is associated with the November 12, 1999 Düzce earthquake (M=7.1). This region starts from Karadere segment which forms the eastern edge of the August 17, 1999 event and Gölkaya pull-apart basin and continues to the east of Kaynaşlı in the east (Akyüz et al., 2002). This segmentation reaches its highest vertical slip at the south of Eften Lake and coincides with the 9 km section which constitutes the eastern section of the August 17, 1999 event (Akyüz et al., 2002). The final segmentation in the study area is located to the south of the area, starting from Geyve and named as middle Marmara strand by Barka and Kadinsky-Cade (1988). It is known that this region has not endured a destructive earthquake in 200 years (Barka and Kadinsky-Cade, 1988) and may be considered to be a seismically quiet region.
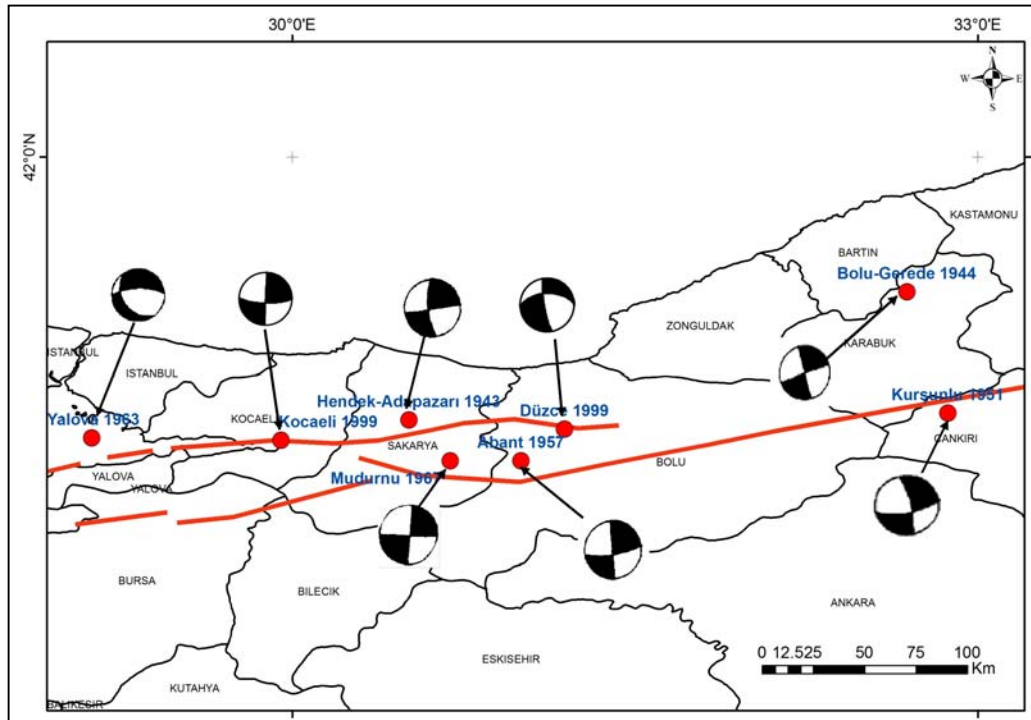
Figure 5. Large Earthquakes and their focal mechanisms (Active faults modified from Şaroğlu et al., 1992 and Barka et al., 2002; focal mechanisms reproduced from Barka, 1992; Ayhan et al., 2002 and Ayhan and Koçyiğit, 2010)

10

CHAPTER 3

IMAGE PROCESSING

3.1 Introduction

Use of remotely sensed data is widespread in geological application and interpretation. The source of this data can be either aerial photographs or satellite imagery. There are advantages and disadvantages related with these images in relation to the purpose and scale of the study.

Considering the scope of this study; formation of a reliable fault model for the eastern Marmara region, aerial photographs remain at a rather large scale for the purpose and also insufficient in terms of geological representation. Although it is known that stereographically overlapped aerial photographs are known to be a good source for topographical and therefore, structural interpretation, the time required for this type of a process in the extent of the study area can be excessively time consuming when the areal coverage of a single photograph is considered. Along with this, satellite imagery can also be used in conjunction with the topography by methods and softwares of Digital Elevation Models (DEMs) acquired from different satellite sources. Furthermore, the wavelength range of the satellite sensors and visualization techniques of these remotely sensed data in different wavelengths of electromagnetic spectrum is unique in geological applications and interpretations (e.g., lineament detection, volcano detection, mineral exploration) as discussed below.

Therefore, time considerations and extent of utilization have logically directed the medium of interpretation to satellite imagery. At this stage, the financial considerations and most efficient utilization is considered in the determination of the type of satellite image to be acquired.

The most commonly used satellite images for geological applications are images (also known as scenes) of Landsat (ETM or TM) and ASTER sensors both mounted on Terra satellite. Superiority of ASTER images and the reasons are explained below.

3.2 General Information on ASTER Sensor and Imagery

ASTER (Advanced Spaceborne Thermal Emission and Reflection Radiometer) sensor mounted on the TERRA satellite is a sensor that has three different wavelength ranges, namely; Visible-Near Infrared (VNIR), Short Wave Infrared (SWIR) and Thermal Infrared (TIR). Spatial and spectral ranges of the bands are given in Table 2. Spatial resolution of the sensor is 15, 30 and 90 meters for VNIR, SWIR and TIR bands respectively. Spectral and spatial analyses carried out by using VNIR and SWIR bands of the sensor gives more accurate results due to the relative high spatial resolution of the aforesaid bands (Figure 6).

Table 2. Characteristics of the sub-systems of the ASTER sensor.

Sub-system	Band No.	Spectral Range (μm)	Spectral Resolution (m)	Quantization Levels
VNIR	1	0.52-0.60	15	8 bits
	2	0.63-0.69		
	3N	0.78-0.86		
	3B	0.78-0.86		
SWIR	4	1.60-1.70	30	8 bits
	5	2.145-2.185		
	6	2.185-2.225		
	7	2.235-2.285		
	8	2.295-2.365		
	9	2.360-2.430		
TIR	10	8.125-8.475	90	12 bits
	11	8.475-8.825		
	12	8.925-9.275		
	13	10.25-10.95		
	14	10.95-11.65		
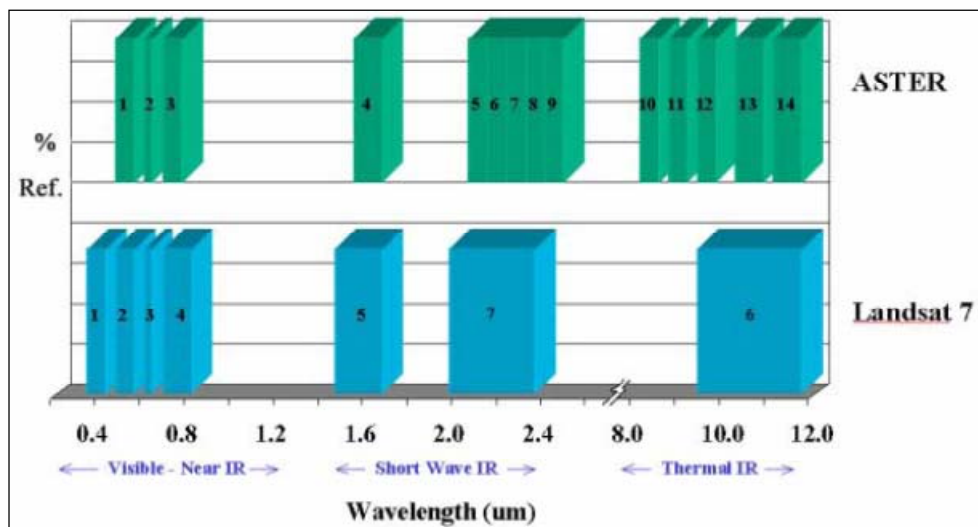
Figure 6. Spectral band comparison between ASTER and Landsat-7 TM (ASTER User's Guide, 2003)

Depending on the different version (level) of the ASTER data, some corrections may be necessary for accurate interpretation. The initial image is ortho-rectified and georeferenced for spatial placement. Following this, cross-talk error present in the SWIR band of the satellite should be corrected. This error is basically present between 5th and 9th bands, as well as all the remaining SWIR bands. For correction of this error, 'ASTER Crosstalk Correction tool is developed and therefore correction of this cross-talk error was made possible via following the basic steps of this program. Along with this, the east-west shift of the SWIR bands should also be corrected. This can be performed by following a series of steps and interchanging the data between several different softwares (i.e., ENVI and ER Mapper). The details of this application can be found in Gozzard (2006). Only after all these corrections can an ASTER scene be used for geological applications, and can be defined as an ASTER Level 1B data. Following this data level, the ASTER scenes are named as higher-level products. The obtained ASTER scenes for this study are ASTER Level 3A products (Figure 7 and Table 3). Therefore all the above indicated corrections are performed on these scenes as well as the atmospheric correction. Along with these error removals, the level 3A scenes include a DEM map generated from 3N and 3B bands of the sensor either absolutely or relatively. The letters N and B indicates 'nadir' and 'back' sensor at the same wavelength (Table 2) located at the sensor in two different positions; one directed vertically and one looking backward, respectively. The terms absolute and relative DEM indicates whether the data generated on-demand or an already present data was utilized, respectively. On this study a relative Level 3A data was acquired.
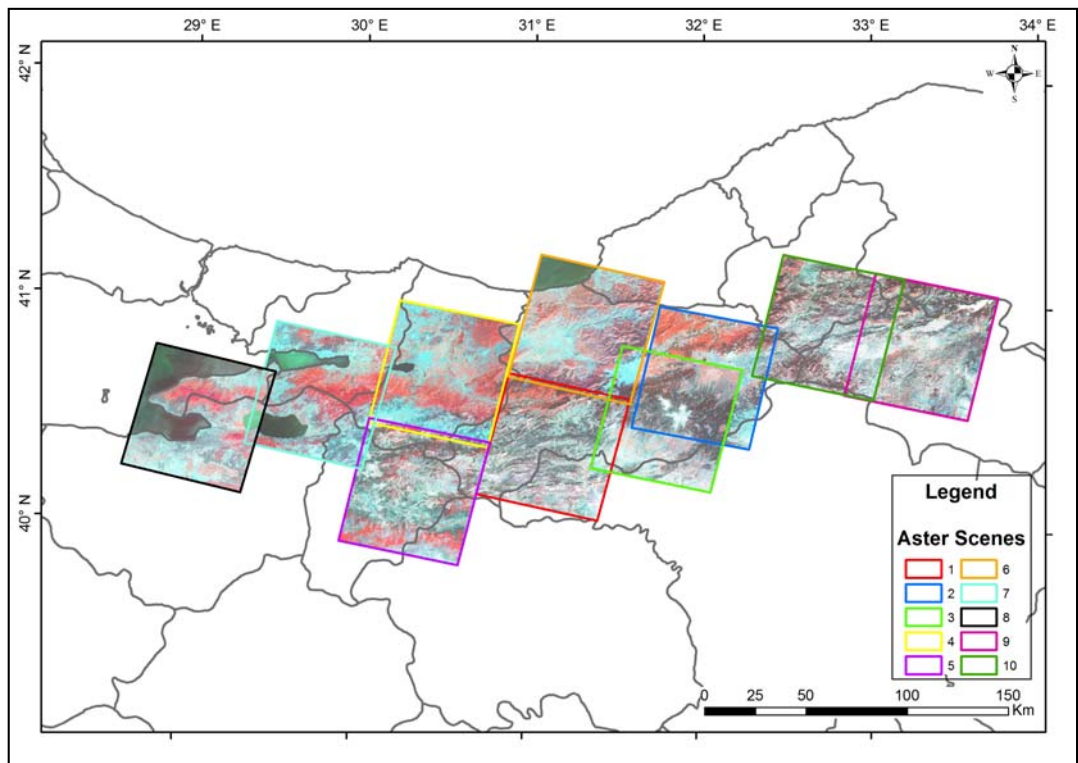
Figure 7. False color composite (R:3 G:1 B:2) of ASTER images.

Table 3. ASTER scenes used in this study.

Image No.	Image Code	Acquisition Date
1	AST3A1_030922085635_0907030003	22.09.2003
2	AST3A1_040724084421_0903030703	24.07.2004
3	AST3A1_070505085052_0809241108	05.05.2007
4	AST3A1_070708085100_0809241142	08.07.2007
5	AST3A1_070708085108_0805090964	08.07.2007
6	ASTL3A1_030922085626_031004058	22.09.2003
7	ASTL3A1_040722085643_040809054	22.07.2004
8	ASTL3A1_040814090241_040828022	14.08.2004
9	AST3A1_040410085030_1001050438	10.04.2004
10	AST3A1 041104084932_0801100004	04.11.2004

3.3 Methodology

ASTER satellite image data is highly suitable for lineament extraction in terms of its intermediate-high spatial resolution in VNIR and SWIR bands as well as high applicability of these data in geological interpretations. Lineament extraction from satellite imagery in conjunction either with the field surveys or correlation with the literature is an effective method in determination of fault (or possible fault) locations in the study area (Gupta, 1991; Fu and Lin, 2002; Akman and Tüfekçi, 2004; Fu et al., 2004; Koç, 2005; Sarp, 2005; Gozzard, 2006). There are various methods for lineament extraction from satellite images. Although many of these were considered during the initial phase of this study, only one method was utilized for final lineament extractions as described below in detail and with reasonings.

Lineament extraction from satellite images were especially performed from Landsat and ASTER images due to the presence of data in the SWIR range of the electromagnetic spectrum which is known for reflection (and absorbance) that includes many of the geological formations (minerals) (Gupta, 1991; Rowan and Mars, 2003). Although Landsat sensors (ETM or TM) have VNIR and SWIR bands as the ASTER sensor does, the spatial resolution (pixel size) of Landsat data is lower (30 m) in VNIR band and there are only two bands present in the SWIR range (Figure 6) while the ASTER sensor have 15 m pixel size in VNIR range and have 6 bands in the SWIR spectral range (Abrams et al., 2000). Thus ASTER images are superior both in spatial sense and spectral sense, and distinction in surficial information in the SWIR range (i.e., geological formations) is much more accurate in ASTER images. Therefore, as ASTER scenes were utilized in this study, it is possible to comment that both the methods used for lineament extraction from Landsat were possible to be used and also the results are much more reliable.

Lineament extraction methods can mainly be divided into two as; manual and automated extraction. Automated methods are based on extraction of lineaments through various softwares via integration of several parameters. Segment tracing algorithm (STA) (Koike et al., 1995 and 1998), Lineament Extraction and Stripe Statistical Analysis (LESSA) (Zlatoposky, 1992 and 1997), Haar transform (Wang et al., 1990), LINDENS software (Casas et al., 2000) and finally LINE algorithm of PCI Geomatica software (2003) are some examples for these automated lineament extraction softwares (or codes). Although these automated lineament extraction programs process all images with the same sensitivity and considerably decrease the process time, they depend on user supplied parameters (i.e., filtering diameter, line length threshold, line fitting threshold, etc.) PCI Geomatica (2003) and disregards the general geological and structural data readily present for the study area. Therefore these automated methods tend to extract each and every linear feature that fits the input parameters and restrictions. These are the basic reasons why automated lineament extraction was not utilized in this study.

There are several methods present for manual extraction of lineaments. Filtering operations, spectral ratios, color composites and principal component analyses are some of the most commonly used image interpretation methods in terms of lineament extraction.

Filtering operation is a spatial enhancement of images through the digital number (DN) value of each pixel along with the neighboring pixels in terms of a matrix operation. Filtering operation is based on a moving window Kernel analyses (matrix) of distinct sizes (e.g., 3x3, 5x5, 9x9, etc.) throughout the image. Different filtering operations can be performed by different Kernel (values) and different Kernel sizes. The Directional Filtering Method (edge detection filters) is one of the many filtering methods used for lineament detection and extraction, and Low Pass (Majority or Average) Filters are also used to acquire a smoother image (Table 4).

Commonly used directional filters are Gradient-Sobel and Gradient Preweitt (Table 5).

Table 4. 3x3 Low Pass (Majority Filter)

1	1	1
1	1	1
1	1	1

Table 5. Examples of different filters in main directions.

	N-S			NE-SW			E-W			NW-SE		
Sobel	-1	0	1	-2	-1	0	-1	-2	-1	0	1	2
	-2	0	2	-1	0	1	0	0	0	-1	0	1
	-1	0	1	0	1	2	1	2	1	-2	-1	0
Prewitt	-1	0	1	-1	-1	0	-1	-1	-1	0	1	1
	-1	0	1	-1	0	1	0	0	0	-1	0	1
	-1	0	1	0	1	1	1	1	1	-1	-1	0

The example filters given in Table 5 may be used for edge detection in different directions. Each image should be filtered for each direction, each filtered image should be interpreted and therefore a final lineament map can be obtained. But this method may not be used effectively in areas of low contrast, where land features (topography) is parallel to the sun angle and where shadows of elevated areas are present (Koike et al., 1995). Hence, only a single band can be utilized in this method, commonly being band 7 of Landsat images, but ASTER sensor has 5 different bands within this geologically important SWIR wavelength. Thus this method was determined to be insufficient for lineament extraction from ASTER images.

The spectral ratios method is another method used for lineament extraction. In this method, rather than absolute reflectance values, changes in the slopes of the spectral reflectance curves were obtained by rationing specific bands in order to pronounce specific spectral signatures (Lillesand, 1999). Resultant images obtained from ratios of specific bands can either be visualized as a single band or as a RGB (Red-Green-Blue) color composite, thus sharper contrasts can be obtained. However, even with the RGB color composites, a total of 6 bands can be utilized in this method. Although this number can be considered sufficient in Landsat images containing 7 bands, it is inadequate when ASTER images are considered; containing 9 bands in VNIR and SWIR spectral range aside from 5 additional TIR bands.

A third commonly used method for manual lineament extraction from satellite images is color composites. In this method, the determined bands are visualized as RGB color composites where this method is also insufficient as only 3 bands can be used which limits the large spectral range of the ASTER images in different bands.

Finally, Principal Component Analysis (PCA) is considered for lineament extraction. This method is used for decreasing dimensionality in bands of a single image (Richards, 1999). In other words, PCA allows reduction of noise component, determination of correlated bands and thus allowing collection of all bands in as a little band as possible by conversion into uncorrelated bands (Gupta, 2003). Therefore, data on multispectral satellite images such as Landsat or ASTER images can be collected in the first three principle components (PCs), mainly on the first principle component. In this study, the first three PCs were visualized as RGB color composite for each scene and thus as many reduction of data redundancy and noise as possible was obtained along with visualizing the highest possible proportion of data as a single image in RGB composite. At least 97.8% of

the total data was visualized by combining the first three principal components in RGB color composite (Table 6). Thus ideal image was obtained for extraction and interpretation of lineaments (Nama, 2004).

Table 6. Percentages and cumulative percentages of PCs for each ASTER scene.

| | | Principal Component | | |
		1	2	3
Scene 1	%	90.570	4.822	3.777
	Cumulative Percentage	90.570	95.392	99.169
Scene 2	%	83.516	11.518	4.048
	Cumulative Percentage	83.516	95.034	99.082
Scene 3	%	77.677	14.825	6.670
	Cumulative Percentage	77.677	92.502	99.172
Scene 4	%	73.658	20.293	4.959
	Cumulative Percentage	73.658	93.950	98.909
Scene 5	%	84.115	7.545	7.053
	Cumulative Percentage	84.115	91.660	98.713
Scene 6	%	72.513	22.285	3.700
	Cumulative Percentage	72.513	94.799	98.499
Scene 7	%	69.494	26.351	3.295
	Cumulative Percentage	69.494	95.845	99.140
Scene 8	%	83.540	13.643	2.136
	Cumulative Percentage	83.540	97.183	99.319
Scene 9	%	65.330	31.848	1.978
	Cumulative Percentage	65.330	97.178	99.156
Scene 10	%	93.449	3.783	2.083
	Cumulative Percentage	93.449	97.232	99.315

Following acquisition of PCs (Principal Components), each ASTER scene was visualized as R:PC1, B:PC2 and G:PC3 colour composite within the GIS environment (Figure 8). Along with this, DEM model of each scene and 3x3 Low Pass (Majority) Filter of the first PC was inspected in order to observe elevation dependent and more general (larger scale) lineaments, respectively (Figure 9).
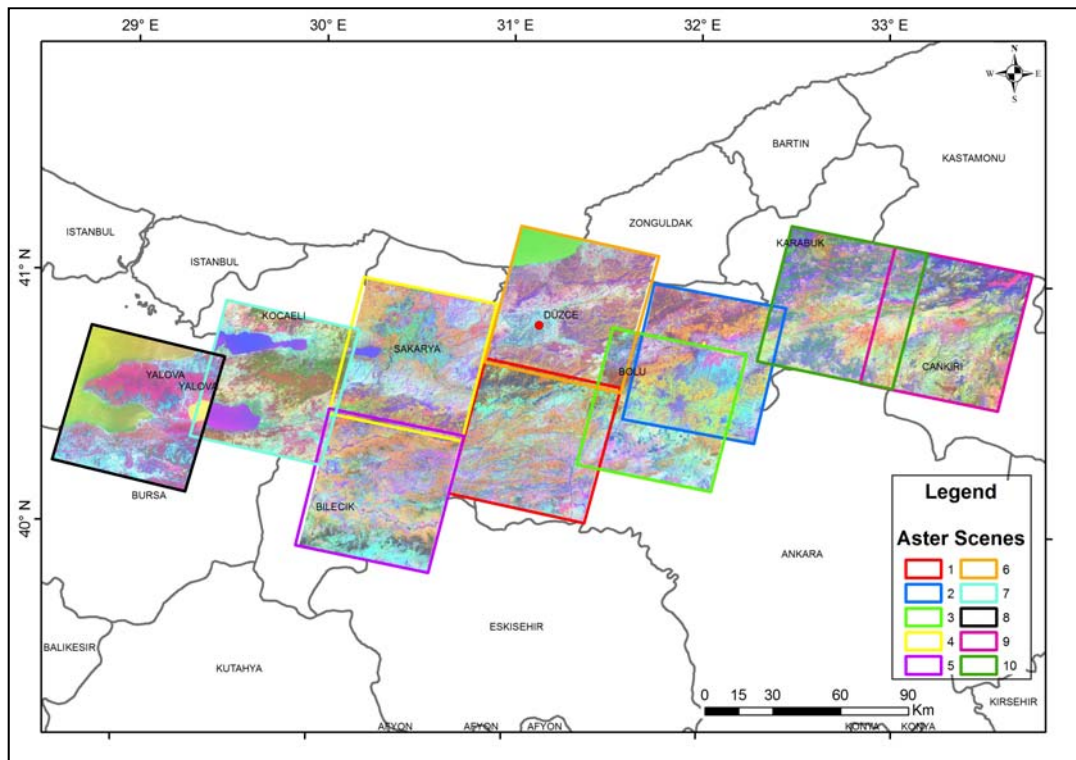
Figure 8. RGB colour composites of PCs of each ASTER scene.
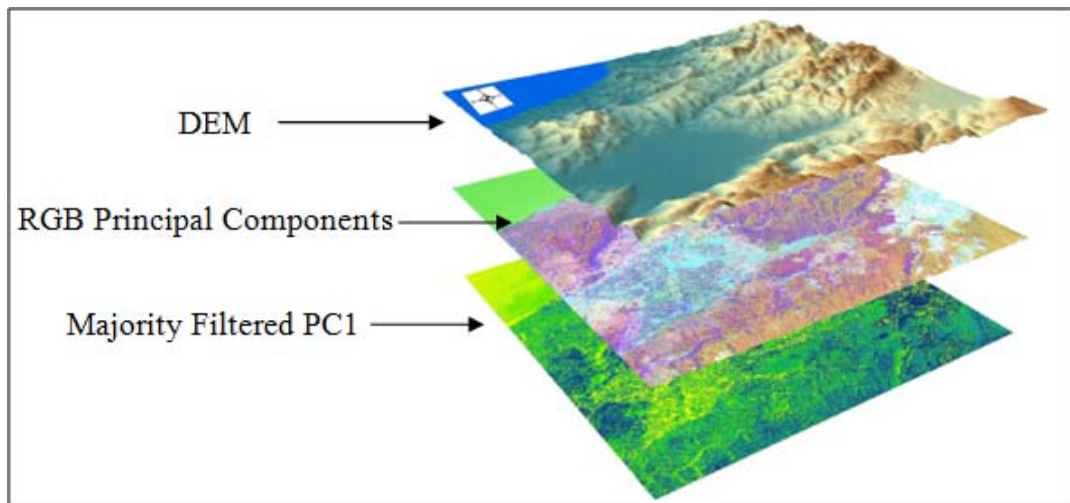
Figure 9. Overlaid view for DEM, PC and Majority Filter of scene 6.

After each scene was inspected in accordance with these image data (i.e. PCs, Filtered PC1 bands and DEM) the final lineament map was produced. A total of 2454 lineaments were extracted from 10 ASTER images and the length of these line features change between 85 m and 13133 m with a mean length of 1984 m (Figure 10). The final lineament map covering the study area can be seen in Figure 11.

Inspection of the directional analysis of the extracted lineaments in terms of length weighted rose diagram method (Figure 11b) revealed that the dominant direction was oriented between N50°E and N80°E where the highest frequency was accumulated at N70°E direction with total of 282 lineaments oriented in that direction. Each inner circle at the rose diagram shown in Figure 11b represents 70 line features. The discussion on directional analysis (strike direction distribution) can be found at the following chapter in detail as each source zone shall be investigated individually in conjunction with the literature.
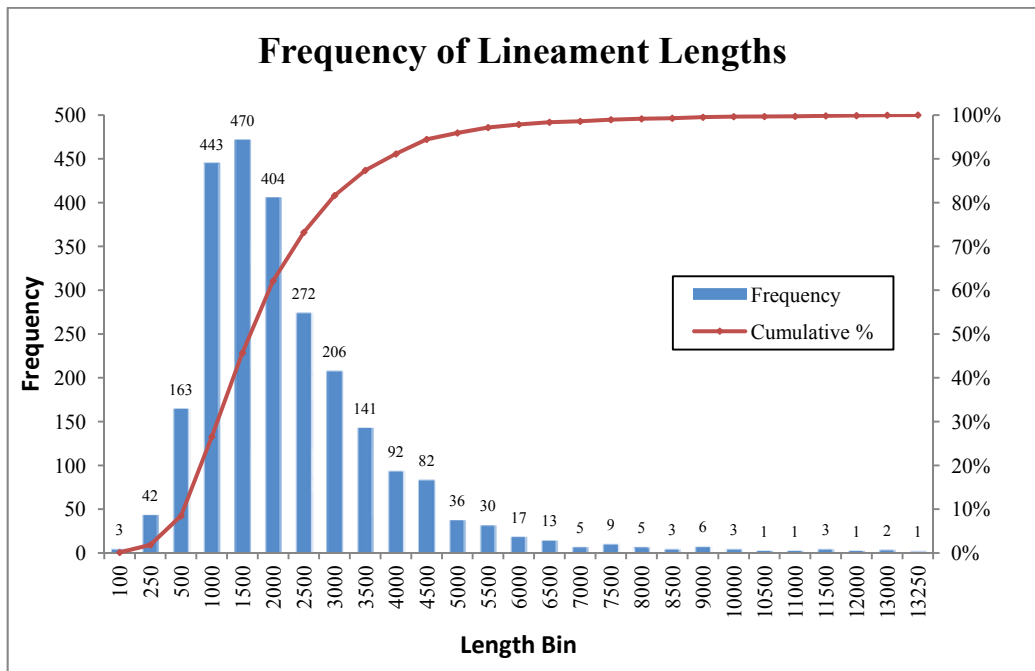
Figure 10. Frequency histogram of extracted lineament lengths.
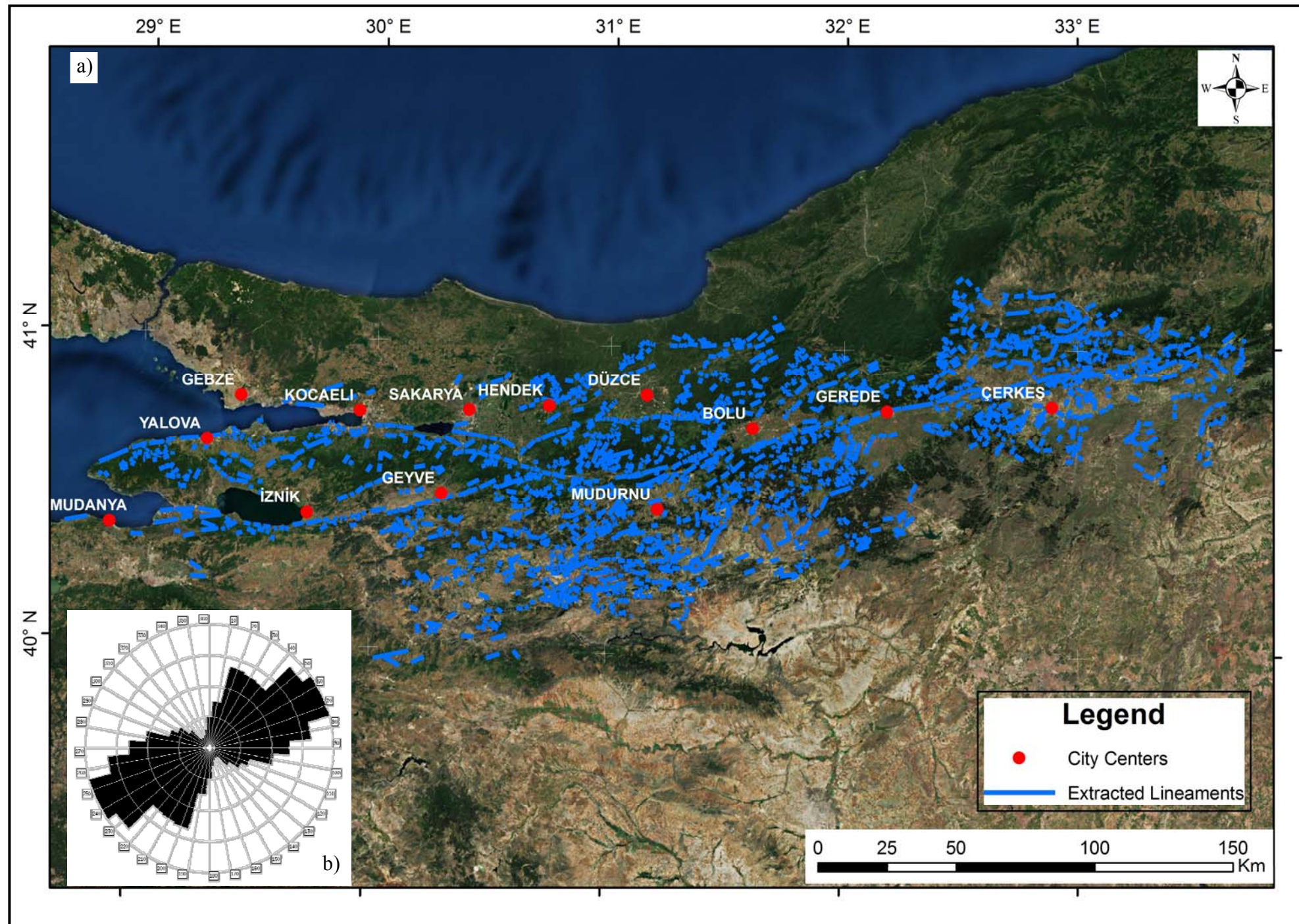
Figure 11. a) Extracted lineaments and b) their directional distribution.

CHAPTER 4

INTERPRETATIONS OF THE LINEAMENT ANALYSIS

4.1 Concordance with the Literature

Following the lineament extraction via utilizing PC analyses, DEM and Majority Images, the resultant lineaments were investigated in terms of their lengths and orientations, and their concordance with the literature was checked. Therefore the resultant lineament map could be utilized in the seismic hazard assessment as an active source model of the area.

Primarily, all the lineaments were included in the model as previously discussed and then their orientations were grouped in accordance with their determined seismic sources. In order to determine the initial extent of the seismic sources, fault maps of different researchers (Ambraseys and Zatopek, 1969; Ambraseys, 1970; Barka and Kadinsky-Cade, 1988; Şaroğlu et al., 1992; Emre et al., 1998; METU and MTA, 1999; Okay et al., 2000; Armijo et al., 2002; Akyüz et al., 2002; Barka et al., 2002; Harris et al., 2002; MTA, 2003a; Duman et al., 2005; Kondo et al., 2005; Pucci et al., 2007) were digitized and visualized within the GIS environment (Figure 12).
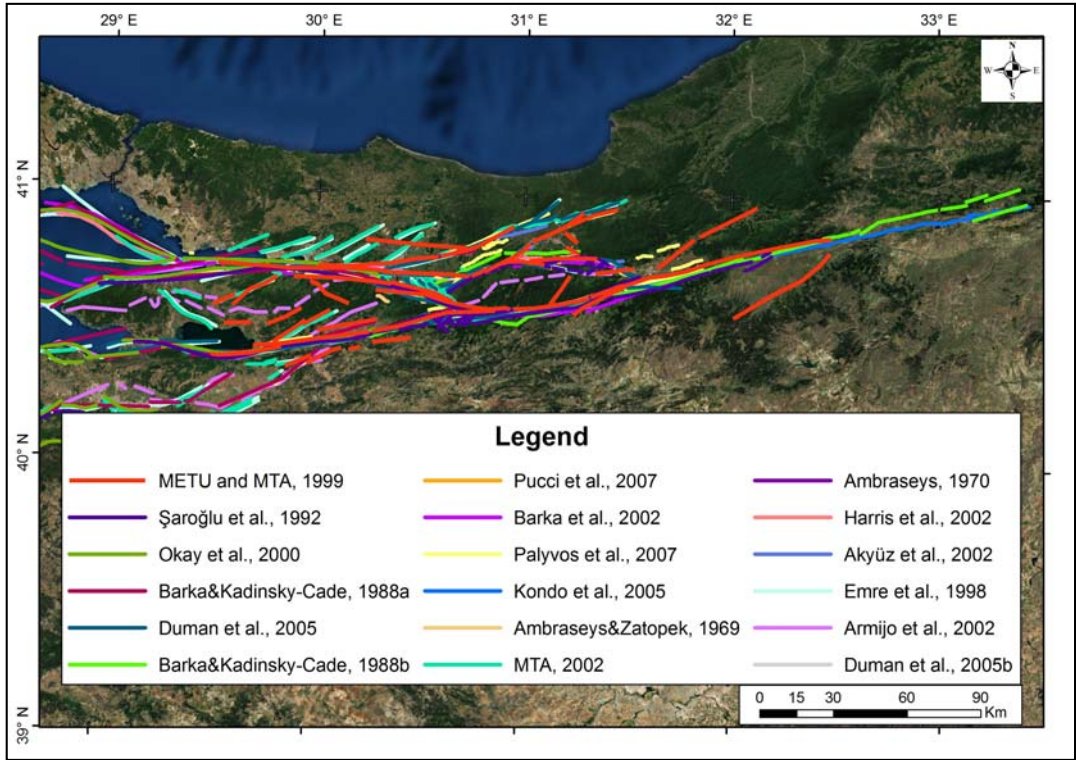
Figure 12. Digitized fault models of different researchers.

The key point in determining these areas was the major seismic activities in the 20th century. In other words, five major events in the 20th century: namely November 12, 1999 Düzce earthquake; August 17, 1999 Kocaeli earthquake; July 22, 1967 Mudurnu earthquake, May 26, 1957 Abant Earthquake and February 1st, 1944 Bolu-Gerede Earthquake. Apart from these main event sources, three more sources were included as well, namely Hendek, Çınarcık and Geyve-İznik areas (Figure 13). All of the following directional analysis were performed in terms of length weighted rose diagram method.
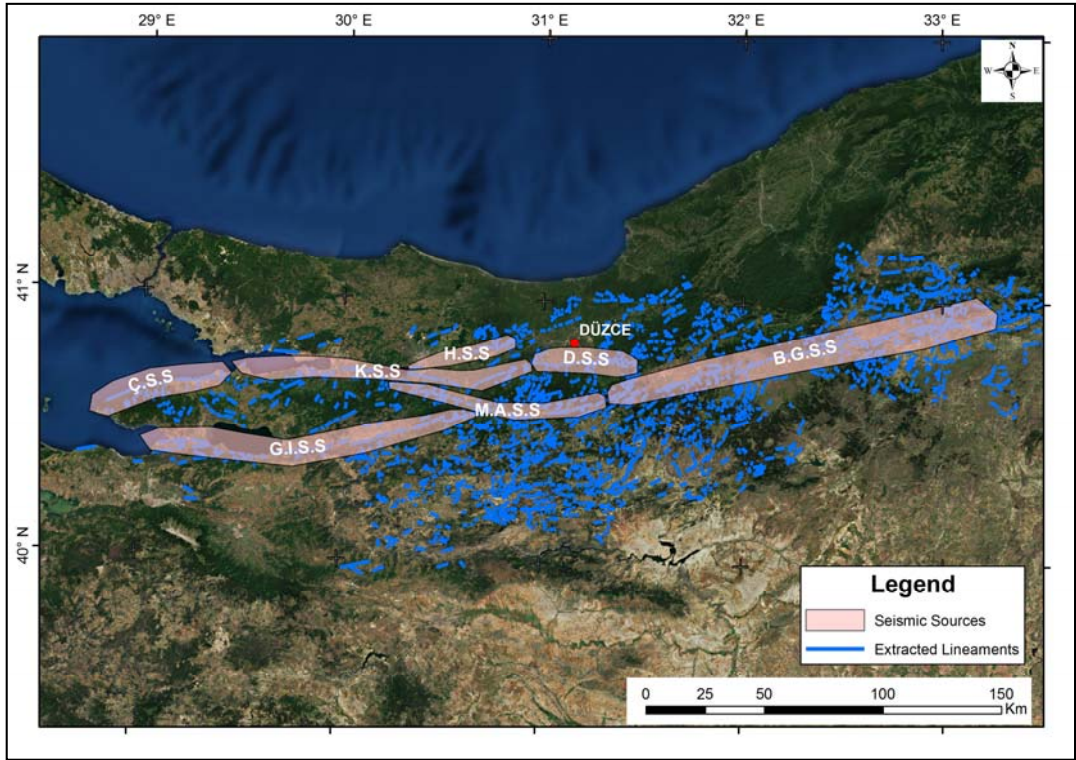
Figure 13. Seismic sources and extracted lineaments (B.G.S.S: Bolu-Gerede
Seismic Source, Ç.S.S: Çınarcık Seismic Source, D.S.S: Düzce Seismic Source,
G.I.S.S: Geyve-İznik Seismic Source, H.S.S: Hendek Seismic Source, K.S.S:
Kocaeli Seismic Source, M.A.S.S: Mudurnu-Abant Seismic Source).

4.1.1 Rupture Zone of 1999 Kocaeli Earthquake

There are different interpretations for the August 17, 1999 earthquake in terms of
segmentation. These different interpretations are summarized in Table 7 according
to their references and their segmentation nomenclature. Nonetheless, the total
rupture area of the Kocaeli earthquake is estimated to be between 125 (Lettis et al,
2002) and 145 km (Barka et al., 2002). However there are different surface rupture
values present in the literature; i.e. Langridge et al. (2002) who includes Yalova
off-shore segment as 'probably ruptured' to the surface rupture of the event. In this

study, the surface rupture segmentation proposed by Barka et al., 2002 was adopted and the lineaments extracted from the ASTER imagery and these lineaments were grouped and joined according to this nomenclature. According to MTA, 2003 and Barka et al., 2002 as well as Langridge et al., 2002 and Lettis et al., 2002; the Hersek and Gölcük segments lies mostly offshore where Hersek segment has a surface presence at the Hersek Peninsula while Gölcük segment follows the coastline in a straight manner and can be observed at its eastern part where Gölcük Navy Base is located (Lettis et al., 2002). However, in the study executed by MTA (2003a) the Gölcük segment was mapped as an offshore fault where only the section at the Navy Base is present as a surface trace.

Following the Hersek and Gölcük segments, three onland segments are differentiated. These were named by Barka et al (2002) as İzmit – Sapanca Lake, Sapanca–Akyazı and Karadere segments (Table 7 gives different segment nomenclatures in the literature).

Table 7. Segmentations for the 1999 Kocaeli Earthquake in literature (MTA, 2003a).

MTA, 2003a	Barka et al., 2002	Lettis et al., 2002	Rockwell et al., 2002	Langridge et al., 2002	Hartleb et al., 2002
Hersek	Hersek	Yalova		Yalova	
Gölcük	Karamürsel – Gölcük	Gölcük	Gölcük	Gölcük	Gölcük
Tepetarla	İzmit – Lake Sapanca	Sapanca	Sapanca	İzmit - Sapanca	Sapanca
Arifiye	Sapanca – Akyazı	Sakarya	Sakarya	Sakarya	Sakarya
Karadere	Karadere	Karadere	Karadere	Karadere	Karadere
Aksu					

In this study, the five segments proposed by Barka et al., 2002 were investigated as the Kocaeli surface rupture zone. Therefore, according to directional analysis of the lineaments, the dominant strike direction of all the lineaments extracted from ASTER images is N70°E and the majority of the lineaments were accumulated in the N60°E to N100°E direction (Figure 14). This range is consistent with the strike directions between N68°E and N98°E proposed by MTA, 2003a and between N65E and N90E proposed by Barka et al. (2002). Furthermore, as the segmentations were investigated individually (Figure 15) their directional analysis results are consistent with the literature as well (Table 8). Therefore these segmentations was modified according to literature and included in the final source model as can be seen in Figure 16.
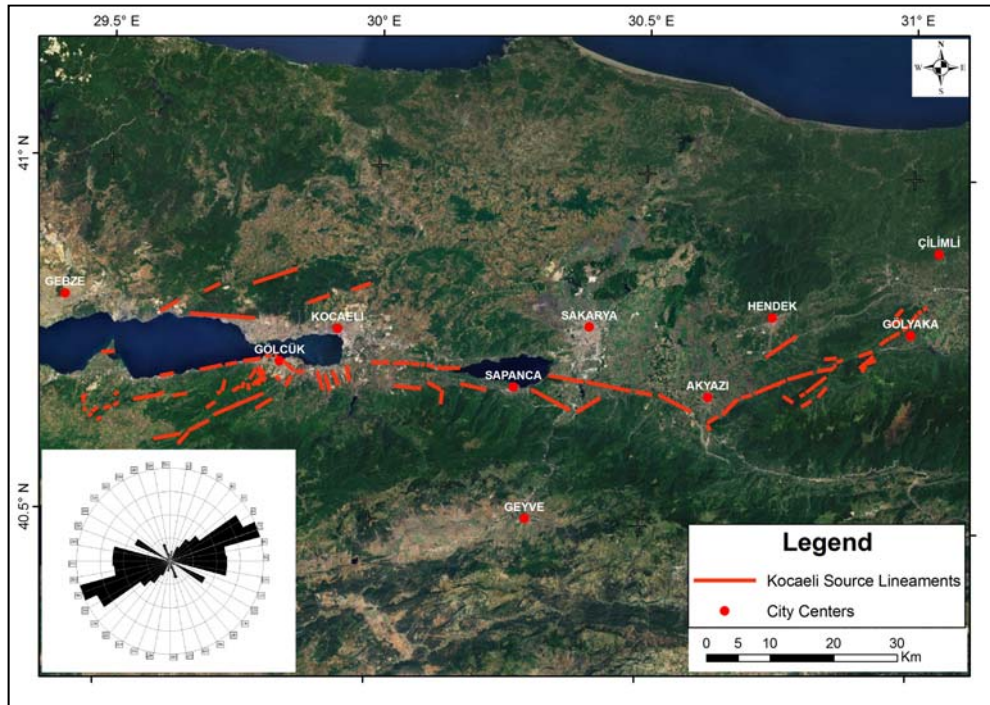
Figure 14. Extracted Lineaments of Kocaeli Source Zone and their Rose Diagram.

Table 8. Directional analysis results for Kocaeli source.

Segment Name / Study	General Strike Direction of Lineaments	MTA, 2003a	Barka et al., 2002	Lettis et al., 2002
Hersek	88°	91° *	80° *	-
Karamürsel – Gölcük	75°- 100°	98°*	70° – 80°	78° – 84°
İzmit – Lake Sapanca	86° - 109°	91°	80° – 90°	89°
Sapanca – Akyazı	100°	95°	75° – 85°	87°
Karadere	50° – 75° (Dominantly 70°)	68°-73°	65°	50° - 80°
* Mapped as offshore segment.				
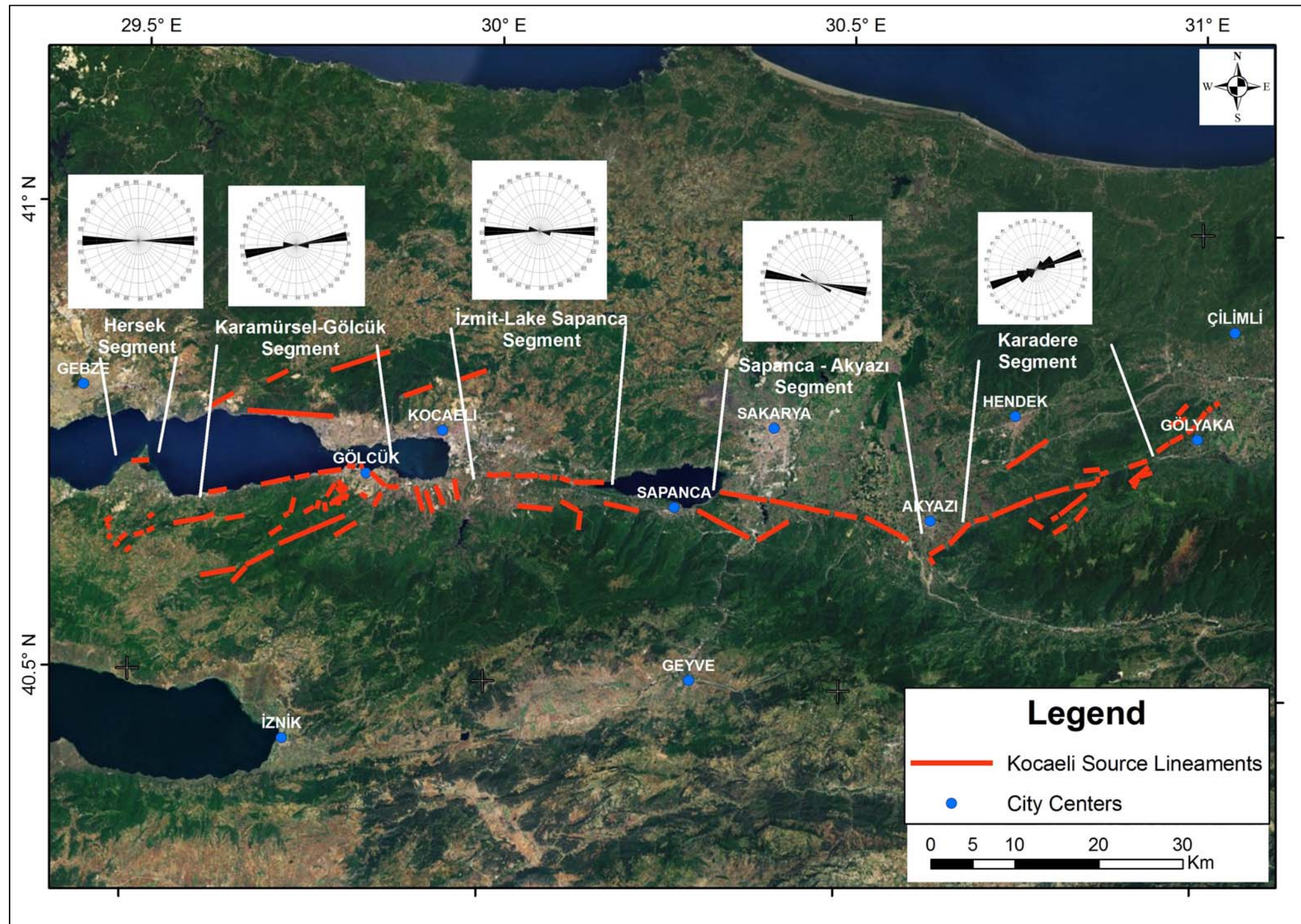
Figure 15. Directional analysis of segments of the Kocaeli source.
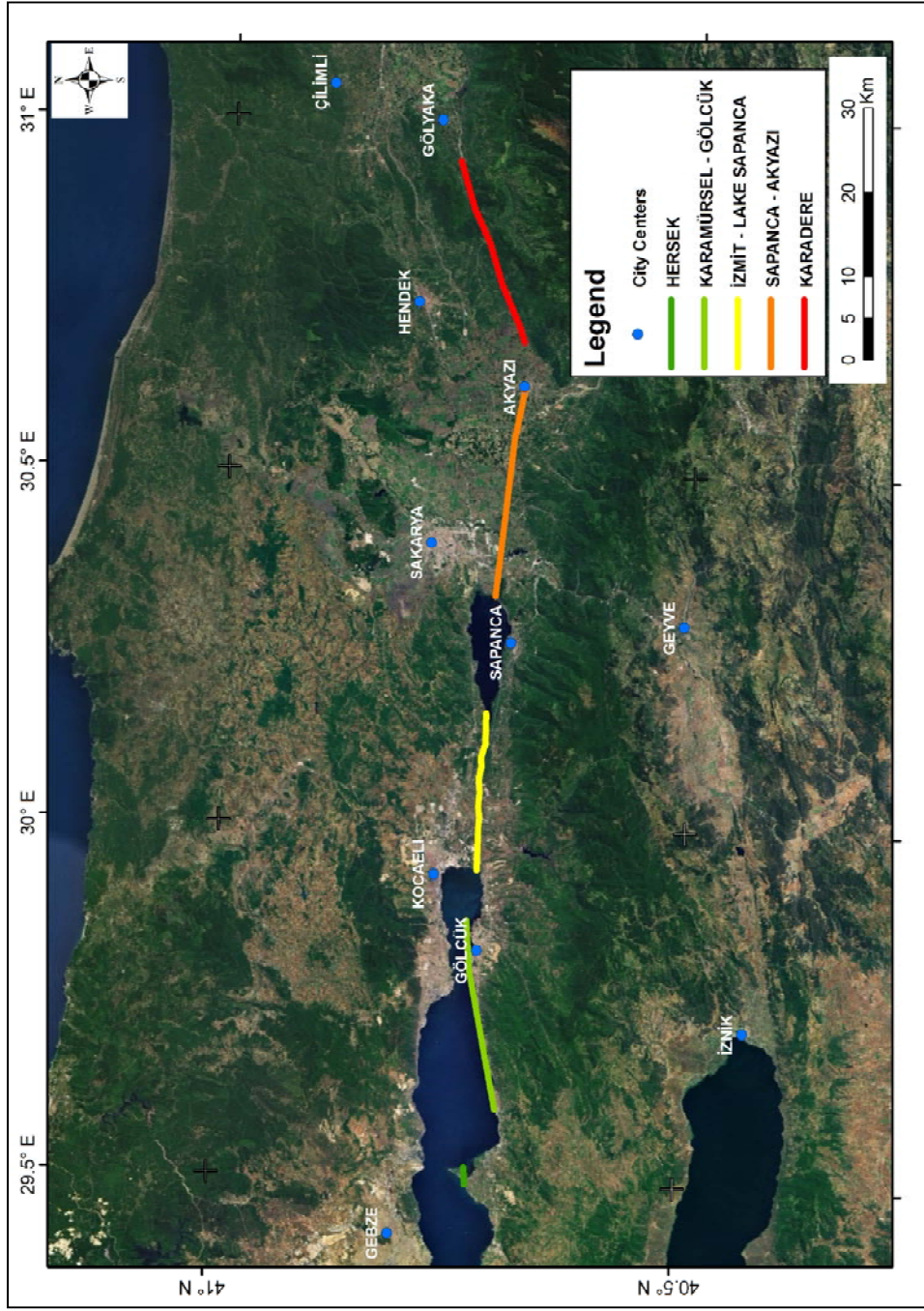
Figure 16. Segmentation of the Kocaeli source

4.1.2 Rupture Zone of 1999 Düzce Earthquake

Following 1999, Kocaeli surface rupture zone, the rupture zone of November 12, 1999 Düzce earthquake was investigated. The surface rupture of the earthquake was reported to be between 30 and 45 (Barka et al., 1999; Demirtaş et al., 2000; Özden et al., 2000, Duman et al., 2005. The surface rupture of approximately 40 km overlaps the eastern termination of 17 August 1999 event at Karadere segment for 9 km (Akyüz et al, 2000; Hartleb et al., 2002). The faulting characteristics of the Düzce rupture changes throughout the surface rupture area. Although the main rupture zone is dominated by right lateral strike-slip motion (Akyüz et al, 2002) there are normal (near Gölkaya) and thrust (at Düzce rupture zone) features present (Akyüz et al, 2002; Pucci et al., 2007). According to Duman et al. (2005) the surface rupture of the earthquake has three distinct segments delineated by Beyköy and Kaynaşlı restraining step-overs, therefore naming these segments as Eften, Dağdibi and Kaynaşlı segments. On the other hand, according to Pucci et al (2007) the Düzce Fault was divided into two segments as western and eastern near Cakırhacıibrahim according to co-seismic fault trace. The rupture trend is reported to be in the E-W direction (Çakır et al., 2003; Umutlu et al., 2004; Duman et al., 2005). Directional analysis of the extracted lineaments yielded the same result with trends ranging between N80°E and N100°E (Figure 17). In this study, the segmentation proposed by Duman et al. (2005) was adopted to the model (Figure 18).
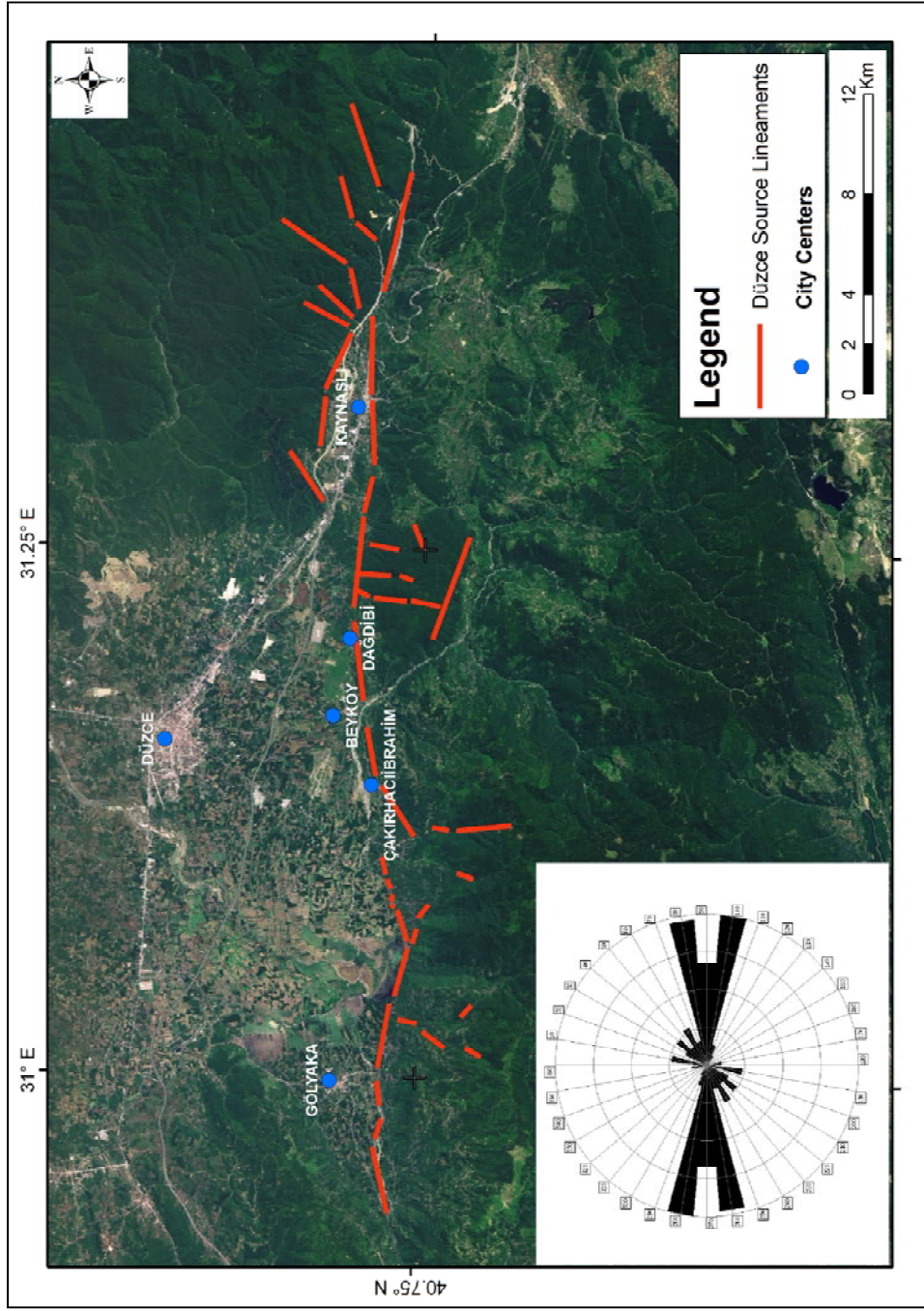
Figure 17. Directional analysis of Düzce seismic source extracted lineaments.
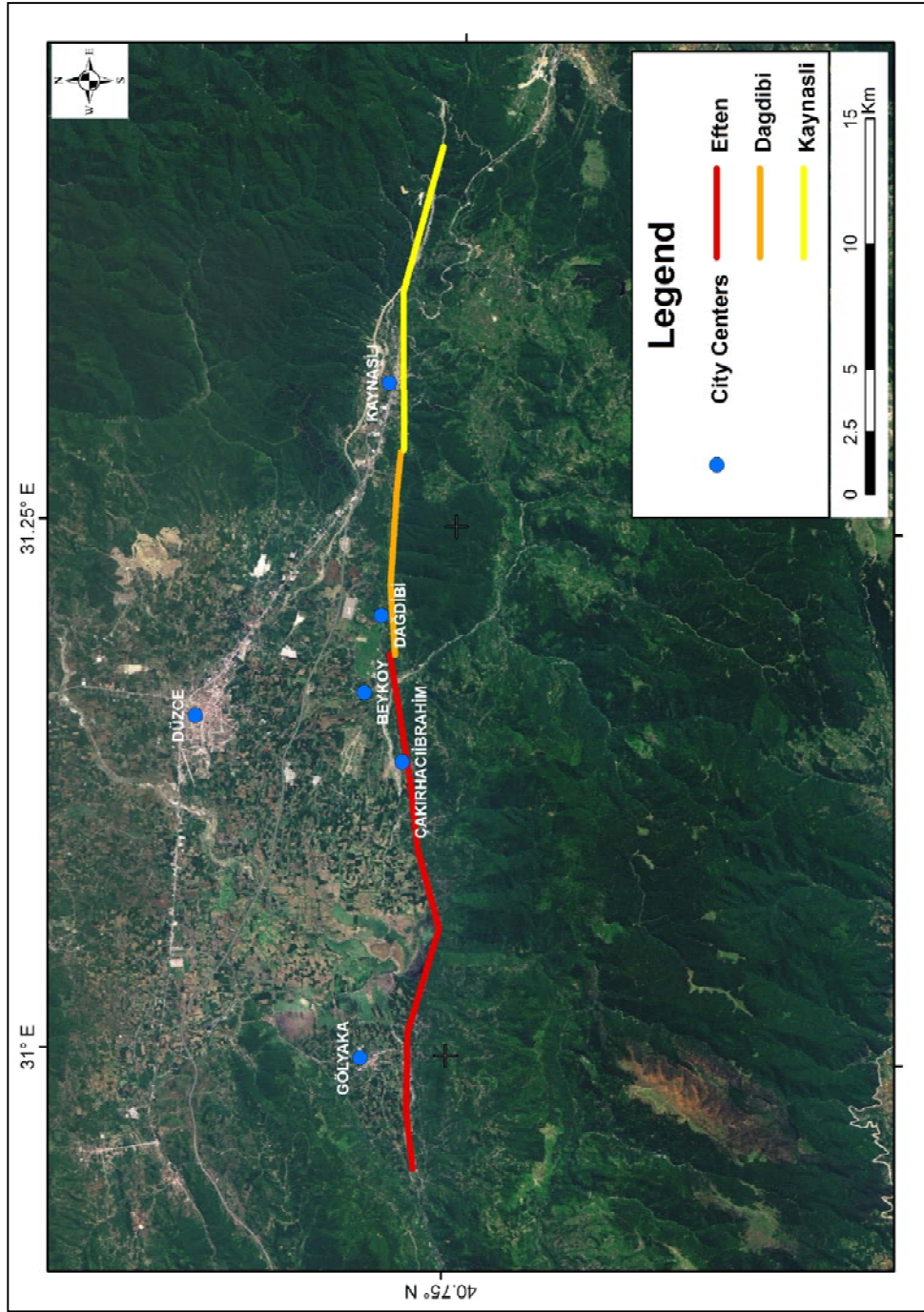
Figure 18. Segmentation of Düzce seismic source.

4.1.3 Rupture Zones of the 1967 Mudurnu and the 1957 Abant Earthquakes and Their Western Continuation

Another source zone for the model was determined to be the surface rupture areas of May 26, 1957 Abant; June 22, 1967 Mudurnu earthquakes and western continuation of these events up to Sapanca Lake -from east to west- (Palyvos et al., 2007). The 1967 Mudurnu earthquake is associated with approximately 55 km of rupture zone and the rupture zone overlaps at the eastern part with the 1957 Abant earthquake surface rupture with approximately 25 km (Ambraseys et al., 1968; Ambraseys and Zatopek, 1969) According to extensive mapping executed by Ambraseys and Zatopek (1969) the trend of the surface rupture varies between N75°-150°E with dominantly trending in N100°-120°E direction. The focal mechanism solution of the 1967 earthquake, performed by McKenzie (1972), indicates 93° striking, vertical fault plane having pure right-lateral strike-slip motion. The deformation zone continues approximately another 25 km to the west (Ambraseys et. al., 1968).

The 1957 Abant earthquake has an approximate surface rupture of 30 km (Barka, 1996), and according to Ambraseys and Zatopek (1969), the surface rupture of the 1957 Abant earthquake is approximately 40 km and located between Lake Abant and near Dokurcun. According to McKenzie (1972), the dip and strike of the slipped fault in 1957 has been reported as 78° and 87°, respectively, with right-lateral strike slip motion. Thus, this source zone was divided into three segments as western continuation, 1967 surface rupture and 1957 surface rupture, respectively from west to east (Figure 20).

According to directional analysis of the three segments, a) the western continuation has a strike range trending between N40°E and N120°E; b) Mudurnu segment has a dominant trend direction of N110°E, which is consistent with the

findings of Ambraseys and Zatopek (1969); and c) the Abant segment has a dominant strike direction of N70°E, which is consistent with McKenzie (1972) (Figure 19).
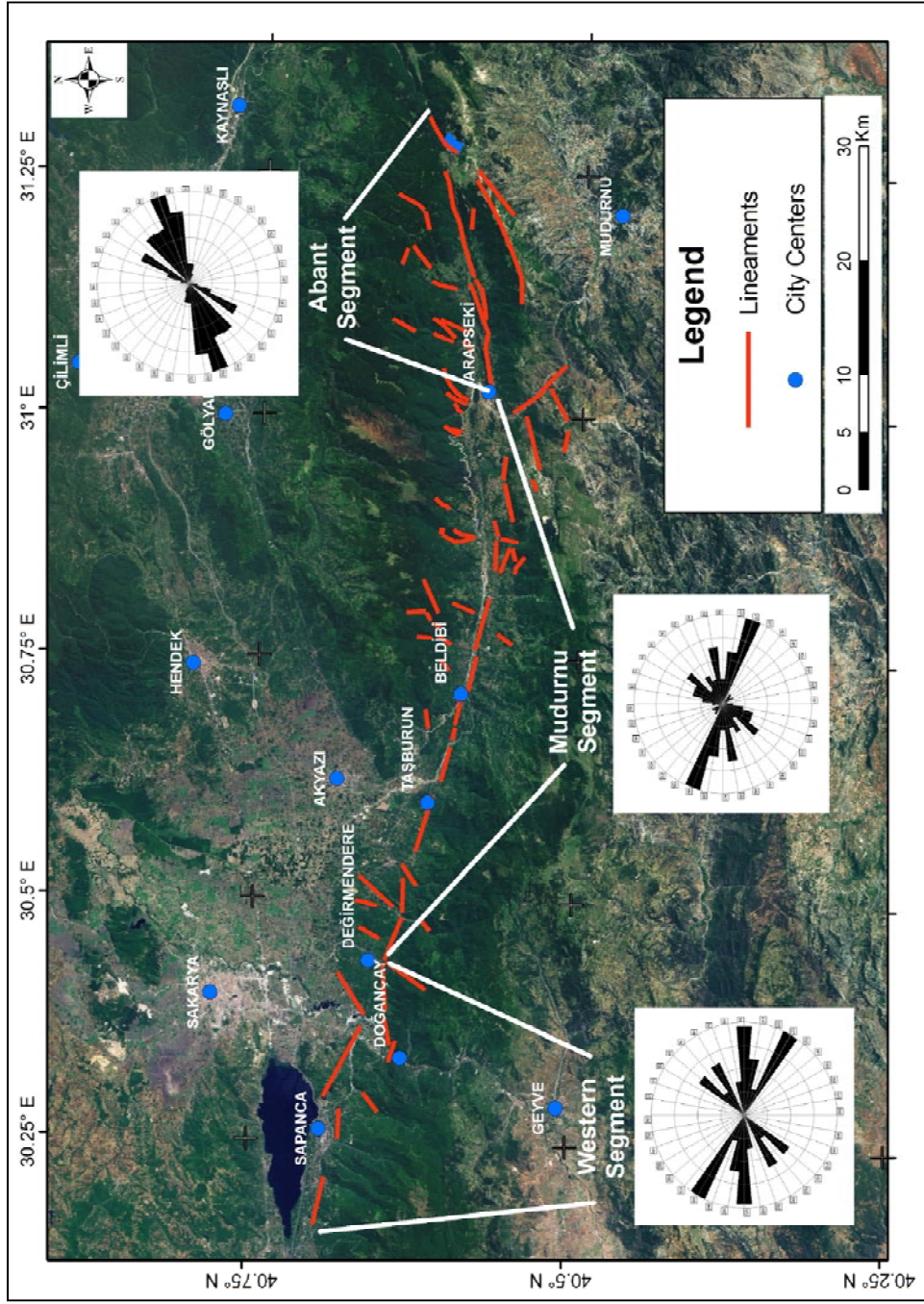
Figure 19. Directional analysis of the Mudurnu-Abant seismic source extracted lineaments.
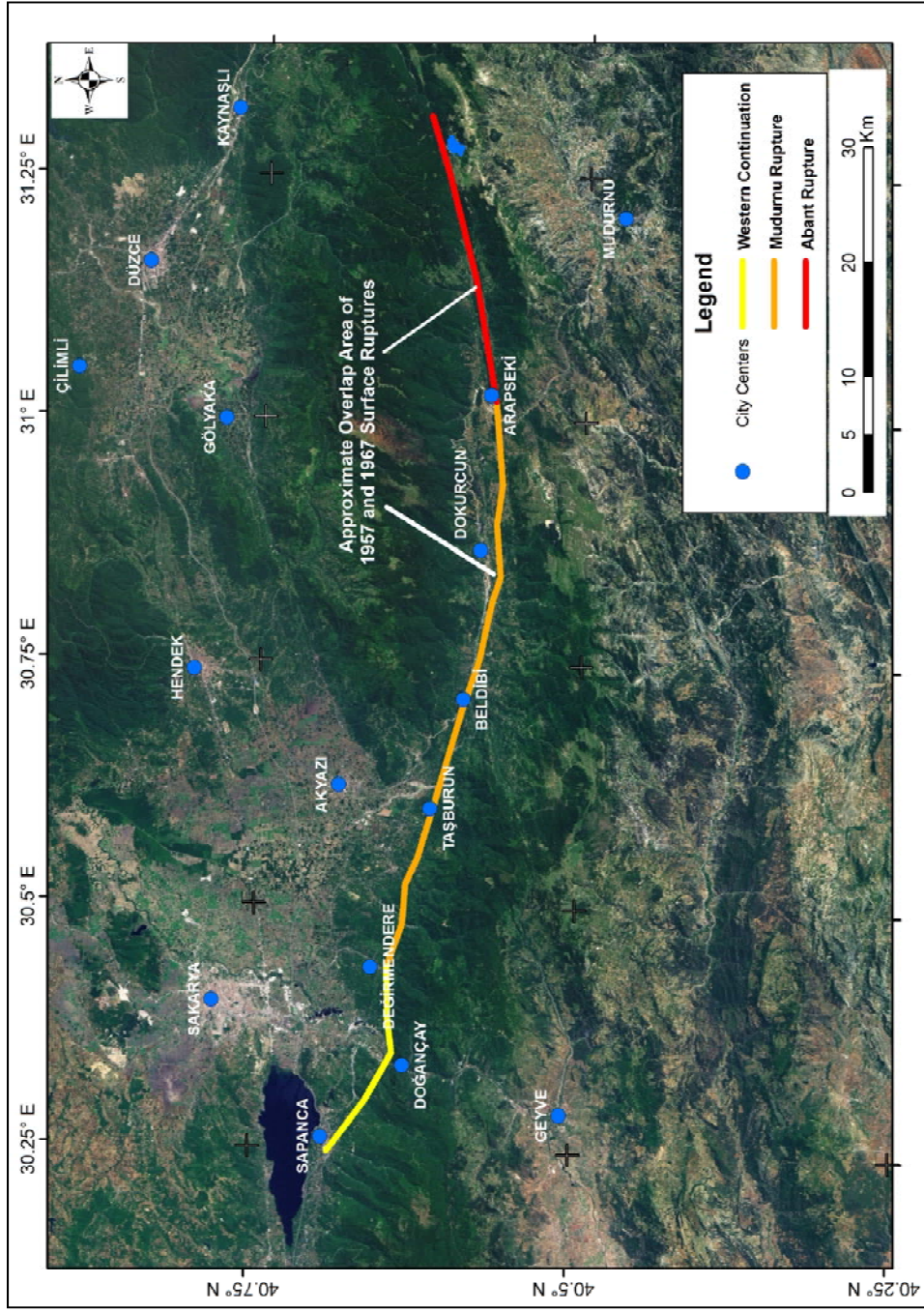
Figure 20. Segmentation of the Mudurnu Abant seismic source.

4.1.4 Rupture Zone of the 1944 Bolu –Gerede Earthquake

As the area of interest for this study (Düzce) is located towards the east of the Marmara Region as well as within the western Black Sea Region, one of the most important earthquakes that occurred at the east of this location; i.e. February 1st, 1944, Bolu-Gerede earthquake; was also included in this study. The base map for this source was the study by Barka and Kadinsky-Cade (1988) where the rupture zone was delineated into three segments between Lake Abant and Bayramören in west and east, respectfully (Ketin, 1969; Öztürk et al., 1985). In addition, the rupture geometry proposed by Kondo et al. (2005) was also utilized in order to determine the fault geometry more precisely.

The initial 37 km section of the fault starting from Lake Abant at the west has a trend variation between N68°E and N78°E and the remaining section until the termination point near Bayramören in the east has a strike direction of N80°E in general (Kondo et al., 2005). According to Ayhan and Koçyiğit (2010), the rupture strikes in the N76°E direction. The same observation can be made from directional analysis of the extracted lineament at this source area where strike direction varies dominantly between N60°E and N90°E, and the most dominant direction is N80°E (Figure 21).

According to Barka and Kadinsky-Cade (1988) and Barka (1996), the rupture zone is separated by a restraining bend south of Bayındır (32.6°E) and İsmetpaşa, therefore dividing the rupture zone into three segments (Figure 22).
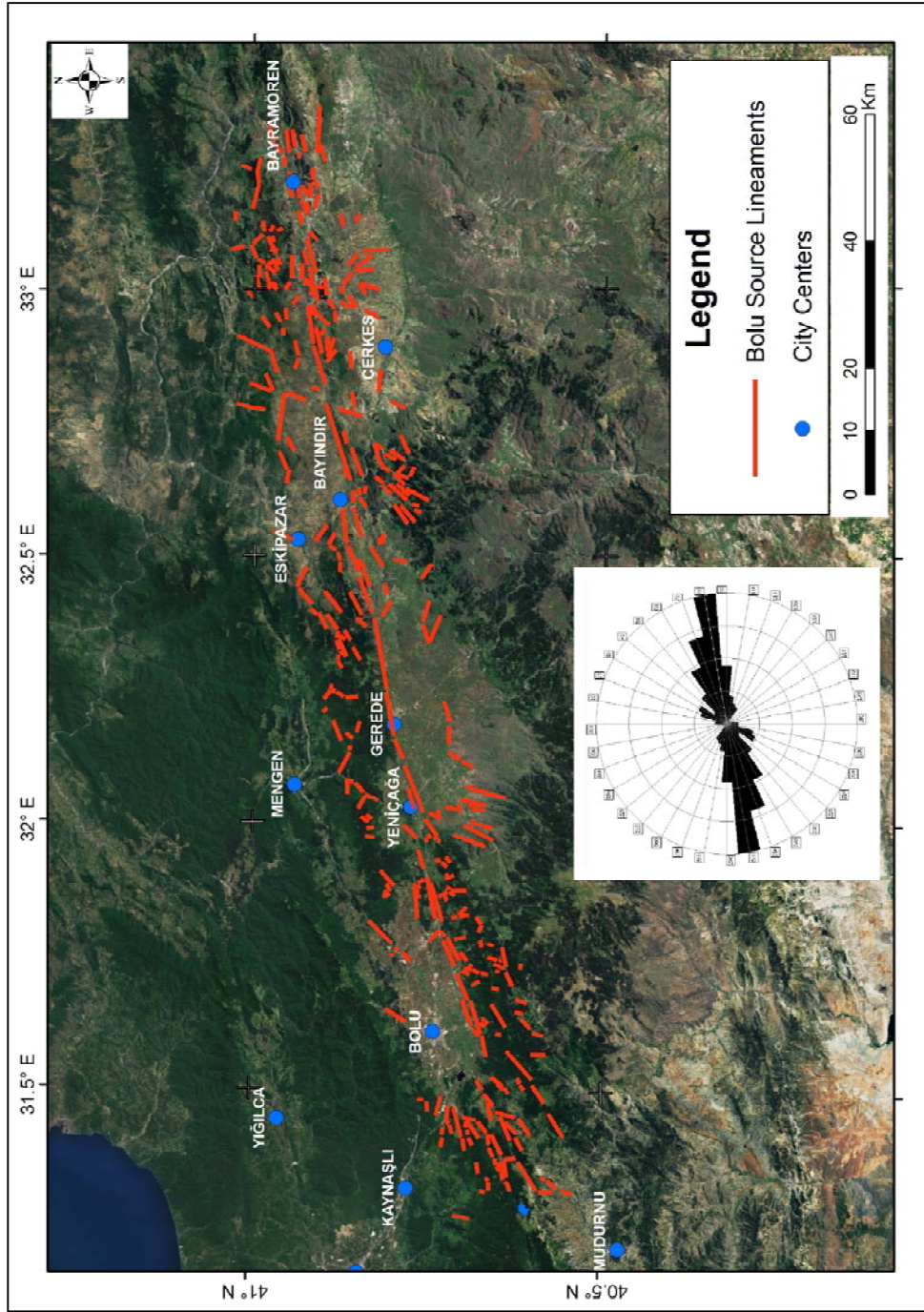
Figure 21. Directional analysis result of the extracted lineaments of Bolu seismic source.
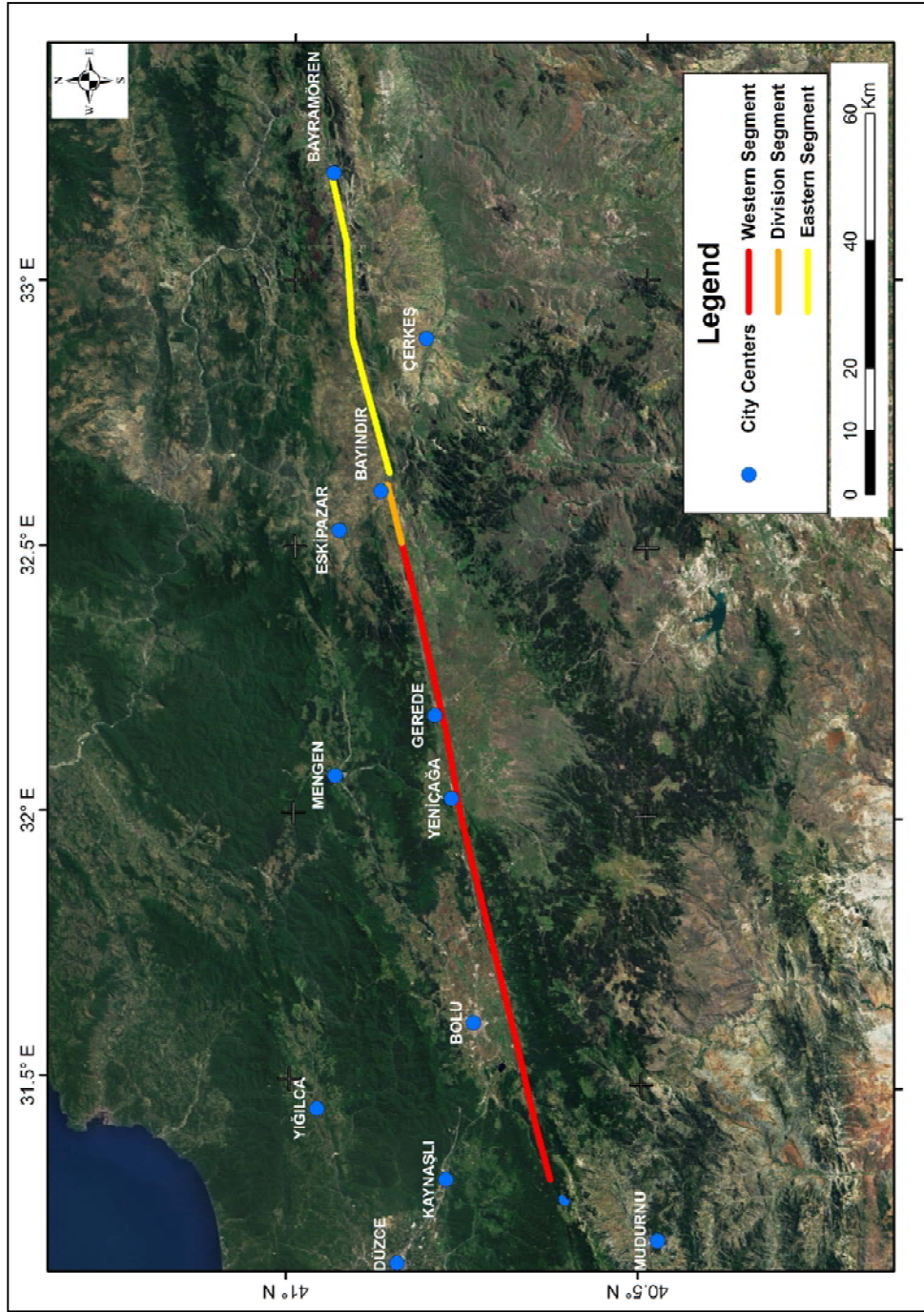
Figure 22. Segmentation of the Bolu seismic source.

4.1.5 Hendek Fault

The next segmentation has been performed on Hendek fault where a 5 km rupture has occurred during the August 17, 1999 Kocaeli earthquake (MTA, 2003b). From satellite images, the fault can be observed at the west of Lake Sapanca up to Hanlı and after Quaternary alluvial cover where Adapazarı is located, its continuation can be observed again starting from approximately 1 km south-west of Akarca. It continues approximately in the N45°E direction for 6.3 km and terminates at approximately 1 km northeast of Güldibi Village, which is consistent with the interpretation of Emre et al. (1998) where the section buried by the Adapazari alluvium has also been mapped as an active fault and with MTA, 2003b where the section east of the Adapazarı cover has been mapped, and the dominant strike direction was identified as N70°E (Figure 23).

Therefore, as the section under the Quaternary cover which is thought to be present due to continuation of the western and eastern interpretations and which has been mapped by Şaroğlu et al., 1992 and Emre et al., 1998; and also the following eastern section has been mapped by MTA, 2003b; this fault has also been added into the final model as a single segment (Figure 24).
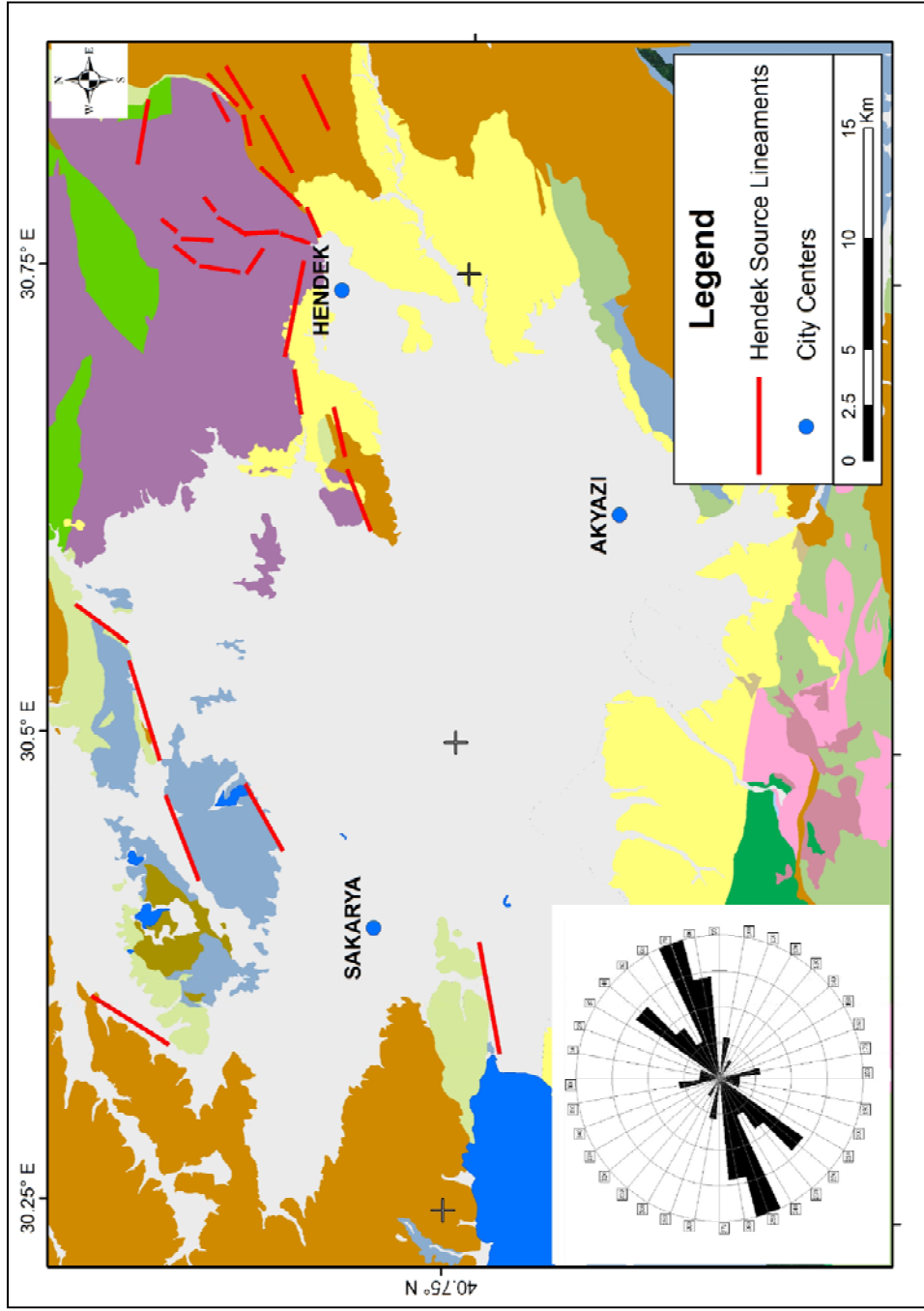
Figure 23. Directional analysis of extracted lineaments of Hendek seismic source.
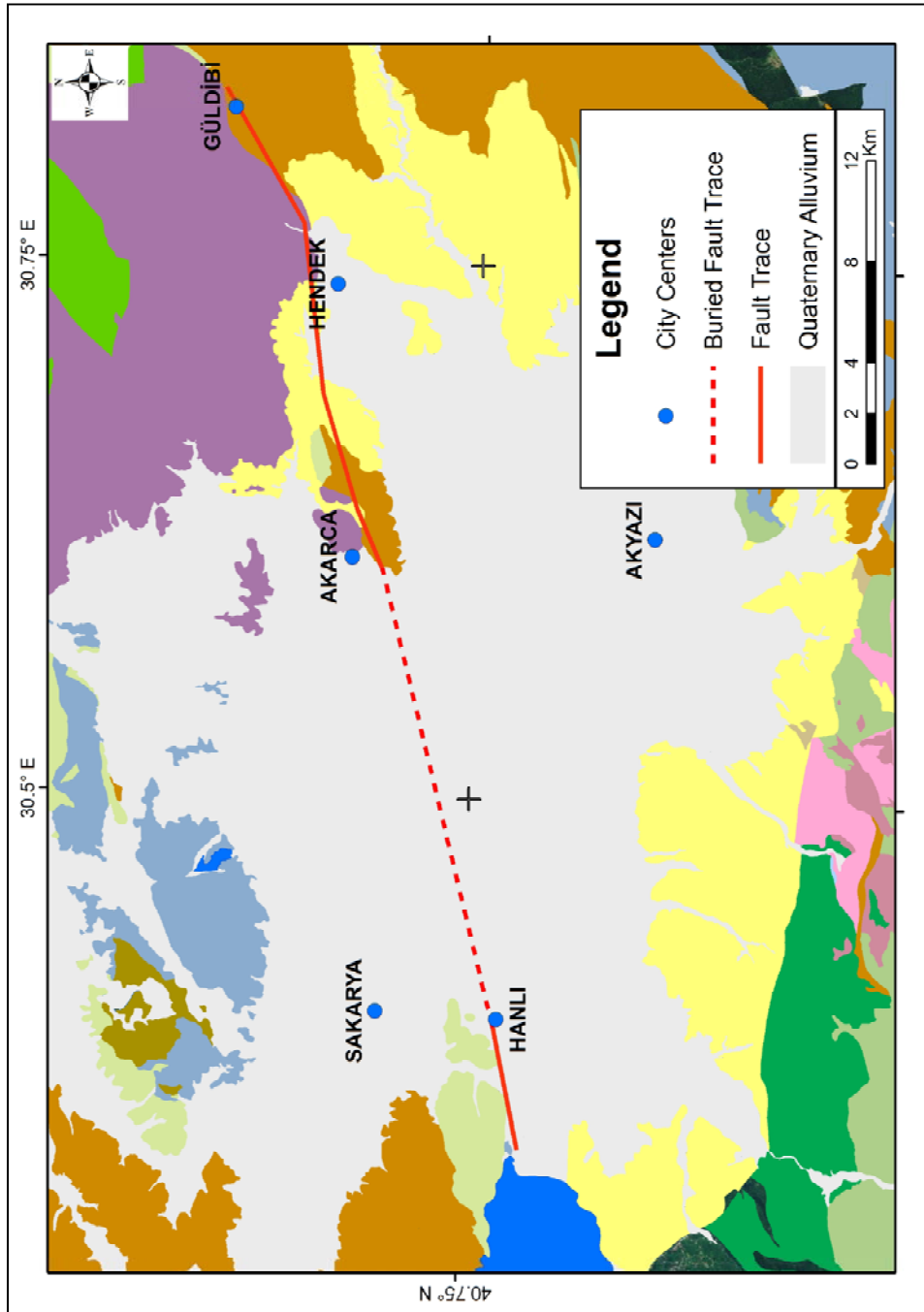
Figure 24. Segment of Hendek fault seismic source.

4.1.6 Geyve-İznik Fault Zone

The following source segment was delineated as Geyve-İznik Fault Zone which is defined as a seismically quiescent (seismic gap) zone (Barka and Kadinsky-Cade, 1988; Barka, 1992). This segmentation (identified as Middle Strand by Barka and Kadinsky-Cade, 1988) starts from the west at the rupture zone of the 1967 Mudurnu earthquake as a branch and continues until Gemlik Bay in the west. In this study, this fault zone was divided into three segments via adopting segmentation designated by Barka and Kadinsky-Cade (1988). According to directional analysis, trend directions range mainly between N60°E and N100°E with a dominant direction of N80E (Figures 25 and 26).

4.1.7 Çınarcık Fault

The final fault source included in this study is the Çınarcık Fault which has been mapped by different researches as on land fault bounding the northern shore of the Çınarcık Peninsula (Şaroğlu et al., 1992; Emre et al., 1998; MTA, 2003b) and also as an offshore fault following the trace of the northern trend of the Çınarcık Peninsula (Barka and Kadinsky-Cade, 1988; Wong et al., 1994; Barka et al., 2002). This source was included in the model as two segments. According to directional analysis of lineaments, the general trend direction ranges between N70°E and N90°E and the highest frequency was observed in the N80°E direction (Figures 25 and 26).
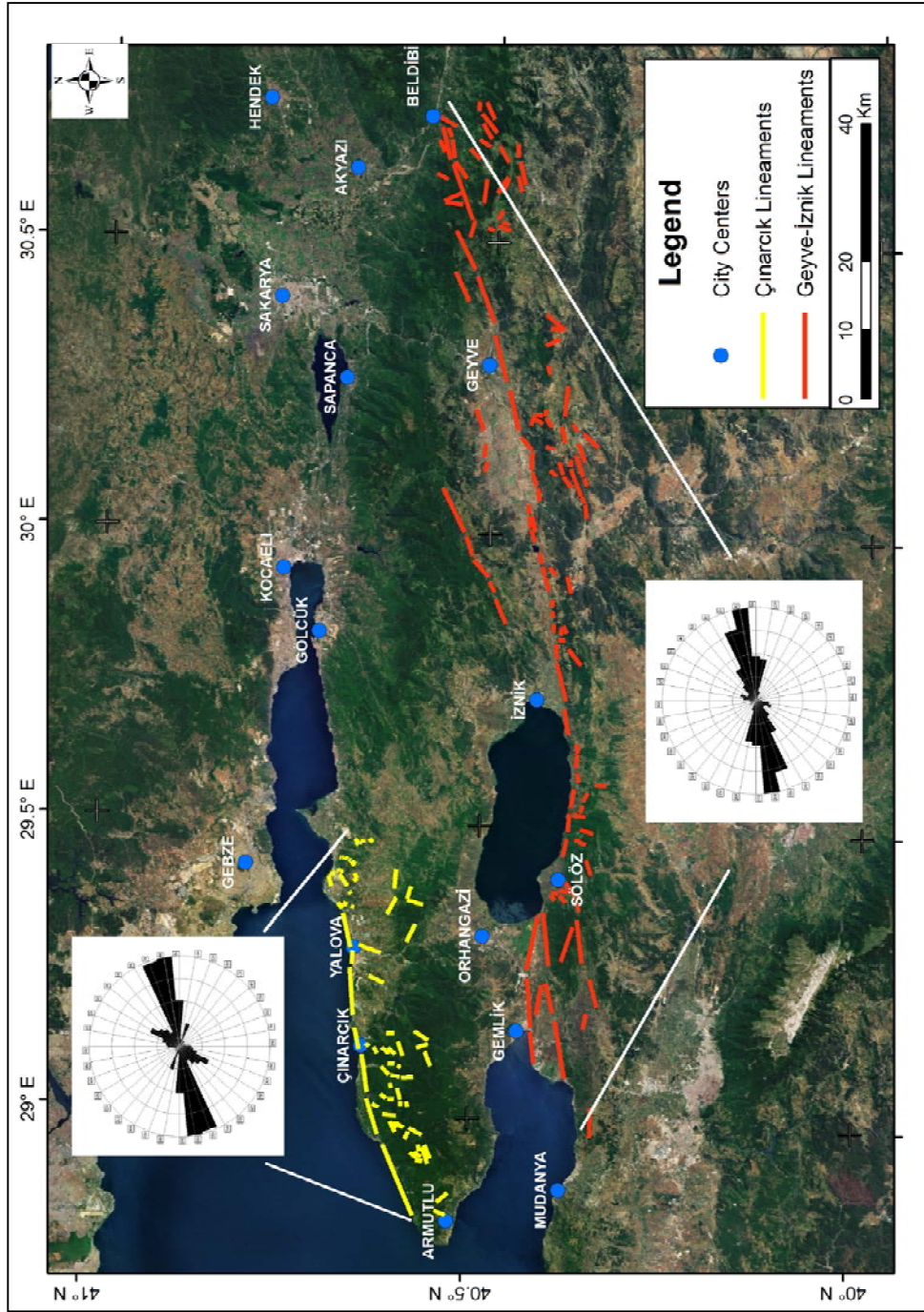
Figure 25. Directional analysis of extracted lineaments of Çınarcık and Geyve-İznik seismic sources.
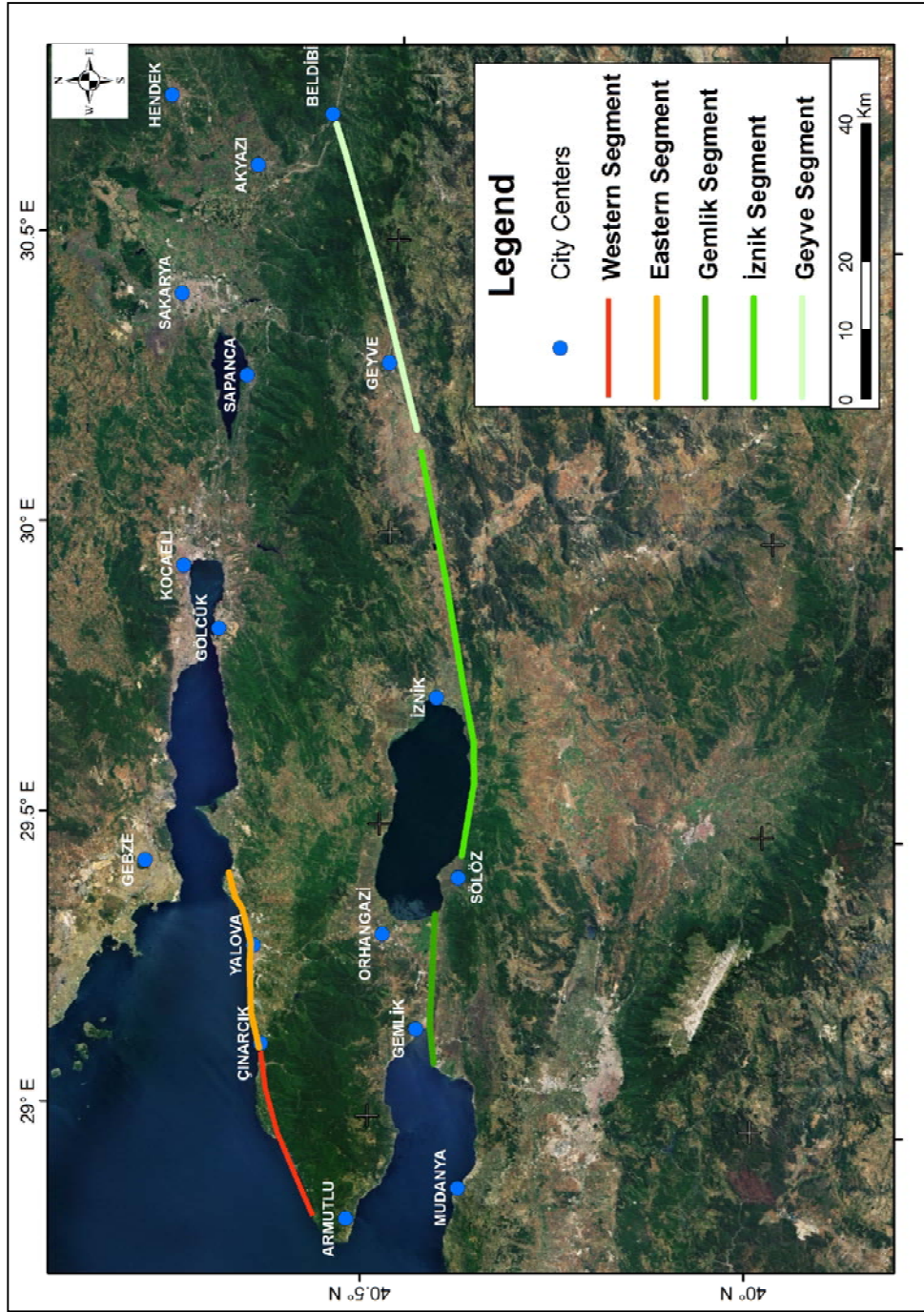
Figure 26. Segments of Çınarcık and Geyve-İznik seismic sources.

49

4.2 Final Source Model and Parameters

After determination of the above mentioned seven source zones, their lengths were extracted from the database and maximum credible earthquake values for each fault segment was determined in accordance with the surface rupture length relationship proposed by Wells and Coppersmith (1994) for strike slip faults:

$$M_w = 5.16 + 1.12* \log (SRL) \qquad (1)$$

where, M_w is the moment magnitude of maximum credible earthquake (characteristic magnitude) and SRL is the surface rupture length in kilometers.

However, each fault has different depth (rupture width) values as determined in accordance with the literature and seismic data. Thus, the relationship proposed by Wells and Coppersmith (1994) for strike slip faults is:

$$M_w = 3.98 + 1.02* \log (RA) \qquad (2)$$

where, RA is the rupture area determined from SRL and RW (rupture width) in kilometers. Rupture width values for each source zone is given by Table 9. Therefore, the characteristic magnitudes for these surface rupture length (Tables 10 and 12) and rupture area values (Tables 11 and 13) were calculated.

Table 9. Rupture width values for the seismic sources.

Seismic Source	Rupture Width (km)			
	From Seismic Data	From Literature	Reference	Utilized Value
Kocaeli Earthquake Source	17	15 - 25	Reilinger et al. 2006	17
		6 - 12	Delouis et al., 2002	
		17	Meade et al., 2002	
		16	Burgmann et al., 2002a	
Düzce Earthquake Source	10	16 - 20	Ayhan et al., 1999	30*
		14 – 24.5	Burgmann et al., 2002b	
		20	Utkucu et al., 2003	
Mudurnu-Abant Source	18	15 - 25	Reilinger et al. 2006	18
Bolu Earthquake Source	16	17	Ayhan and Koçyiğit, 2010	16
		16	Koçyigit et al., 2006;	
		17	Özalaybey et al., 2002	
		31 ± 2	Zor et al., 2006	
		15 - 21	Nakiboğlu et al. 1998; Meade et al. 2002; Koçyiğit et al. 2006; Reilinger et al. 2006	
Hendek Fault Source	14	-	-	17*
Geyve-İznik Fault Source	11	-	-	11
Çınarcık Fault Source	12	-	-	12
* See Chapter 5.6 for details.				

Table 10. Characteristic magnitudes according to surface rupture lengths for each segment.

Source	Segment	Length (km)	M.Char - 1σ	M. Char.	M.Char + 1σ
Kocaeli Earthquake	Hersek	2.15	5.25	**5.53**	5.81
	Karamürsel - Gölcük	22.88	6.40	**6.68**	6.96
	Sapanca	25.51	6.46	**6.74**	7.02
	İzmit - Lake Sapanca	18.83	6.31	**6.59**	6.87
	Karadere	23.05	6.41	**6.69**	6.97
Düzce Earthquake	Eften	20.77	6.36	**6.64**	6.92
	Dagdibi	8.17	5.90	**6.18**	6.46
	Kaynasli	12.32	6.10	**6.38**	6.66
Mudurnu-Abant Earthquakes	Western Continuation	17.69	6.28	**6.56**	6.84
	Mudurnu Rupture	50.67	6.79	**7.07**	7.35
	Abant Rupture	25.46	6.45	**6.73**	7.01
Bolu Earthquake	Western	102.98	7.13	**7.41**	7.69
	Division	9.46	5.97	**6.25**	6.53
	Eastern	48.25	6.77	**7.05**	7.33
Hendek Fault	Hendek Fault	43.93	6.72	**7.00**	7.28
Geyve-İznik Fault	Gemlik	21.72	6.38	**6.66**	6.94
	İznik	59.51	6.87	**7.15**	7.43
	Geyve	45.90	6.74	**7.02**	7.30
Çınarcık Fault	Western	25.17	6.45	**6.73**	7.01
	Eastern	26.11	6.47	**6.75**	7.03

Table 11. Characteristic magnitudes according to rupture areas for each segment.

Source	Segment	Rupture Width (km)	Length (km)	Rupture Area (km²)	M.Char - 1σ	M. Char.	M.Char + 1σ
Kocaeli Earthquake	Hersek	18	2.15	38.64	5.37	**5.60**	5.83
	Karamürsel - Gölcük	18	22.88	411.80	6.42	**6.65**	6.88
	Sapanca	18	25.51	459.16	6.47	**6.70**	6.93
	İzmit - Lake Sapanca	18	18.83	338.93	6.33	**6.56**	6.79
	Karadere	18	23.05	414.92	6.42	**6.65**	6.88
Düzce Earthquake	Eften	30	20.77	623.08	6.60	**6.83**	7.06
	Dagdibi	30	8.17	245.11	6.19	**6.42**	6.65
	Kaynasli	30	12.32	369.46	6.37	**6.60**	6.83
Mudurnu - Abant Earthquakes	Western Continuation	18	17.69	318.35	6.30	**6.53**	6.76
	Mudurnu Rupture	18	50.67	912.08	6.77	**7.00**	7.23
	Abant Rupture	18	25.46	458.32	6.46	**6.69**	6.92
Bolu Earthquake	Western	16	102.98	1647.71	7.03	**7.26**	7.49
	Division	16	9.46	151.35	5.97	**6.20**	6.43
	Eastern	16	48.25	772.04	6.70	**6.93**	7.16
Hendek Fault	Hendek Fault	16	43.93	702.94	6.65	**6.88**	7.11
Geyve-İznik Fault	Gemlik	13	21.72	282.33	6.25	**6.48**	6.71
	İznik	13	59.51	773.67	6.70	**6.93**	7.16
	Geyve	13	45.90	596.69	6.58	**6.81**	7.04
Çınarcık Fault	Western	12	25.17	302.01	6.28	**6.51**	6.74
	Eastern	16	26.11	772.04	6.47	**6.75**	7.03

Table 12. Characteristic magnitudes according to surface rupture lengths for each segment.

Seismic Source	Length (km)	MChar - 1σ	M.Char.	MChar + 1σ
Kocaeli Earthquake	92.41*	7.08	**7.36**	7.64
Düzce Earthquake	41.25	6.69	**6.97**	7.25
Mudurnu – Abant Earthquakes	93.82	7.09	**7.37**	7.65
Bolu Earthquake	160.69	7.35	**7.63**	7.91
Hendek Fault	43.93	6.72	**7**	7.28
Geyve – İznik Fault	127.13	7.24	**7.52**	7.8
Çınarcık Fault	51.28	6.8	**7.08**	7.36
* See Chapter 5.6 for details on model and surface rupture modification.				

Table 13. Characteristic magnitudes according to rupture areas for each seismic source.

Seismic Source	Rupture Area (km)	MChar - 1σ	M.Char.	MChar + 1σ
Kocaeli Earthquake	1663.45	7.04	**7.27**	7.50
Düzce Earthquake	1237.64	6.90	**7.13**	7.36
Mudurnu – Abant Earthquakes	1688.75	7.04	**7.27**	7.50
Bolu Earthquake	2571.10	7.23	**7.46**	7.69
Hendek Fault	702.94	6.65	**6.88**	7.11
Geyve – İznik Fault	1652.69	7.03	**7.26**	7.49
Çınarcık Fault	615.32	6.59	**6.82**	7.05
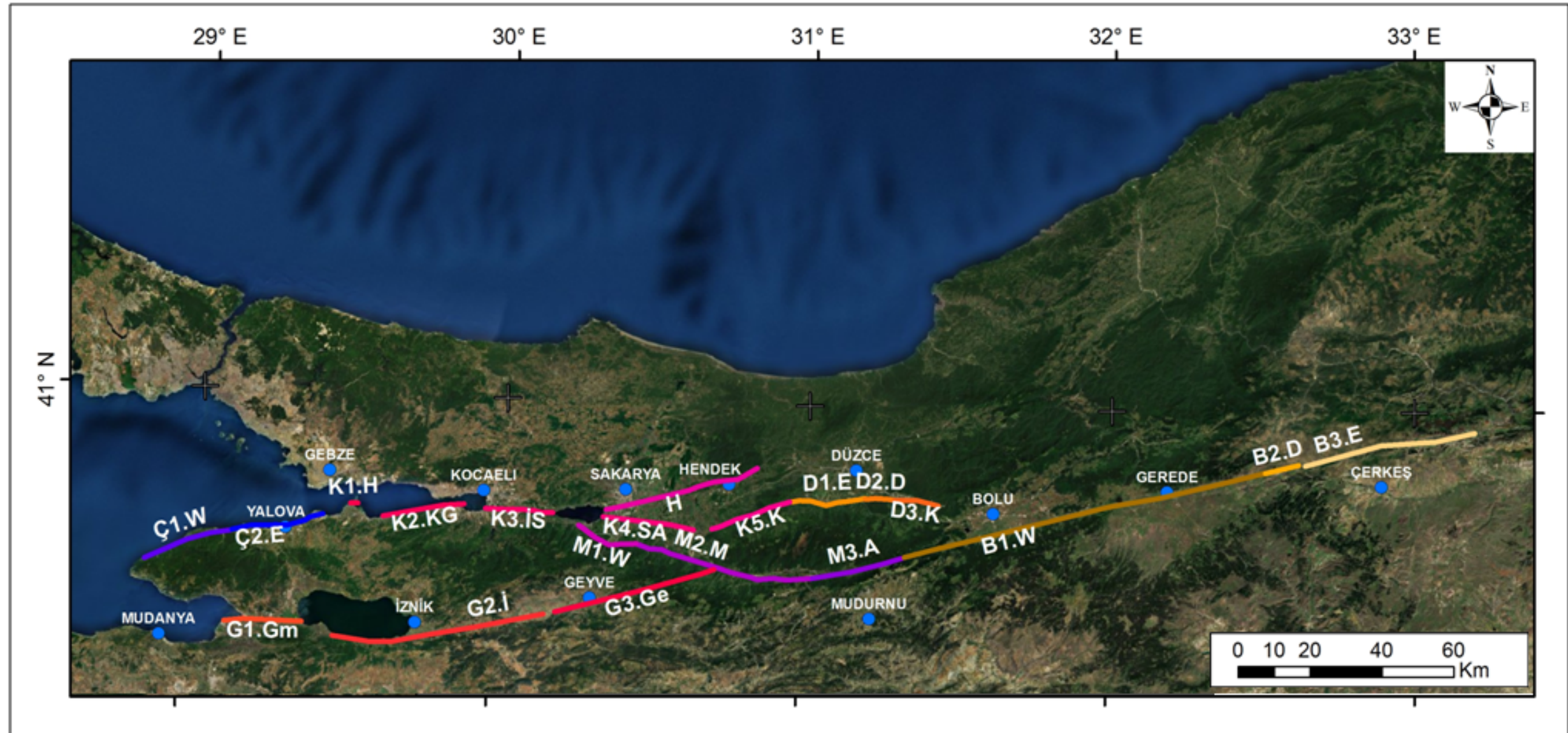
Figure 27. Source model for the study area.
(Ç1.W: Çınarcık, West; Ç2.E: Çınarcık, East; K1.H: Kocaeli, Hersek; K2.KG: Kocaeli, Karamürsel-Gölcük; K3.İS: Kocaeli, İzmit-Lake Sapanca; K4.SA: Kocaeli, Sapanca-Akyazı; K5.K: Kocaeli, Karadere; G1.Gm: Geyve-İznik, Gemlik; G2.İ: Geyve-İznik, İznik; G3.Ge: Geyve-İznik, Geyve; M1.W: Mudurnu-Abant, Western Continuation; M2.M: Mudurnu-Abant, Mudurnu; M3.A: Mudurnu-Abant, Abant; B1.W: Bolu-Gerede, West; B2.D: Bolu-Gerede, Divide; B3.E: Bolu-Gerede, East; D1.E: Düzce, Eften; D2.D: Düzce, Dağdibi; D3.K: Düzce Kaynaşlı; H: Hendek segments)

CHAPTER 5

PROBABILISTIC SEISMIC HAZARD ASSESSMENT

5.1 Introduction

Earthquake hazard analyses are performed in terms of deterministic (Krinitzsky, 1993) and probabilistic (Cornell, 1968) approaches since recent decades. There are uncertainties regarding the magnitude, time and location of an earthquake, and due to these uncertainties the method to be applied should be carefully selected. As deterministic approaches focus on a single fault, fault segment, fault system which can cause the largest earthquake in the closest vicinity of the area of interest (100 km, 250 km, etc.) and depend on uncertain data inputs, these are deemed poor for engineering decisions (Gupta, 2002). Deterministic seismic hazard analysis is a practical method for assessment of worst-case ground motions. However, this approach does not give information on uncertainties of the occurrence probability of this earthquake event, its possibility of occurrence at a specific location, level of ground shaking in a certain time interval and characteristics of the ground motion to be calculated in different steps (Kramer, 1996).

On the other hand, probabilistic seismic hazard assessment enables to consider geological, geophysical, seismologic and historical data in a more compatible and logical manner (Erdik et al., 2006). Probabilistic seismic hazard assessments allow systematic modeling and estimation of parameters of ground motions which have a certain probability of exceedance and which may occur within the design period of

area of interest where there are uncertainties in the input parameters. This approach, which is a more successful method in the estimation of ground motions in the area of interest, when compared with deterministic approaches due to the nature of the earthquake phenomena which have uncertainties from source location to distance to event, is being used since it was first proposed by Cornell (1968) and has a larger area of application since. Although this approach has undergone some modifications in terms of randomization of parameters, the main approach has resumed as is in essence (Çetin et al., 2004).

All probable and relevant deterministic earthquake scenarios (all possible location and earthquake combinations) are considered in probabilistic approach. Along with this, plus/minus standard deviation (σ) values of median value (μ) are considered for all possible ground motion probability levels.

The main steps in probabilistic approaches have been summarized below as indicated by Erdik et al. (2006) and Yücemen (2008):

a) Collection of geological and seismological data: Determination of the area of influence and preparation of a seismic database by utilizing earthquake catalogue(s) which include previous earthquakes that have occurred in the area. Assurance that the compiled earthquake catalogue is complete and unbiased with the necessary changes and adjustments.

b) Determination of seismic zones: Determination of the area and line seismic source zones in the study area, preparation of active fault zones and determination of the parameters that define these identified faults.

c) Determination of the statistical properties and seismicity parameters of the earthquake occurrence in these seismic zones: Preparation of a seismo-tectonic map in order to assess earthquake epicenters and their relation with active faults. Assignment of earthquake epicenters to

seismic source zones in terms of their locations and determination of magnitude probability distribution according to magnitude-recurrence relations to be determined for each source zone and determination of other seismic parameters. Identification of background seismic zones for epicentral distribution which could not be assigned to any seismic source zones (this approach was not utilized in this study).

d) Determining and/or compiling the appropriate ground motion prediction equations (GMPEs) which can be utilized for the seismic source zones along with their uncertainty coefficients.

e) Acquisition of distribution of maximum magnitude and maximum horizontal ground acceleration exceedance probabilities based on computer software(s). Acquisition of a probabilistic distribution of the earthquake magnitude (intensity) or ground motion parameter according to a calculation algorithm which shall combine to the contribution of the seismic source zones in the study area to the seismic hazard. As numerical calculation shall be executed with software(s) compiled for this purpose; determination of the appropriate software(s).

f) Either direct assessment of uncertainties of different types or reflection of effects of epistemic uncertainties due to lack of information via sensitivity analyses and logic-tree or similar approaches.

Therefore, probabilistic seismic hazard assessment which contained the following three input data sets was utilized in this study:

a) Seismic source
b) Earthquake catalogue
c) Ground Motion Prediction Equation.

As stated previously, all these datasets included a certain level of uncertainty in them. When the main objective of this study is considered along with previous chapters and especially Chapter 4, the first input data set is considered to be accurate. On the other hand, the utilized earthquake catalogue has certain aspects (as discussed below) which should be considered prior to utilization, i.e., declustering and catalogue completeness analyses. Finally, GMPEs to be utilized have a certain uncertainty and as shall be discussed in the below sections, this uncertainty was included by inclusion of standard deviations in the analyses.

Seismic source models in a seismic hazard analyses can be point, line or area sources (Cornell, 1968). In this study, line sources were utilized, and total of 7 seismic sources were determined.

5.2 Probability Distribution of Earthquake Magnitude

Probability distribution of earthquake magnitudes is derived from recurrence relations, which indicate the relationship between magnitudes and their occurrence frequency. The most commonly utilized relationship is the linear magnitude-frequency relationship proposed by Gutenberg and Richter (1949) and given below:

$$(log)_{10} N(M) = a + bM \qquad (3)$$

where; N(M) is the number of earthquakes with magnitude equal or larger than M in unit time; a and b are regression coefficients determined for the area and M is the Richter magnitude. The coefficient 'a' changes according to extent of the study area, observation period and level of earthquake activity, while the coefficient 'b' is the seismo-tectonic parameter and this coefficient has a significant importance

in statistical analysis of earthquakes as it is directly related to the physical characteristics of earthquake occurrence. The calculated '*b*' values change according to utilized data, methods, normal and cumulative frequencies of earthquakes. Gutenberg and Richter (1949) have reported *b*=0.9±0.2 and *b*=1.2±0.2 values for shallow (depth < 70 km) and moderate and deep earthquakes, respectively.

In seismic hazard analyses a lower bound of (M_0) is generally defined and earthquakes having a magnitude smaller than this lower bound are not included in hazard assessments as they are deemed insignificant in terms of engineering applications. Along with this, since statistical analyses of these earthquakes are generally are reliable (Yücemen, 2008), earthquakes having a magnitude equal or smaller than M_w=4.0 were neglected in this study and the earthquake catalogue was selected concordant with this criterion.

Previous earthquake records show that infinite energy release is impossible. In other words, there is an upper bound (M_1) for magnitude. This upper bound is determined by the maximum magnitude earthquake to be expected to occur in the area. By considering that there is an upper and a lower bound for magnitude, the exponential probability density function, $f_m(M)$ that is given below is obtained for magnitude:

$$f_m(M) = k\beta e^{-\beta(M-M_0)} \qquad\qquad M_0 < M < M_1 \qquad\qquad (4)$$

$$= 0 \qquad\qquad\qquad \text{elsewhere}$$

$$k = \left[1 - e^{-\beta(M_1-M_0)}\right]^{-1} \qquad\qquad (5)$$

The 'k' parameter given in Eq. (5) is the standardization coefficient which satisfies that $M = M_1$ is equal to 1 in cumulative distribution. Therefore the magnitude probability density function can be expressed as:

$$f(m) = \frac{\beta . e^{[-\beta(M - M_o)]}}{1 - e^{\{-\beta(M_1 - M_o)\}}} \tag{6}$$

The $\beta = b$ (ln 10), which is a parameter of exponential distribution with upper and lower bounds demonstrated in Eq. (3) is related to the tectonic structure of the region and indicates the relative ratio relationship between small and large earthquakes. An example of this double bound exponential density function is shown in Figure 28 for magnitude truncation at magnitudes 5.0 and 7.0.
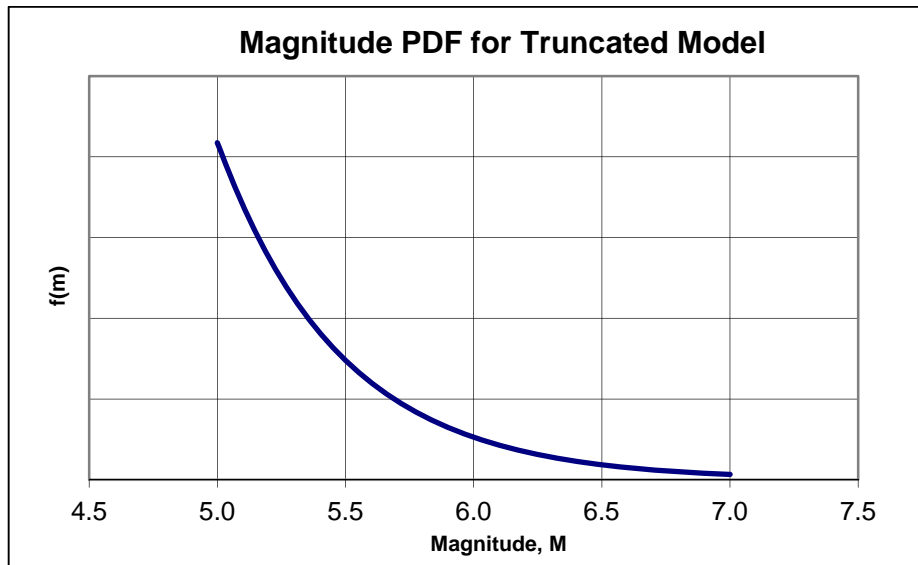
Figure 28. Magnitude probability density function for a double bound exponential model.

Different statistical methods can be used for estimation of parameters of exponential distribution based on observed values. Linear regression and maximum likelihood estimations are the two most common methods (Deniz, 2006; Yücemen, 2008).

Following these explanations, a discussion regarding earthquake catalogue and its completeness along with declustering is explained in the sections below.

5.3 Earthquake Catalogue

The earthquake catalogue data to be utilized in estimation of exponential probability density function should be complete in each magnitude interval. The quality and number of earthquakes decrease with decreasing time. Although both large and small magnitude earthquakes are recorded in recent years, older records include only large earthquakes. Along with this, these recorded large earthquakes are mostly located in settled areas and large earthquakes at non-habited areas may not even be included in the earthquake catalogues. Thus, these deficiencies in earthquake catalogs cause bias both in time and also in space (Stepp, 1973; Deniz and Yücemen, 2010). Thus, since recurrence relations may not represent occurrence frequencies in a realistic manner, it is necessary to use an interval that is short enough to be complete in small events or long enough that is complete in large events (Stepp, 1973). In addition, in order to assume that the distribution fits a Poisson process, the catalogue should be declustered, homogenized and its completeness should be checked. In this study, 'The revised and extended earthquake catalogue for Turkey since 1900' (KOERI, 2007) was utilized as an earthquake catalogue. This is a homogenized catalogue in terms of magnitude scales with a standard format. This catalogue reports the events with each magnitude scales rather than different magnitude scales which causes non-

homogeneity (KOERI, 2007). Therefore, the clustering and completeness analysis of this catalogue is checked in the subsequent sections.

5.3.1 Declustering Analysis of the Catalogue

As previously mentioned, the earthquake catalogue should be declustered, i.e. secondary events should be excluded from the catalogue in order to preserve mutually exclusiveness of the events as well as to guarantee that the catalogue can be represented by Poisson process which is utilized to describe earthquake phenomena in time domain (Gardner and Knopoff, 1974). For this purpose, catalogue having 337 earthquakes (see Appendix A) were primarily processed in accordance with the previously stated main earthquake events both in terms of time and space via utilizing the temporal-spatial bounds proposed by Deniz (2006) which combines bounds proposed by Gardner and Knopoff, 1974; Prozorov and Dziewonski, 1982; Reasenberg, 1985; Savage and Rupp, 2000 and Kagan, 2002 (Table 14).

Table 14. Temporal-Spatial windows for declustering analysis.

Moment Magnitude (Mw)	Distance (km)	Time (Days)
4.5	35.5	42
5	44.5	83
5.5	52.5	155
6	63	290
6.5	79.4	510
7	100.0	790
7.5	125.9	1326
8	151.4	2471

Following this primary declustering analysis, the remaining earthquakes were secondarily checked manually for further related events. Therefore the final catalogue having 120 events were utilized in further analyses (Table 15).

Table 15. Earthquake magnitude frequency before and after declustering analysis.

Magnitude Bins	Initial Catalogue	Final Catalogue
< 4.6	197	61
4.6 - 5.5	117	45
> 5.5	23	14
Total	**337**	**120**

5.3.2 Catalogue Completeness

Following de-clustering analysis, one final catalogue correction, namely catalogue completeness analysis was performed in order to ensure that the catalogue fits to the above given earthquake recurrence relation which is considered to represent true long-term relations (Stepp, 1973). This analysis was based on the research executed by Stepp (1973) where events with different magnitudes were analyzed in time bins in order to check that the catalogue, whether the catalogue is complete in small events for short period, and in large events for a long period of time or not. Stepp (1973) states that all earthquake catalogues are biased due to less dense deployment of seismograms and lack of settlement in the earlier earthquake records. Therefore, the de-clustered catalogue (having minimum and maximum event dates for 1905 and 2005, respectively) was checked for the distribution of magnitudes in time (Figure 29) and completeness proposed by Stepp (1973).
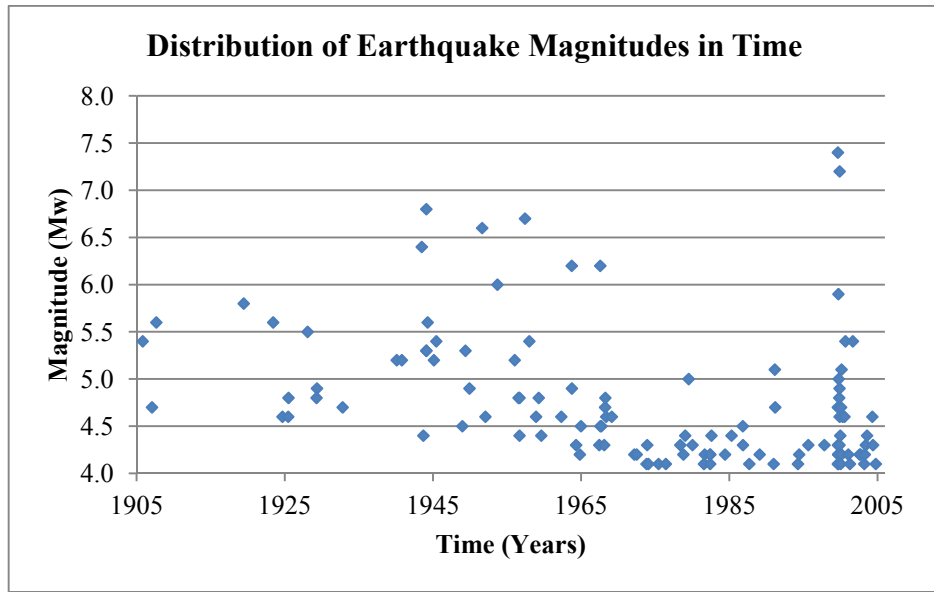
Figure 29. Distribution of earthquakes in time.

As can be seen from Figure 29, the catalogue is observed to be biased for small magnitude events having $M_w<4.6$ before 1964. This observation is also mentioned in the study of Atakan et al. (2002) where the records for the modern instrumental period were stated to have begun from 1964, and the same observation was also made by Kalkan et al. (2009).

In order to ensure this observation, the catalogue was divided into three magnitude bins (events; smaller than 4.6, between 4.6 and 5.5, and larger than 5.6) and 10 year time intervals. In accordance with the methodology proposed by Stepp (1973):

$$\lambda = \frac{1}{n} \sum_{i:1}^{n} k_i \qquad (7)$$

where, λ is recurrence, n is number of time intervals and k is the number of events. Thus, the variance is:

$$\sigma_\lambda^2 = \lambda/n \tag{8}$$

and as the unit time interval (*n*) is taken as one year, the following equation may be presented:

$$\sigma_\lambda = \sqrt{\lambda}/\sqrt{T} \tag{9}$$

where, σ_λ is the standard deviation and *T* is the sample length. Therefore, standard deviation is expected to behave as $1\sqrt{T}$, where mean rate recurrence of a magnitude class is constant in a time-bin within complete catalogue under the assumption of stationarity (Stepp, 1973; Gupta, 2002). Completeness plot was constructed under these assumption where σ_λ was plotted as a function of *T*.

Two scenarios where catalogue was taken to be complete for whole time span, and events with magnitudes <4.6 was taken as complete for only 41 years and the rest of the catalogue was taken as complete for whole time span (i.e., 100 years) (Figures 30 and 31, respectively).
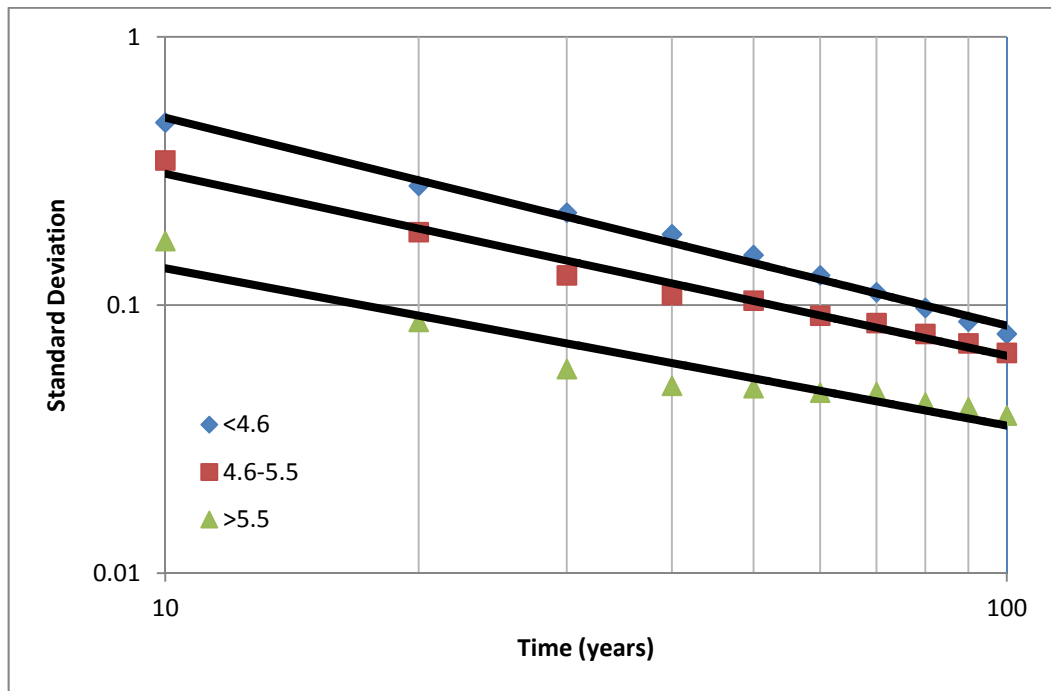
Figure 30. All magnitude bins complete for 100 years.

As can be seen from Figure 30, where all magnitude bins were considered complete for all catalogue interval, there is a distinct departure in the linearity for events having magnitudes smaller than 4.6. Therefore, the small magnitude events (M_w<4.6) were plotted in accordance with the previous observation that the catalogue can be divided into two main time intervals where 1964 is the boundary time. Thus small events were assumed to be complete for 41 years and intermediate (M_w between 4.6 and 5.5) and large (M_w>5.5) events were considered complete for all catalogue interval (i.e. 100 years) (Figure 31).

67
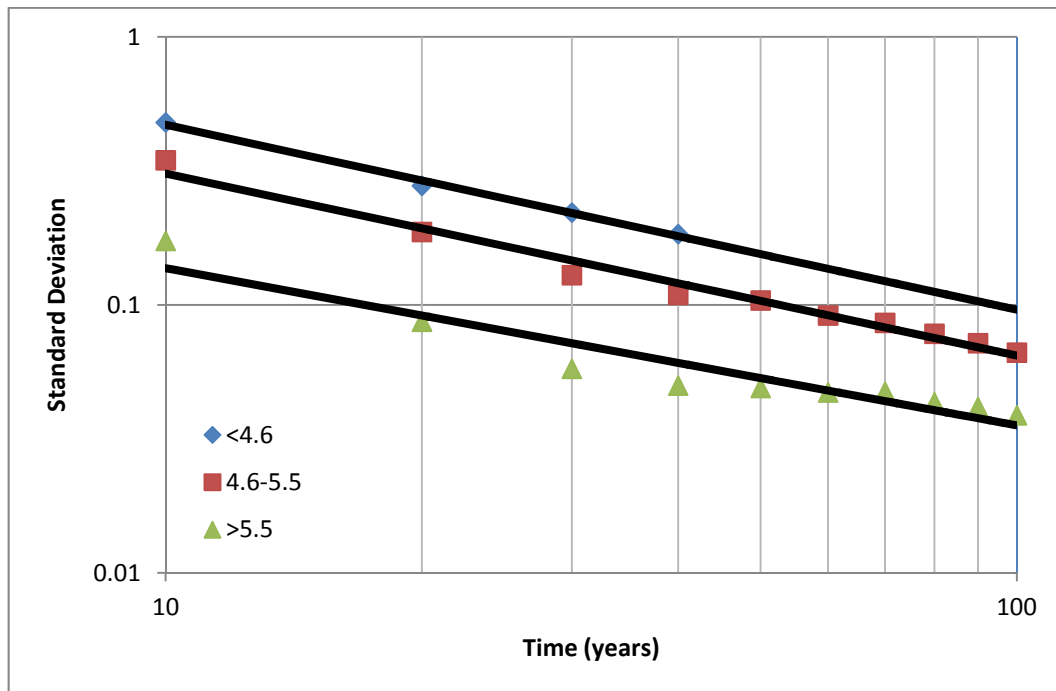
Figure 31. Magnitudes <4.6 complete for 41 years and remaining bins complete for 100 years.

As can be seen from Figure 31, the observation that small magnitude events are complete only for 41 years of time holds as the linearity of the magnitude bins are consistent within themselves. Thus the catalogue was investigated in accordance with these two time intervals for small, and intermediate and large events, namely 41 years and 100 years of completeness, respectively. Distribution of events for the three magnitude bins in 10 years of time intervals can be seen in Figure 32.
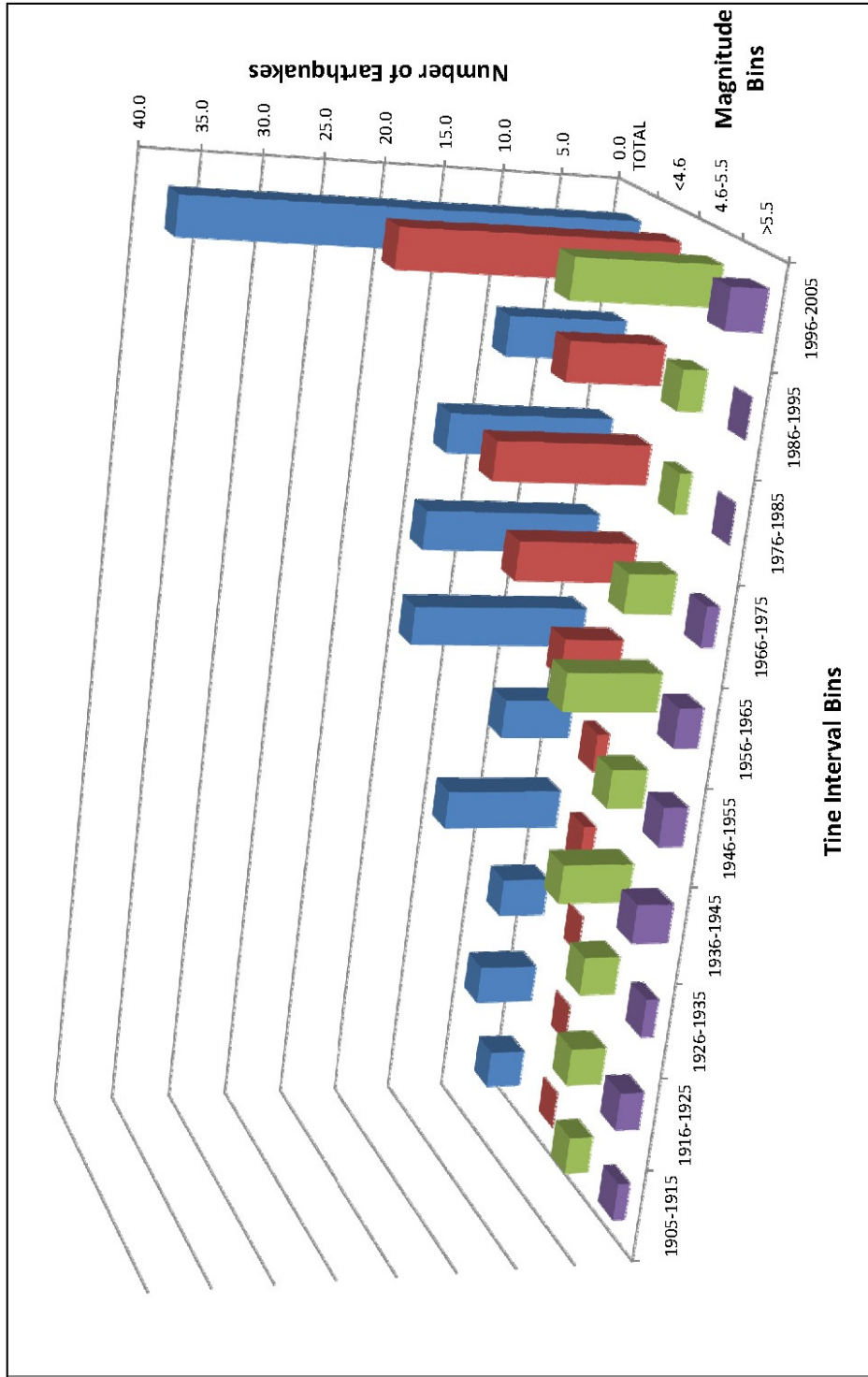
Figure 32. Distribution of events in 10 year bins according to three magnitude bins.

In light of these findings, the regression coefficients '*a*' and especially '*b*' were determined according to these final catalogue parameters (Figure 33).
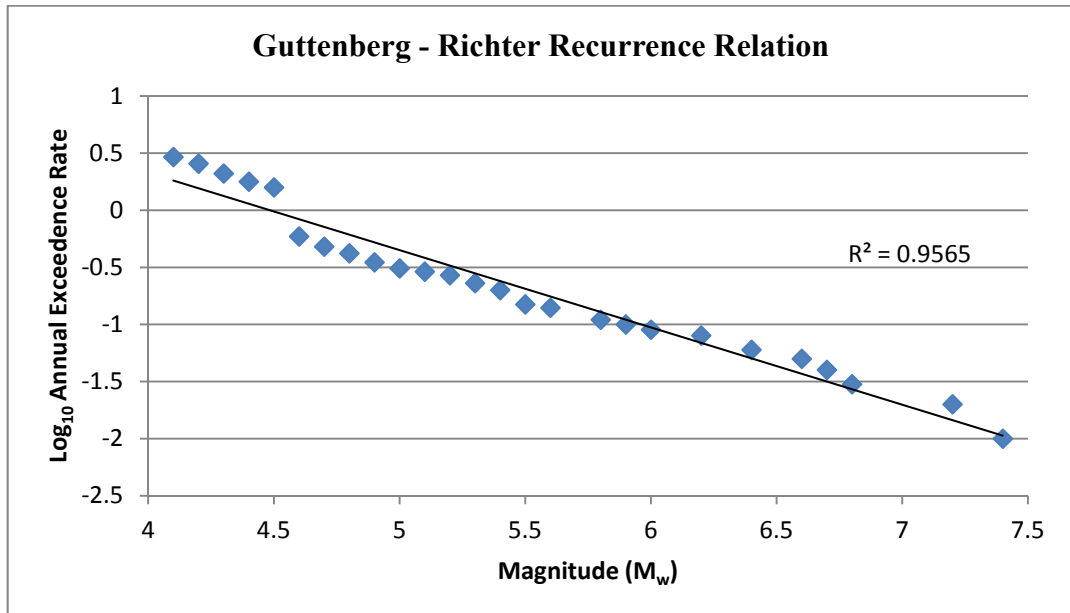
Figure 33. Guttenberg-Richter Parameters for $\log_{10}$ mean annual exceedance rate.

Therefore, the Guttenberg-Richter '*b*' value for $\log_{10}$ mean annual exceedance rate was acquired according to both least squares method and maximum likelihood method (Aki, 1965) as well, as given below for the entire region, i.e. individual *b* values for each seismic source was not considered as it was observed during declustering analysis that each large magnitude earthquake has an effect on individual seismic sources, therefore triggering different seismic sources.

Table 16. 'b' and 'β' values for the study area.

METHOD	*b* value	*β* value
Least Squares	0,6765	1.5577
Maximum Likelihood	0,7417	1.70783
Average	**0,7091**	**1.63276**

The average '*b*' value of 0.71 is compatible with the range of 0.9 ± 0.2 for shallow (>70 km) earthquakes proposed by Guttenberg and Richter (1949). Along with this general value, a comparison of the *b* value acquired in this study with the previous studies is presented in Table 17, and as can be seen, the *b*-value acquired in this study is highly compatible with the previous studies.

Along with this, if temporal threshold was to be taken as 1964 and only 80 post-1964 records were to be utilized, the equally weighted average 'b' value would have been 0.706, which is identical to the presently acquired 'b' value when rounded down to two decimal values. However, as historical seismicity of each pre-determined seismic source zone was to be evaluated via records from the earthquake catalogue, this temporal threshold approach was not considered in order to represent the historical seismicity of the zones more accurately in terms of pre-1964 events.

Table 17. b-values acquired in this study and previous studies.

Study	b value
Erdik et al. (2004)	0.8
Atakan et al. (2002)	1.00 – 1.12
Crowley and Bommer (2006).	0.69
Deniz (2006)	0.58 – 0.68
Kalkan et al. (2009)	0.72
This Study	**0.71**

5.4 Ground Motion Prediction Equations

In this study, four different Next Generation Attenuation (NGA) Ground Motion Prediction Equations (GMPEs) were utilized during probabilistic seismic hazard assessment, these are: Abrahamson and Silva (2008), Boore and Atkinson (2008), Campbell and Bozorgnia (2008), and Chiou and Youngs (2008) (from now on referred as AS08, BA08, CB08 and CY08, respectively) as all four of these GMPE's found applications for worldwide shallow crustal (<70 km) data and for Europe and Middle East (Stafford et al., 2008, Douglas, 2011). These four GMPE include earthquake and strong motion records of events from Turkey as well (Table 18).

Table 18. Number of strong motion record included in the GMPEs.

Earthquake	Year	Number of Strong Motion Records			
		A&S 2008	B&A 2008	C&B 2008	C&Y 2008
Izmir	1977	0	0	0	1
Dursunbey	1979	1	0	0	1
Erzincan	1992	1	0	1	1
Dinar	1995	2	4	2	2
Kocaeli	1999	17	26	22	17
Düzce	1999	13	22	14	12
Caldiran	1976	1	0	1	1
Total		**35**	**52**	**40**	**36**

The general form of the equation proposed by Abrahamson and Silva (2008) NGA GMPE is given in Equation 10. This attenuation relation is developed by considering worldwide shallow crustal movements.

$$\ln Sa(g) = f1(M, R_{rup}) + a_{12}F_{RV} + a_{13}F_{NM} + a_{15}F_{AS} + f_5(PGA_{1100}, V_{S30}) +$$
$$F_{HW}f_4(R_{jb}, R_{rup}, R_x, W, \delta, Z_{TOR}, M) + f_6(Z_{TOR}) + f_8(R_{rup}, M) + f_{10}(Z_{1.0}, V_{S30}) \qquad (10)$$

As can be observed in Equation 10, this equation is a function of distance to rupture (R_{rup}), Joyner-Boore distance (R_{jb}), minimum distance to fault (R_x), fault type, dip amount of the fault, hanging wall effect, distance to coseismic rupture, magnitude, fault width, layer thickness equal to 1000 m/s shear wave velocity ($Z_{1.0}$), soil effect (Vs_{30}), aftershock effect parameters. The standard deviation of the model is a function of magnitude, time and distance parameters.

The general form of the NGA GMPE proposed by Boore and Atkinson (2008) is given in Equation 11. This GMPE is also applicable for worldwide shallow crustal movements as was AS08.

$$\ln Y = F_M(M) + FD(R_{JB}, M) + FS(V_{S30}, R_{JB}, M) \tag{11}$$

As can be observed in Equation 11, this GMPE is a function of magnitude, V_{S30} (average shear wave velocity of the top 30 m), Joyner-Boore distance.

The general form of the NGA GMPE proposed by Campbell and Bozorgnia (2008) is given in Equation 12.

$$\ln Y = f_{mag} + f_{dis} + f_{flt} + f_{hng} + f_{site} + f_{sed} \tag{12}$$

As can be seen in Equation 12, the GMPE proposed by Campbell and Bozorgnia (2008) is a function of magnitude, distance, fault mechanism, site conditions and sediment thickness and "*explicitly includes the effects of magnitude saturation, magnitude-dependent attenuation, style of faulting, rupture depth, hanging-wall geometry, linear and nonlinear site response, 3-D basin response, and inter-event and intra-event variability*" (Campbell and Bozorgnia, 2008).

The final NGA GMPE considered in the probabilistic seismic hazard analysis is the one proposed by Chiou and Youngs (2008). The general form of the GMPE is given in Equation 13.

$$\ln(y) = \ln(y_{ref}) + \Phi_1 \min\left[\ln\left(\frac{V_{S30}}{1130}\right), 0\right]$$

$$+ \Phi_1\left\{e^{\Phi_3 \left[\min(V_{S30}, 1130) - 360\right]} - e^{\Phi_3 (1130 - 360)}\right\} ln\left(\frac{y_{ref}e^{\eta} + \Phi_4}{\Phi_4}\right)$$

$$+ \Phi_5\left\{1 - \frac{1}{cosh\left[\Phi_6 \max(Z_{1.0} - \Phi_7)\right]}\right\} \tag{13}$$

$$+ \frac{\Phi_8}{cosh\left[0.15 max(0, \ Z_{1.0} - 15\right]}$$

The magnitude and distance applicabilities of these four GMPE is summarized in Table 19. The comparison of these four GMPEs with the earthquake recorded at the Düzce Meteorology Station strong motion station (40.843 and 31.149 latitude and longitude, respectively) is presented in Figure 34.
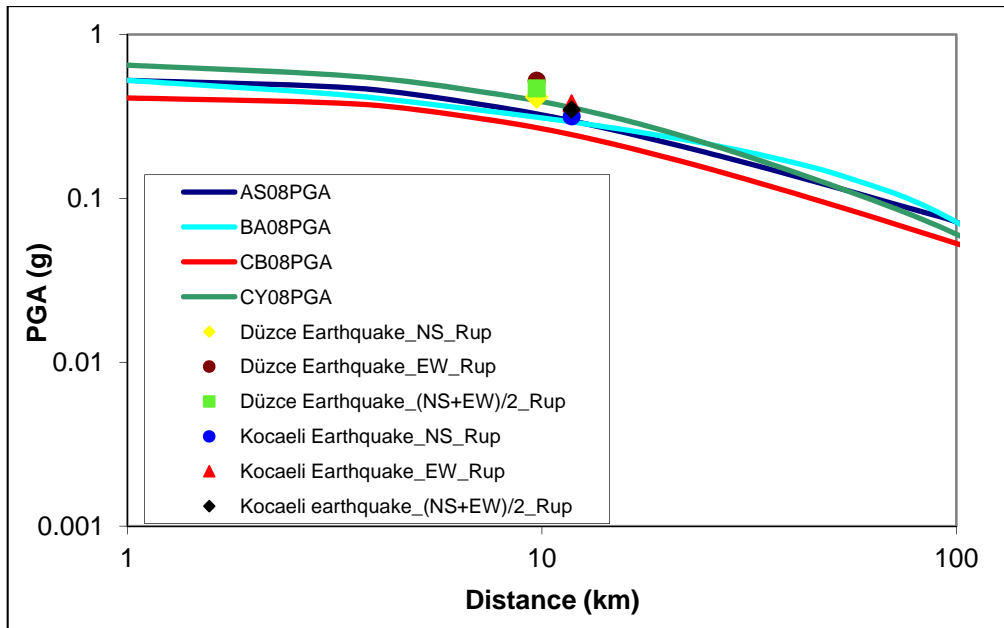
Figure 34. Comparison of earthquake records and GMPEs.

Table 19. Applicabilities of GMPEs.

GMPE	Area	M_{min}	M_{max}	M_{scale}	r_{min} (km)	r_{max} (km)	r_{scale}
Abrahamson and Silva (2008)	Worldwide – shallow crustal	4.27[1]	7.9	M_w	0.06	200	r_{rup}
Boore and Atkinson (2008)	Worldwide – shallow crustal	4.27	8	M_w	0.00	280	r_{jb}
Campbell and Bozorgnia (2008)	Worldwide – shallow crustal	4.27[1]	7.9	M_w	0.07	199.27	r_{rup}
Chiou and Youngs (2008)	Worldwide – shallow crustal	4.265[1]	7.9	M_w	0.2	70[2]	r_{rup}
[1] Can be extrapolated down to 4.0 (Douglas, 2011) [2] Can be extrapolated up to 200.0 km (Douglas, 2011)							

5.5 Seismic Source Model

As previously discussed, the study area is divided into seven seismic sources. In order to utilize these segments in the seismic hazard assessment, it is necessary to develop recurrence models via utilizing seismic energy (moment) balancing principle, determine characteristic magnitudes (see Chapter 4.2) and finally to develop segment-source-scenario relationship (see Chapter 5.5.1).

In order to develop recurrence models, it is necessary to calculate seismic moment accumulated on each fault segment, and seismic moment accumulated on each segment is calculated by utilizing the given equation given below (Aki, 1966):

$$M_0{}^T = \mu \ x \ A \ x \ D \tag{14}$$

where, $M_0{}^T$ is total seismic moment, μ is rigidity (dyne/cm^2), A is rupture area (km^2) and D is annual slip rate (mm). The rigidity value is taken as 3.0 x 10^{11} dyne/cm^2 (Youngs and Coppersmith, 1985; Ambraseys, 2002) and rupture areas have been presented previously. The moment released during an earthquake can be calculated by the equation:

$$log_{10} M_0 = cM_w + d \tag{15}$$

where, c is 1.5 and d is 16.05 according to theoretical considerations and empirical observations (Hanks and Kanamori, 1979).

In order to calculate recurrence relation for a given fault, number of earthquakes in a year having a certain magnitude, $N(m)$, should be determined. $N(m)$ can be defined as accumulated moment over probability density of moment release within desired magnitude interval, i.e.:

$$N(m) = \frac{M_0^T}{\int_{mmin}^{mmax} f(m).10^{M_0} dm} \tag{16}$$

where $f(m)$ is the previously described probability density function. Thus, recurrence can be calculated as:

$$\lambda = N(m) \int_{mmin}^{mmax} f(m).dm \tag{17}$$

As the assumption of Youngs and Coppersmith (1985) is adopted, where it is considered that certain fault and fault segments can produce a certain characteristic magnitude and therefore the probability density function is considered in two parts as first part (Eq. 18) is evaluated between minimum magnitude (M_0) and characteristic magnitude $(M_1) - \sigma$ (standard deviation), where $\sigma = 0.25$, and

second part (Eq. 19) is evaluated between characteristic magnitude (M.Char) $\pm$ σ (standard deviation). The characteristic magnitude and $\pm$ σ values for each individual fault were determined in Chapter 4.2.

$$f_1(m) = \frac{\beta.e^{[-\beta(M-M_O)]}.\left[\frac{1}{(1+c)}\right]}{1-e^{\{-\beta(M_1-\Delta m_2-M_O)]}} \qquad (18)$$

$$f_2(m) = \frac{\beta.e^{[-\beta(M_1-\Delta m_1-\Delta m_1-M_O)]}.\left[\frac{1}{(1+c)}\right]}{1-e^{\{-\beta(M_1-\Delta m_2-M_O)]}} \qquad (19)$$

where, c is defined as:

$$c = \frac{\beta.e^{[-\beta(M_1-\Delta m_1-\Delta m_1-M_O)]}.\Delta m_2}{1-e^{\{-\beta(M_1-\Delta m_2-M_O)]}} \qquad (20)$$

where, M_1 is characteristic magnitude (M_{max}) and M_0 is the minimum magnitude.

Therefore, probability distribution function for 7.0 characteristic magnitude can be represented as given by Figure 35.
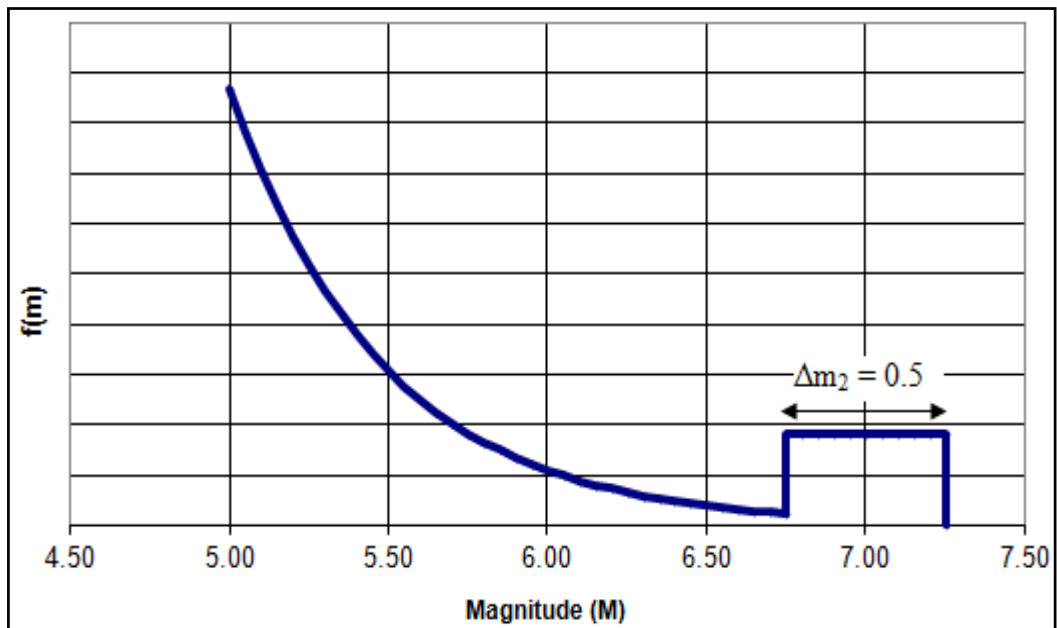
Figure 35. Magnitude probability density function based on Youngs and Coppersmith (1985) characteristic model.

Following the same steps described for the truncated exponential model for the two part probability density function of Youngs and Coppersmith (1985), the magnitude recurrence curve can be obtained as demonstrated by Figure 36.
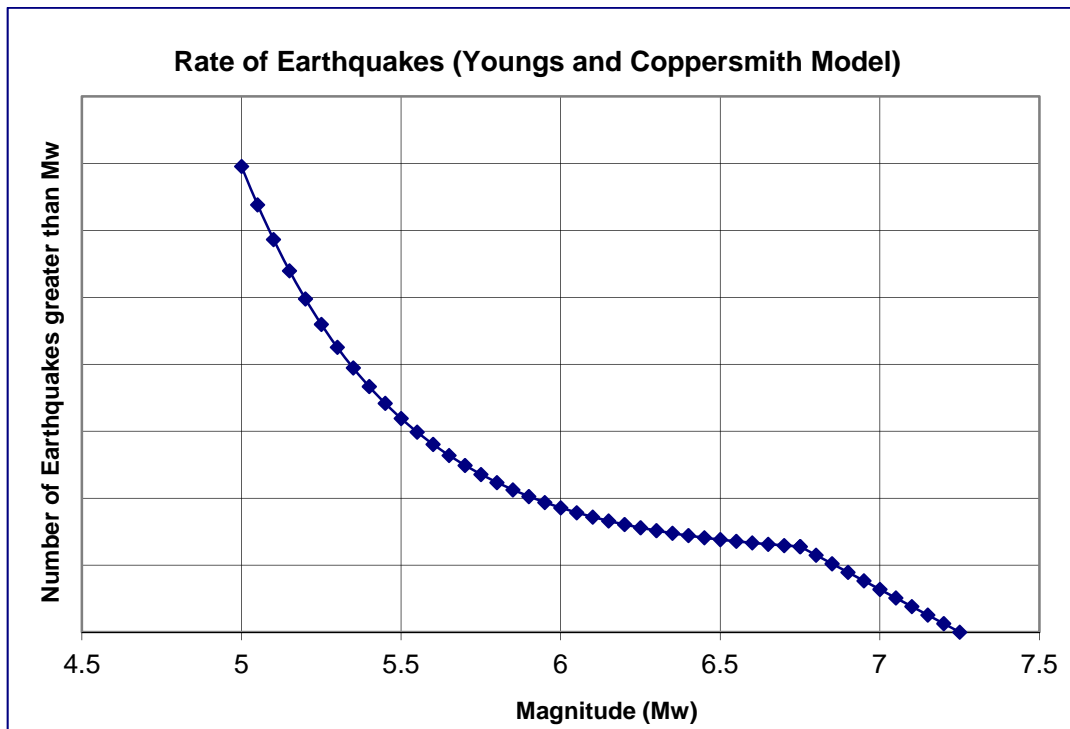
Figure 36. Recurrence relation based on Youngs and Coppersmith characteristic model.

By utilizing this model, both seismicity (first part) and geology (second part) could be represented (Youngs and Coppersmith, 1985). In order to allow a certain error margin for the scenario fitting process in the following section, the methodology proposed by Graf et al. (1966) and investigated by Weichert (1980) was employed where lower (μ_L) and upper (μ_L) bound confidence intervals can be calculated as given below:

$$\mu_L = \tfrac{1}{2}\chi^2 \alpha/2; f \qquad \text{where} \quad f = 2N$$

$$\mu_U = \tfrac{1}{2}\chi^2 1 - (\alpha/2); f \qquad \text{where} \quad f = 2(N+1)$$

(21)

where, *N* is the number of events, *α/2* is the confidence interval which is taken as ± *2σ* (i.e %5 and %95) for the error margin calculation. Considering the above given equations where confidence intervals are calculated, when the annual rate of an event is considered and also the annual rate of these confidence intervals are considered, the error margins can be calculated by extracting annual event rate from annual upper confidence for positive error and extracting lower confidence interval from annual event rate (see Table 20 for example events and error margins).

Table 20. Positive and negative errors for a 100 year catalogue for number of events between 1 and 10.

# of Events	μ_L	μ_U	Annual Event Rate	Annual Lower Confidence Interval	Annual Upper Confidence Interval	Positive Error	Negative Error
1	0.051	4.744	0.01	0.001	0.047	0.037	0.009
2	0.355	6.296	0.02	0.004	0.063	0.043	0.016
3	0.818	7.754	0.03	0.008	0.078	0.048	0.022
4	1.366	9.154	0.04	0.014	0.092	0.052	0.026
5	1.970	10.513	0.05	0.020	0.105	0.055	0.030
6	2.613	11.842	0.06	0.026	0.118	0.058	0.034
7	3.285	13.148	0.07	0.033	0.131	0.061	0.037
8	3.981	14.435	0.08	0.040	0.144	0.064	0.040
9	4.695	15.705	0.09	0.047	0.157	0.067	0.043
10	5.425	16.962	0.10	0.054	0.170	0.070	0.046

However, in order to determine the previously mentioned seismic moment accumulation (Eq. 14) it is necessary to identify slip rates as well, and although regional slip rate, i.e., slip rate in the study area varies between 16 – 25 mm/yr (strike slip) according to geologic data (McClusky et al., 2000; Reilinger et al., 2006) and 25 ± 5 mm/yr (strike slip) according to GPS data (Reilinger et al., 1997

and 2000; Straub et al., 1997; McClusky et al., 2000; Kahle et al., 1999 and 2000; Reilinger et al., 2006) (Figure 37), the slip rates of individual segments, i.e. sub-parallel segments, varies within themselves in order to acquire these total values. Therefore, in order to determine the slip rates of individual segments, the literature sources were utilized and the unknown slip rates were determined via assuming a 25 - 30 mm total slip and extracting known rates.
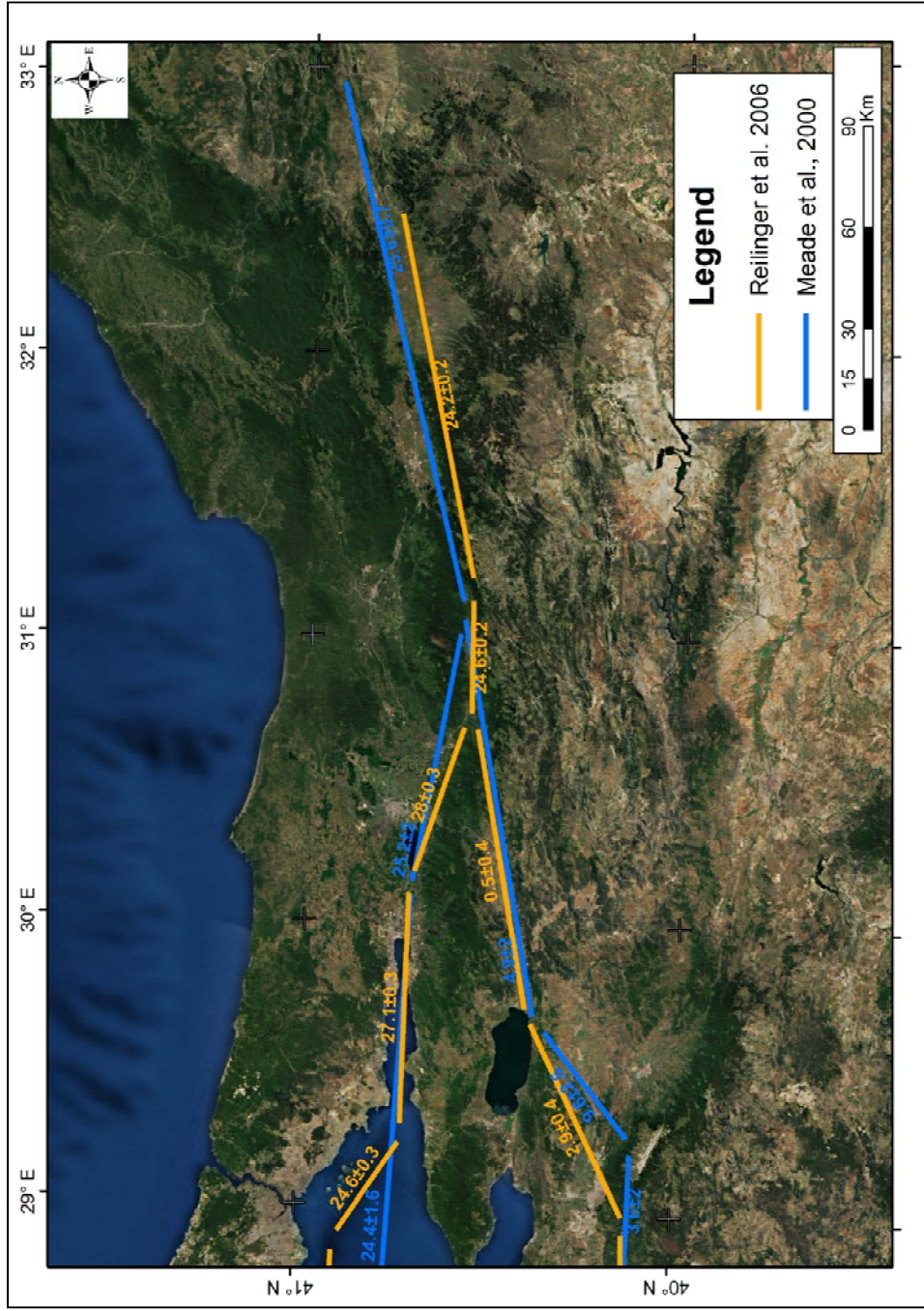
Figure 37. Slip Rates (mm/yr) (Reproduced from Meade et al., 2000 and Rilinger et al., 2006).

Two of the highly problematic areas were where Mudurnu-Abant, Kocaeli and Geyve-İznik seismic sources, and Mudurnu-Abant, Düzce and Hendek seismic sources run sub-parallel to each other (Figure 38, areas *a* and *b,* respectively).
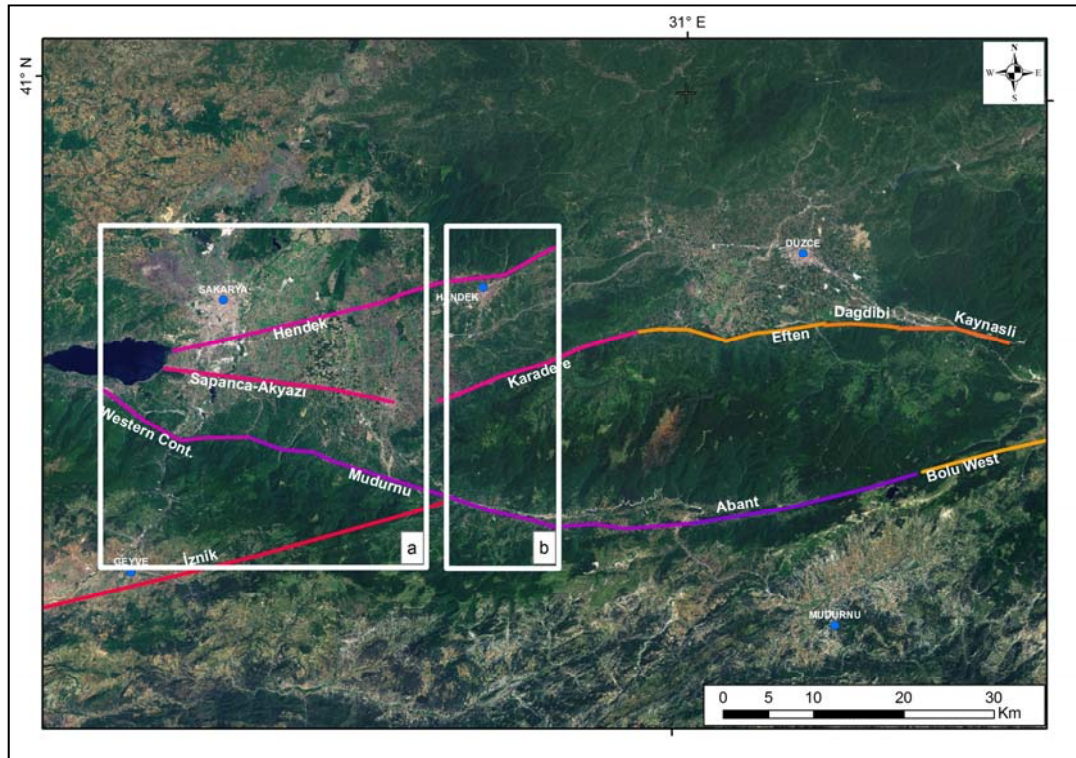
Figure 38. Parallel segments.

It is known that the slip rate at the Düzce segment is 10 mm/yr (Ayhan et al., 2000), on the other hand, slip rate of Bolu segments was taken as 20 mm/yr according to maximum total slip of 30 mm/yr and this value is also compatible with the 16.5 mm/yr (Koçyiğit et al., 2006; Ayhan and Koçyiğit, 2010), 24.2 mm/yr (Reilinger et al., 2006) and 25.6 mm/yr (Meade et al., 2000), 17 mm/yr (Kondo et al., 2005), 20 mm/yr (Okumura et al., 1993).

At area '*b*', for Mudurnu-Abant Source, 12 mm/yr, 14 mm/yr and 16 mm/yr slip rate values were used for western Continuation, Mudurnu and Abant Segments, respectively, which are both compatible with the slip rate values reported by McClusky et al. (2000) and also with the upper bound limit of 30 mm/yr. When Karadere and Sapanca-Akyazi segments and Hendek segment running parallel to these segments are considered, the model is developed in order to allow only one of these parallel faults to be ruptured at the same time as shall be described shortly in Chapter 5.6, therefore allowing to maintain upper slip rate limit and assigning the same (i.e. 13 mm/yr) slip rate to all of these segments.

When area '*a*' is considered; where İznik segment, western Continuation and Mudurnu Segments, Sapanca-Akyazı Segment and Hendek Segments run sub-parallel to each other, and as only either Sapanca-Akyazı or Hendek Segment shall allow to accumulate the 13 mm/yr slip rate as well as western Continuation and Mudurnu Segments have 12 and 14 mm/yr slip rate, respectively; therefore a slip rate of 3 mm/yr was assigned to İznik Segment of Geyve-İznik Seismic Source which also falls within the value range of 0.5 and 4.9 reported by Reilinger et al. (2006) and Meade et al. (2000), respectively.

The slip rates of the remaining western segments, namely – from east to west - İzmit-Lake Sapanca, Karamürsel-Gölcük, Hersek, Çınarcık Eastern and Çınarcık Western at the northern (main) segments and İznik, Geyve and Gemlik segments at south were assigned in accordance with the interpretation of both Reilinger et al. (2006) and Meade et al. (2000) where the slip rate of northern (main) branch decreases from east to west and slip rates at the southern branch increase in the same direction. Therefore, slip rates of Izmit-Lake Sapanca, Karamürsel-Gölcük and Hersek segments were assigned as 21 mm/year and slip rates of both Çınarcık source segments were assigned as 16 mm/yr, while slip rates for Geyve and Gemlik segments of Geyve-İznik Seismic Source was assigned as 6 mm/yr and 8

mm/yr, respectively. Thus both maintaining the upper bound limit as well as compatibility with the values reported by both Reilinger et al. (2006) and Meade et al. (2000). Slip rates of each segment and total slip rates at any north-south section is given in Figure 39. Note that 13 mm/yr slip rates of Hendek segment (orange circle), and Karadere and Sapanca-Akyazı segments (blue circle) were included in the N-S sections of total slip rates as a total slip rate of 13 mm/yr as these segments were not allowed to rupture simultaneously as explained in Chapter 5.6.
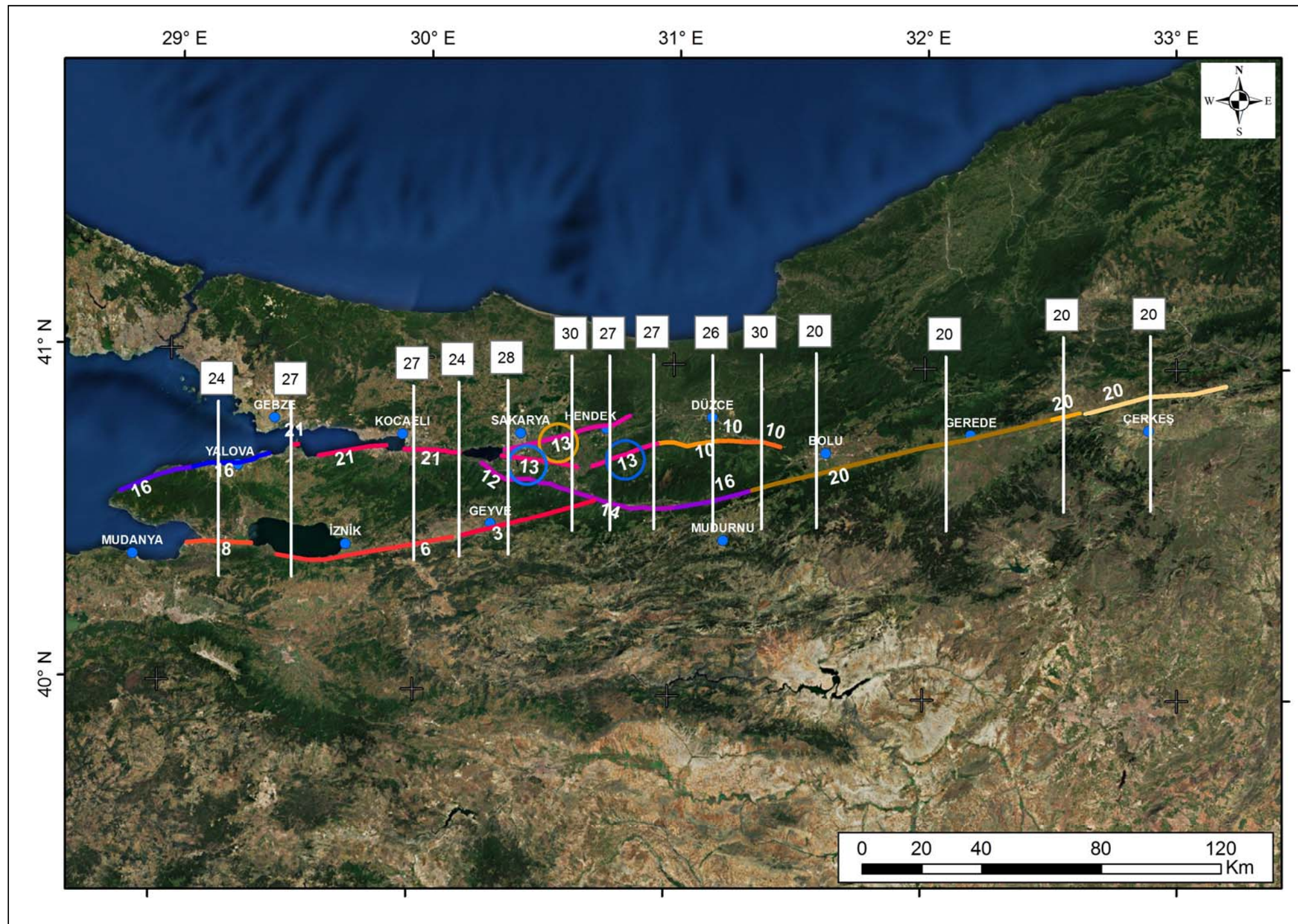
Figure 39. Individual slip rates of segments and total slip rates at N-S sections (slip rates in mm/yr).

Table 21. Slip rates of individual segments.

Source	Segment	Slip Rate (mm/yr)
Kocaeli Earthquake	Hersek	21
	Karamürsel - Gölcük	21
	Sapanca	21
	İzmit - Lake Sapanca	13
	Karadere	13
Düzce Earthquake	Eften	10
	Dağdibi	10
	Kaynaşlı	10
Mudurnu - Abant Earthquakes	Western Continuation	12
	Mudurnu Rupture	14
	Abant Rupture	16
Bolu Earthquake	Western	20
	Division	20
	Eastern	20
Hendek Fault	Hendek Fault	13
Geyve-İznik Fault	Gemlik	8
	İznik	6
	Geyve	3
Çınarcık Fault	Western	16
	Eastern	16

After identifying rupture width and slip rates of each segment, the segment, source and scenario relationship defined by USGS Workgroup on California Earthquake Probabilities San Francisco (SF Bay WG Report, 2003) (Figures 40 and 41, Tables 21 and 22).
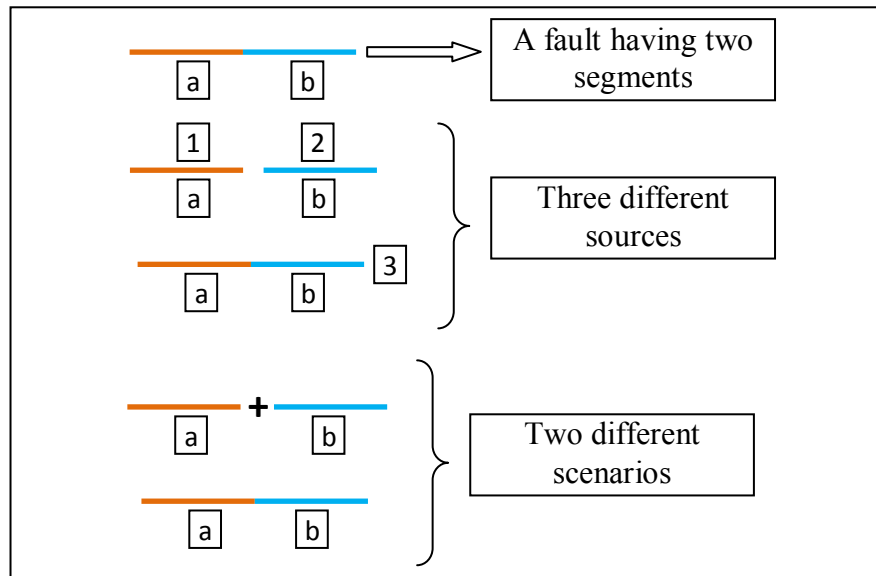
Figure 40. Example source and scenario model for a two segment fault.
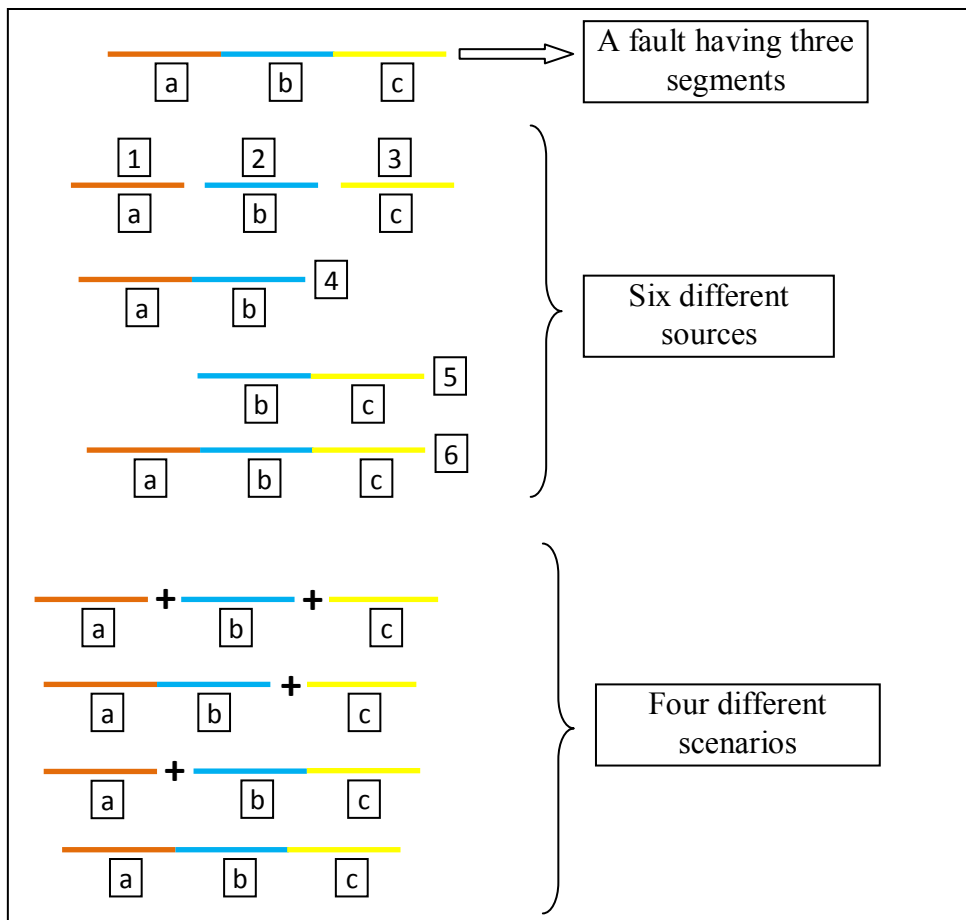
Figure 41. Example source and scenario model for a three segment fault.

Table 22. Example source and scenarios relationship for a two segment fault.

		Source		
		1	2	1+2
Scenario	1 , 2	1	1	0
	1+2	0	0	1

Table 23. Example source and scenarios relationship for a three segment fault.

		Source					
		1	2	3	1+2	2+3	1+2+3
Scenario	1 , 2 , 3	1	1	1	0	0	0
	1+2,3	0	0	1	1	0	0
	1,2+3	1	0	0	0	1	0
	1+2+3	0	0	0	0	0	1

Therefore, each different rupture scenarios regarding rupture of single segments as well as adjacent segments could be modeled. However, in order to incorporate different scenarios into the model, weights of these scenarios should be determined. In order to determine these weights, recurrence models of the seismic sources were developed based on previously discussed Youngs and Coppersmith characteristic model.

5.6 Segment, Source and Scenario Weights for Seismic Sources

As previously mentioned, there are six seismic sources in the final model with the inclusion of Hendek Fault source to the Kocaeli Earthquake seismic source. In order to determine the scenarios to be developed for each seismic source, it is necessary to develop a seismicity database for each seismic source via utilizing the

final catalogue having 120 events. However, before assigning epicenter data to each seismic segment, the issues regarding Kocaeli Seismic Source and Düzce Seismic Source noted above at section 4.2 should be addressed.

As observed in section 4.2, the rupture width of Düzce source was identified as 10 km from seismic data, however as this value is considered along with 41.25 km surface rupture length, the expected $M_w = 7.2$ value which is the magnitude of 12 November 1999 Düzce earthquake, cannot be acquired, i.e.:

$$3.98 + 1.02*\log (41.25*10) = 6.65 \qquad\qquad (22)$$

only 6.65, and with 1 and 2 standard deviation, only 6.88 and 7.11 magnitude values can be obtained. According to literature, the rupture length of this event is expected to reach up to 60 km at depth (Demirtaş et al., 2000) or for another 15 km towards east according to GPS and InSAR interpretation (Çakır et al., 2003). Therefore, as previously indicated, other than extending the rupture length, the rupture width value was modified to 30 km, therefore obtaining 7.13 and 7.36 magnitude values for characteristic and +1 standard deviation according to Wells and Coppersmith (1995) rupture area – magnitude relation.

Another issue previously noted is the surface rupture length of the Kocaeli event which is observed to be 92.41 km as a result of the lineament extraction analysis and comparison with literature. However, the length of the surface rupture is reported to reach up to 150 km (MTA, 2002b). When the continuation of segments under water east and west of Hersek segment, west – to İzmit Bay - and east – to Lake Sapanca – of İzmit-Lake Sapanca segment, and west – to Lake Sapanca – of Sapanca-Akyazi segment was also included in the model according to literature (Emre et al., 1998; Armijo et al., 2002; Barka et al., 2002; MTA, 2002b; Harris et al; 2002; Duman et al., 2005) the surface length of the seismic source reaches

131.8 km (Figure 41 and Table 24). Therefore, the source and scenario weights were identified according to these final values by utilizing seismicity of each source (Figure 42).

Table 24. Characteristic magnitude value of Kocaeli seismic source according to Wells and Coppersmith (1995) rupture area.

Source	Segment	Rupture Width (km)	Length (km)	Total Length (Km)	M.Char - 1σ	M. Char.	M.Char + 1σ
Kocaeli Earthquake	Hersek	18	24.03	131.78	7.19	**7.42**	7.65
	Karamürsel - Gölcük	18	22.88				
	Sapanca	18	33.13				
	İzmit - Lake Sapanca	18	28.69				
	Karadere	18	23.05				
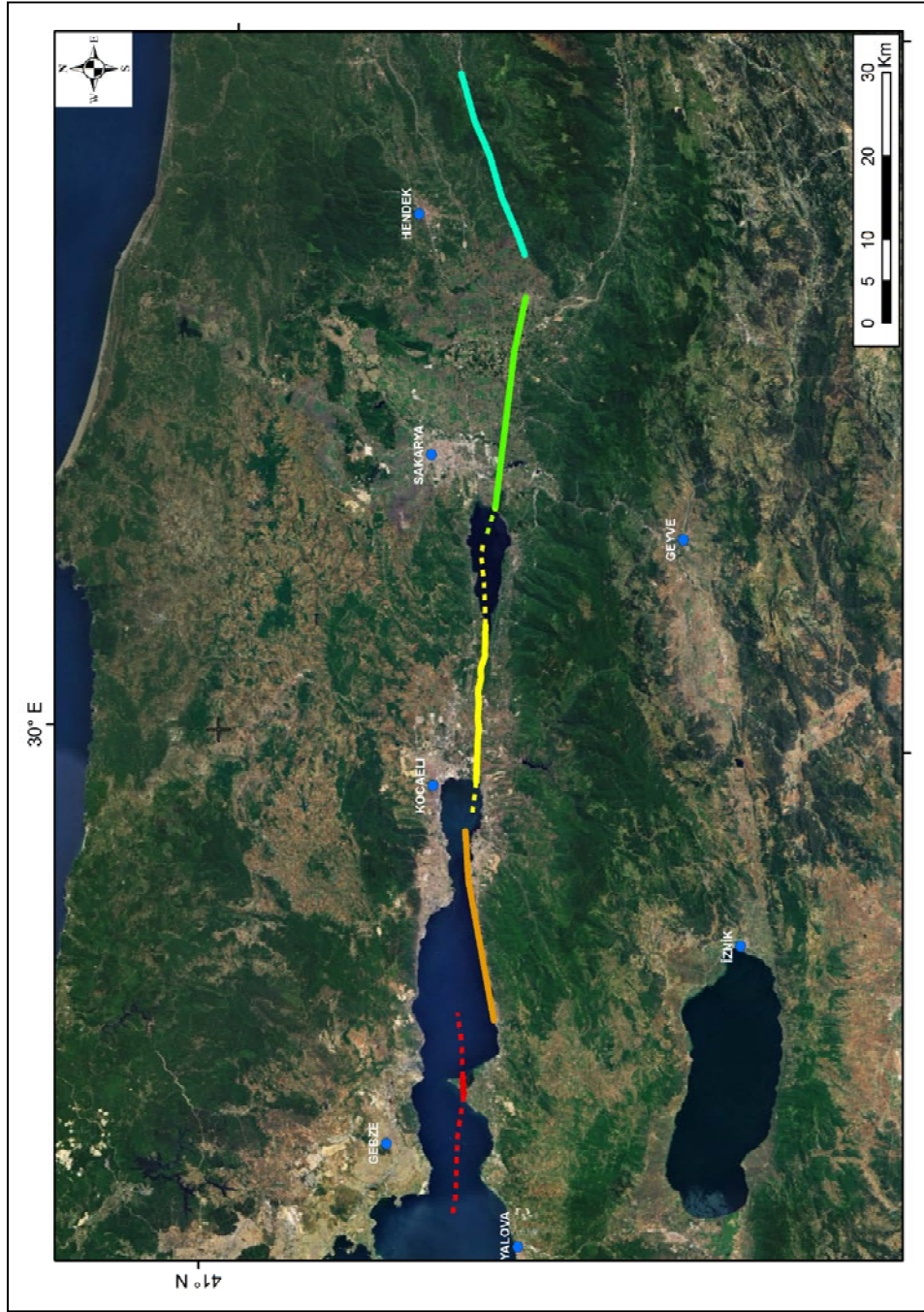
Figure 42. Kocaeli seismic source including offshore extensions.
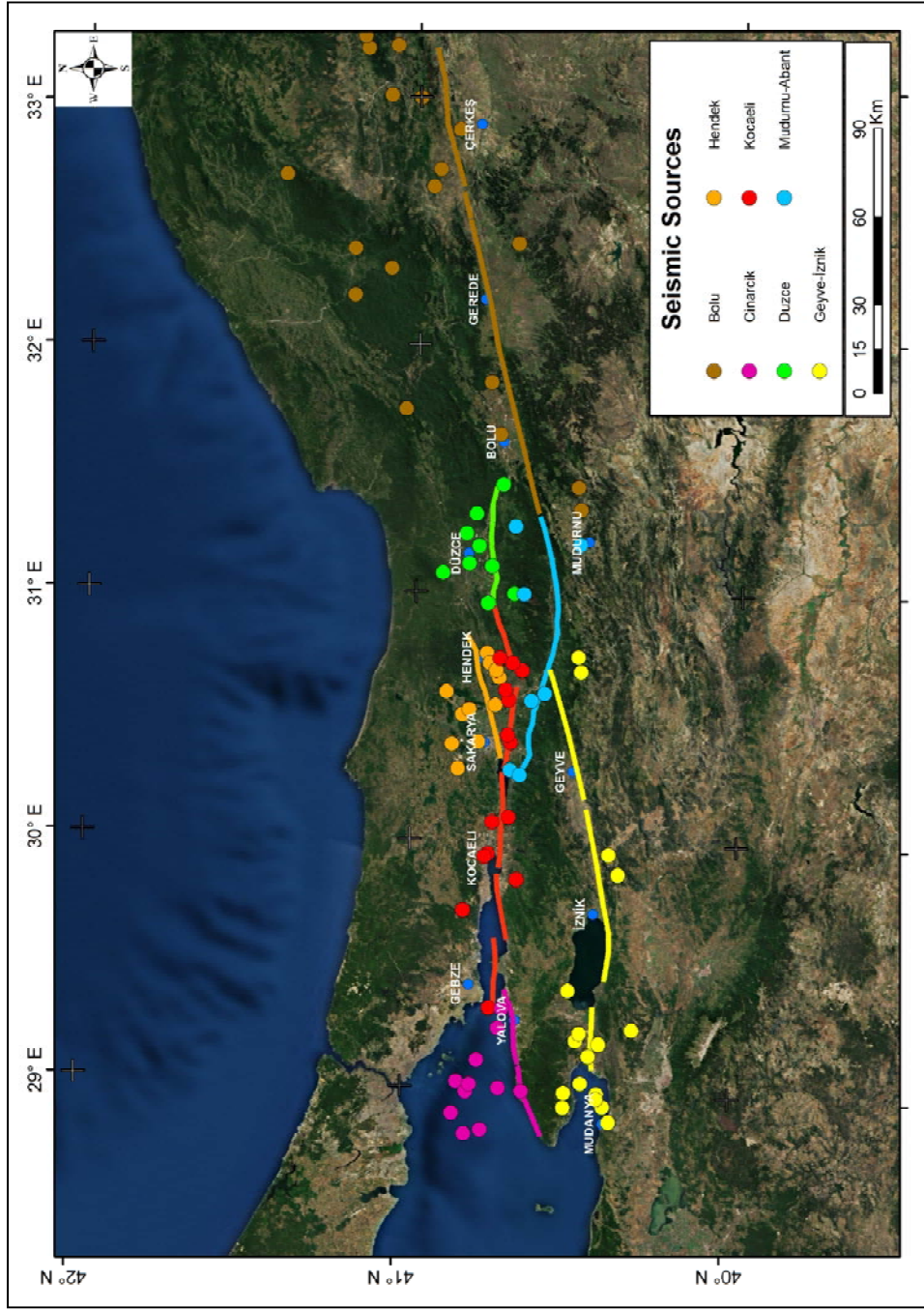
Figure 43. Seismicity of each seismic source.

5.6.1 Kocaeli Earthquake and Hendek Fault Seismic Source

As previously discussed, the seismic source of Kocaeli is joined with Hendek Fault as earthquake activity and surface rupture following August 17, 1999 earthquake was also observed at Hendek fault. 19 sources and 24 scenarios were prepared by considering these six segments (Table 25). In Table 25 '1' indicates that the source ruptured and '0' indicates that the source was not ruptured. A total of 29 events were used to generate the seismicity according to Youngs and Coppersmith (1984) characteristic model. In Table 25: "W1" is Hersek, "W2" is Karamürsel-Gölcük, "C" is İzmit-Lake Sapanca, "E1" is Sapanca-Akyazı, "E2" is Karadere and "H" is Hendek segments.

As can be seen from the source and scenario table below, easternmost two segments of the original Kocaeli source and Hendek fault was never allowed to be ruptured at the same time, therefore allowing propagation of an event starting from Lake Sapanca either to north (to Hendek Fault, grey highlighted cells at Table 25) or to south (Sapanca-Akyazı and Karadere) segments. As for weights, 59% was allocated for the main fault segmentation which also ruptured at the 1999 event and 41% percent was assigned to rupture scenarios with the inclusion of the Hendek fault, therefore maintaining the actual case as much as possible without disregarding the importance of a possibility of an event which may continue through north at the east of Lake Sapanca. The event where all segments may rupture at the same time (scenario numbers 16 and 24) were considered to have a higher weight in order to represent the behavior of the source zone which occurred in the August 1999 event. However, this led to the fact that the small magnitude events (M<4.5) cannot be represented as much as desired, yet this observation can be overlooked as events smaller than M=5.0 are usually not considered for probabilistic seismic hazard assessments (Abrahamson, 2010, unpublished notes on Haz43 code).

Table 25. Source and scenarios for the Kocaeli and Hendek seismic sources.

SCENARIO		W1	W2	C	E1	E2	W1+W2	W2+C	C+E1	E1+E2	W1+W2+C	W2+C+E1	C+E1+E2	W1+W2+C+E1	W2+C+E1+E2	W1+W2+C+E1+E2	H	C+H	W2+C+H	W1+W2+C+H	Weights	
	W1,W2,C,E1,E2	1	1	1	1	1	0	0	0	0	0	0	0	0	0	0	0	0	0	0	0.1	1
	W1+W2,C,E1,E2	0	0	1	1	1	1	0	0	0	0	0	0	0	0	0	0	0	0	0	0.01	2
	W1,W2+C,E1,E2	1	0	0	1	1	0	1	0	0	0	0	0	0	0	0	0	0	0	0	0.01	3
	W1,W2,C+E1,E2	1	1	0	0	1	0	0	1	0	0	0	0	0	0	0	0	0	0	0	0.01	4
	W1,W2,C,E1+E2	1	1	1	0	0	0	0	0	1	0	0	0	0	0	0	0	0	0	0	0.01	5
	W1+W2+C,E1,E2	0	0	0	1	1	0	0	0	0	1	0	0	0	0	0	0	0	0	0	0.01	6
	W1,W2+C+E1,E2	1	0	0	0	1	0	0	0	0	0	1	0	0	0	0	0	0	0	0	0.01	7
	W1,W2,C+E1+E2	1	1	0	0	0	0	0	0	0	0	0	1	0	0	0	0	0	0	0	0.01	8
	W1+W2+C+E1,E2	0	0	0	0	1	0	0	0	0	0	0	0	1	0	0	0	0	0	0	0.01	9
	W1,W2+C+E1+E2	1	0	0	0	0	0	0	0	0	0	0	0	0	1	0	0	0	0	0	0.01	10
	W1+W2,C+E1,E2	0	0	0	0	1	1	0	1	0	0	0	0	0	0	0	0	0	0	0	0.01	11
	W1,W2+C,E1+E2	1	0	0	0	0	0	1	0	1	0	0	0	0	0	0	0	0	0	0	0.01	12
	W1+W2,C+E1+E2	0	0	0	0	0	0	0	0	1	1	0	0	0	0	0	0	0	0	0	0.01	13
	W1+W2,C+E1+E2	0	0	0	0	0	1	0	0	0	0	0	1	0	0	0	0	0	0	0	0.01	14
	W1+W2,C,E1+E2	0	0	1	0	0	1	0	0	1	0	0	0	0	0	0	0	0	0	0	0.01	15
	W1+W2+C+E1+E2	0	0	0	0	0	0	0	0	0	0	0	0	0	0	1	0	0	0	0	0.35	16
	W1.W2.C.H	1	1	1	0	0	0	0	0	0	0	0	0	0	0	0	1	0	0	0	0.1	17
	W1+W2.C.H	0	0	1	0	0	1	0	0	0	0	0	0	0	0	0	1	0	0	0	0.01	18
	W1.W2+C.H	1	0	0	0	0	0	1	0	0	0	0	0	0	0	0	1	0	0	0	0.01	19
	W1.W2.C+H	1	1	0	0	0	0	0	0	0	0	0	0	0	0	0	0	1	0	0	0.01	20
	W1+W2+C.H	0	0	0	0	0	0	0	0	0	1	0	0	0	0	0	1	0	0	0	0.01	21
	W1.W2+C+H	1	0	0	0	0	0	0	0	0	0	0	0	0	0	0	0	0	1	0	0.01	22
	W1+W2.C+H	0	0	0	0	0	1	0	0	0	0	0	0	0	0	0	0	1	0	0	0.01	23
	W1+W2+C+H	0	0	0	0	0	0	0	0	0	0	0	0	0	0	0	0	0	0	1	0.25	24
	Source Number	1	2	3	4	5	6	7	8	9	10	11	12	13	14	15	16	17	18	19		
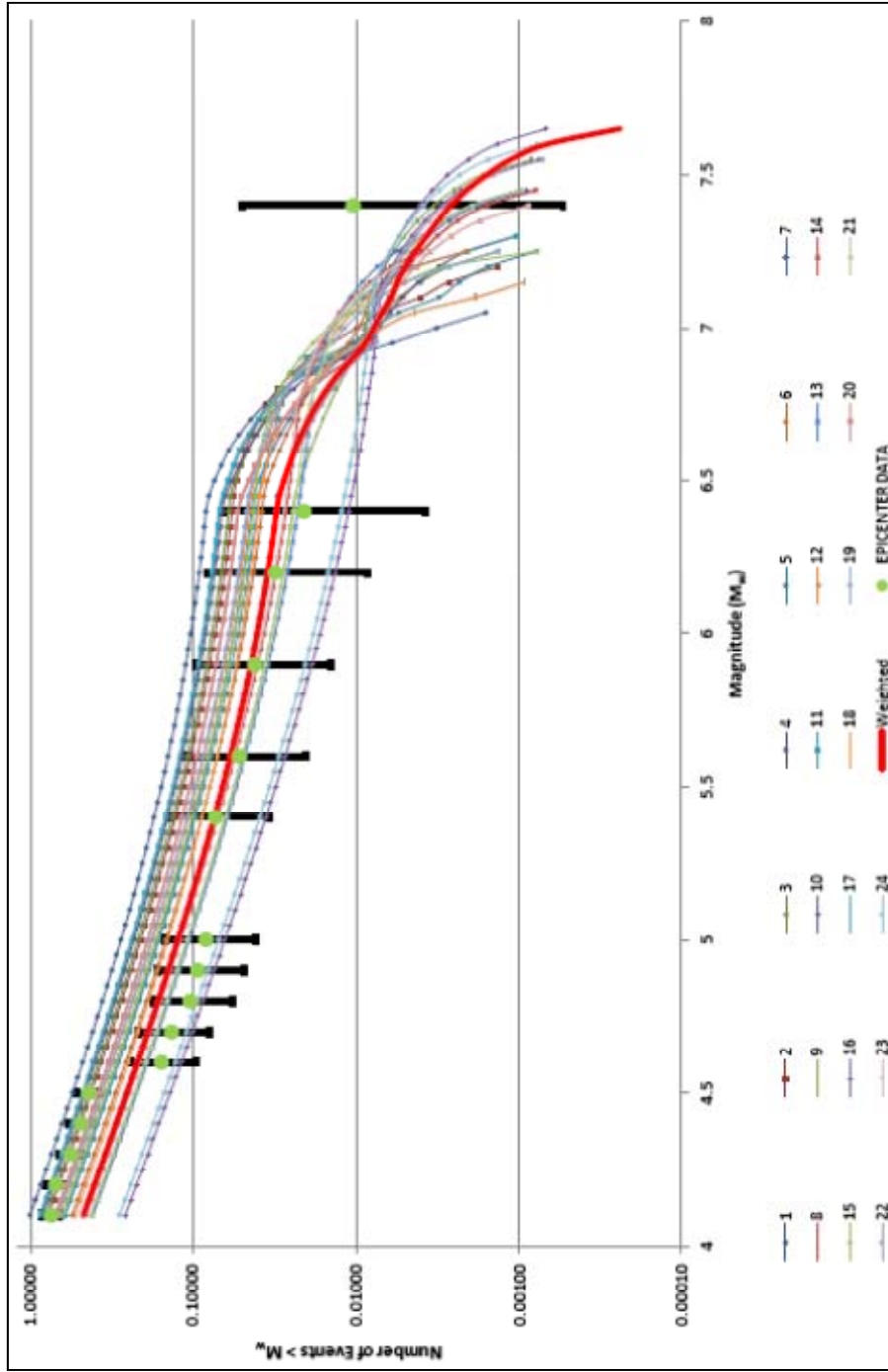
Figure 44. Weighted scenarios for the Kocaeli-Hendek seismic source.

5.6.2 Düzce Earthquake Seismic Source

This seismic source was investigated as three segments as previously indicated in section 4.2.1. The source and scenario relationship as well as weights of each scenario can be seen in Table 26, and fit of the weighted scenario can be observed in Figure 45. In Table 26; "W" is Eften, "C" is Dağdibi and "E" is Kaynaşlı segments. The case that all three segments rupture at the same time have the highest weight (%50) as this was the case for the November 12, 1999 Düzce earthquake. A total of 11 events were used to characterize this seismic source.

5.6.3 1957 Abant and 1967 Mudurnu Earthquakes Seismic Source

For this seismic source, a total of 9 events were considered while developing characteristic model curves (Figure 46) and weights were assigned rather equally (Table 27) as no recorded event in the 100 year catalogue has ruptured all three segments, but as there is a close relationship with the Mudurnu and Abant segments as previously discussed, the weight scenario where all three segments rupture at the same time was kept the highest. In Table 27, "W" is western Continuation, "C" is Mudurnu and "E" is Abant segments.

Table 26. Scenarios, sources and scenario weights for the Düzce seismic source.

		Source						
		W	*C*	*E*	*W+C*	*C+E*	*W+C+E*	*Weights*
Scenario	**W , C , E**	1	1	1	0	0	0	0.3
	W+C,E	0	0	1	1	0	0	0.1
	W,C+E	1	0	0	0	1	0	0.1
	W+C+E	0	0	0	0	0	1	0.5

Figure 45. Weighted scenarios for the Düzce seismic source.

Table 27. Scenarios, sources and scenario weights for the Mudurnu-Abant seismic source.

		Source						
		W	*C*	*E*	*W+C*	*C+E*	*W+C+E*	*Weights*
Scenario	**W , C , E**	1	1	1	0	0	0	0.3
	W+C,E	0	0	1	1	0	0	0.15
	W,C+E	1	0	0	0	1	0	0.15
	W+C+E	0	0	0	0	0	1	0.4

Figure 46. Weighted scenarios for the Mudurnu-Abant seismic source.

5.6.4 Bolu-Gerede Earthquake Seismic Source

The Bolu-Gerede seismic source was included in the model with three segments as previously discussed in accordance with the segmentation proposed by Barka and Kadinsky-Cade (1988) in section 4.1.4. The weights of scenarios was assigned by considering this February 1, 1944 event and the highest weight was assigned to the scenario where all three segment rupture at the same event (Table 28). In Table 28; "W" is the Bolu West, "C" is the Bolu Divide and "E" is the Bolu East segments. A total of 18 events were utilized while fitting the scenarios to the characteristic model.

5.6.5 Geyve-İznik Seismic Source

The Geyve-İznik seismic source is the most problematic as curve fitting to the characteristic model is considered due to its low seismicity (having events only up to 4.8) in spite of its long surface trace (127.1 km), therefore causing hard to represent low magnitude events, and although the weight of the scenario where each segment rupturing separately is kept the highest (60%) and the scenario where all three segments rupture simultaneously is kept the lowest (10%), the weighted model fails to represent the magnitudes 4.3 and 4.2 (Figure 48 and Table 29). This case is actually expected as the slip rate of the source is low (between 3 and 8 mm/yr) and this area is considered to be a relatively seismic quiescence (Tsukuda et al., 1988; Barka, 1997).

Total of 18 events with magnitudes between 4.1 and 4.8 was utilized in source characterization of this seismic source. In Table 29, "W" is the Gemlik, "C" is the İznik-Mekece and "E" is the Geyve segments.

Table 28. Scenarios, sources and scenario weights for the Bolu seismic source.

		Source						
		W	*C*	*E*	*W+C*	*C+E*	*W+C+E*	*Weights*
Scenario	**W , C , E**	1	1	1	0	0	0	0.2
	W+C,E	0	0	1	1	0	0	0.1
	W,C+E	1	0	0	0	1	0	0.1
	W+C+E	0	0	0	0	0	1	0.6
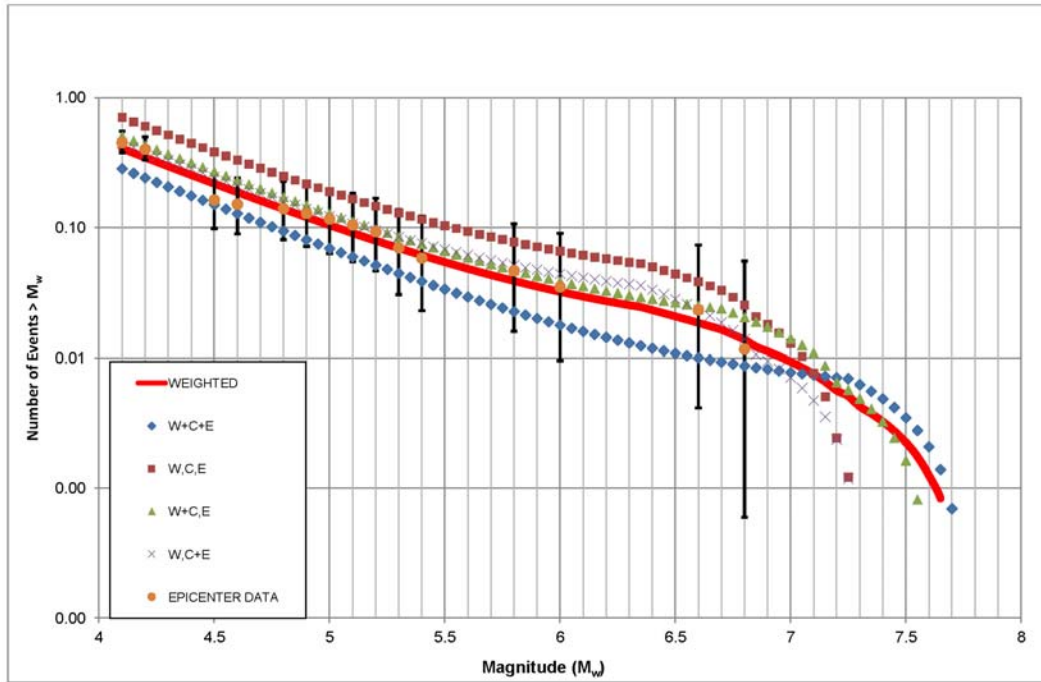
Figure 47. Weighted scenarios for the Bolu seismic source.

Table 29. Scenarios, sources and scenario weights for the Geyve-İznik seismic source.

		Source						
		W	*C*	*E*	*W+C*	*C+E*	*W+C+E*	*Weights*
Scenario	**W , C , E**	1	1	1	0	0	0	0.6
	W+C,E	0	0	1	1	0	0	0.15
	W,C+E	1	0	0	0	1	0	0.15
	W+C+E	0	0	0	0	0	1	0.1

103
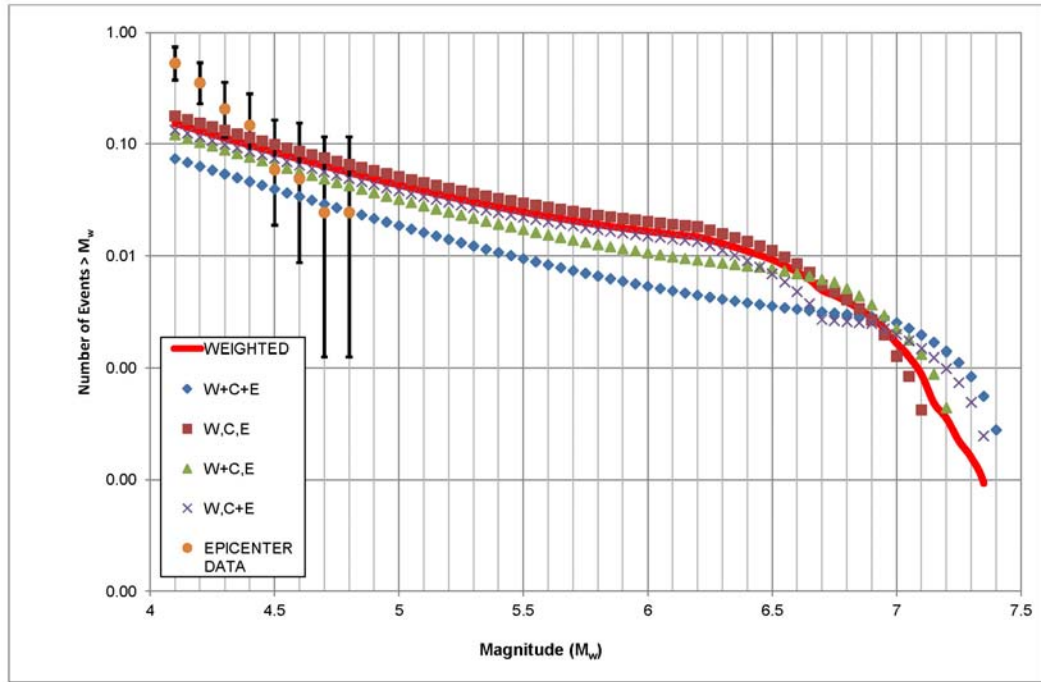
Figure 48. Weighted scenarios for the Geyve-İznik seismic source.

5.6.6 Çınarcık Fault Seismic Source

This seismic source was investigated as two segments as previously discussed and a total of 10 events were utilized in the development of characteristic seismicity model. Weights of each scenario were assigned equally (Table 30) and as can be seen from scenario fitting (Figure 49), the source represents the seismicity both in small and large magnitude events.

Table 30. Scenarios, sources and scenario weights for the Çınarcık seismic source.

		Source			
		W	E	W+E	Weights
Scenario	W , E	1	1	0	0.5
	W+E	0	0	1	0.5
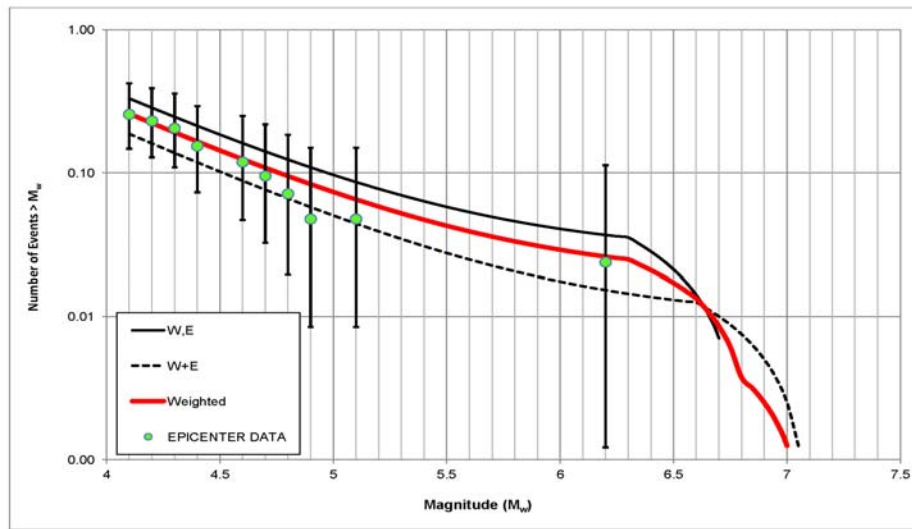
Figure 49. Weighted scenarios for the Çınarcık seismic source.

5.7 Analysis

As previously discussed, probabilistic seismic hazard assessment (PSHA) was performed according to the final source model based on weight determined by utilizing Youngs and Coppersmith (1985) characteristic model and by utilizing the four ground motion prediction equations (GMPEs). Three different standard deviation values, 0, 1 and 3, were used for GMPEs in order to observe the behavior depending on standard deviation. These parameters were incorporated

into Haz43 computer code developed by Norman Abrahamson as an upgrade to Haz38 (Abrahamson, 2006, unpublished) which is validated by Pacific Earthquake Engineering Research (PEER) Center (Thomas et al., 2010). The code computes seismic hazard by utilizing the methodology for probabilistic seismic hazard assessment developed by Cornell (1968), McGuire (1976 and 1978), and with the fundamental assumption that earthquakes within a given source zone is completely random in terms of spatial location and these events occur independently in time which means the events occur as a Poisson process (Shannon and Wilson, Inc., 2009).

The hazard code was run for Düzce Province center having 31.16N 40.84E coordinates with different surface wave velocity values of upper 30 m (Vs_{30}) for soil (360) and rock (760) conditions corresponding to thresholds between site classes D and C, and C and B according to International Code Council, respectively, while roughly corresponding to Z2 and Z4 site classes according to Turkish Seismic Code (2007). All calculations were executed for 10% probability of exceedance for 50 years for peak ground acceleration (PGA) g values, therefore with a return period of 475 years. The result of the analyses will be given and discussed in the following chapter.

CHAPTER 6

RESULTS AND DISCUSSION

6.1   50 Year Total Hazard Curves for Two Vs_{30} Values

Initially, hazard curves in accordance with the previously stated two Vs_{30} values (360 m/s Vs_{30} threshold boundary in between D- (Stiff soil) and C-Sites (Very dense soil and soft rock), and 760 m/s - Vs_{30} threshold boundary in between C- (Very dense soil and soft rock) and B-Sites (Rock); International Code Council, ICC 2006) were generated for the aforementioned four GMPE at each three standard deviation value (0, 1 and 3). Therefore the interpretation on influence of GMPEs and their standard deviation values were investigated. The minimum distance of the analysis point (Düzce city center) to a segment in the analysis is 7.8 km and the maximum distance is 175.5 km (Table 31).

As 50 year exceedance curves are investigated for threshold boundary in between C and B-Sites (Vs_{30}=760 m/s; Figures 50-52) it was observed that Abrahamson and Silva (2008) (henceforth stated as AS08) relationship gives the highest results in all three standard deviation values while Campbell and Bozorgnia (2008) (henceforth stated as CB08) gives the smallest values. In other words, the relationships can be ranked from smallest to largest as Campbell and Bozorgnia (2008), Boore and Atkinson (2008) (henceforth stated as BA08), Chiou and Youngs (2008) (henceforth stated as CY08) and finally Abrahamson and Silva (2008) (Table 32).

The same observation can also be made for the threshold boundary in between D- and C-Sites, (Vs_{30}=360 m/s). However, AS08 and CY08 relationships have more similar value throughout the curves, and CY08 values exceeds AS08 values at a certain point for 3 standard deviation chart (at around 0.8g vs. 6.3% probability of exceedance point). Yet, this knick point is beyond the 10% probability of exceedance value being sought in this study; therefore no further consideration was given regarding this change in trend between these two GMPEs.

Table 31. Minimum rupture distances of segments to the Düzce city center.

Seismic Source	Segment	Distance to Site (km)
Kocaeli	Hersek	135.1
	Karamürsel-Gölcük	109.9
	İzmit-Lake Sapanca	75.6
	Sapanca-Akyazı	48.6
	Karadere	21
	Hendek	28
Düzce	Eften	7.8
	Dağdibi	8
	Kaynaşlı	13.5
Mudurnu-Abant	Western Cont.	65
	Mudurnu	32.4
	Abant	26.6
Bolu	Bolu West	27.3
	Bolu Divide	113.7
	Bolu East	124.7
Geyve-İznik	Gemlik	160.5
	İznik	96.5
	Geyve	48.8
Çınarcık	Çınarcık West	175.5
	Çınarcık East	149.2
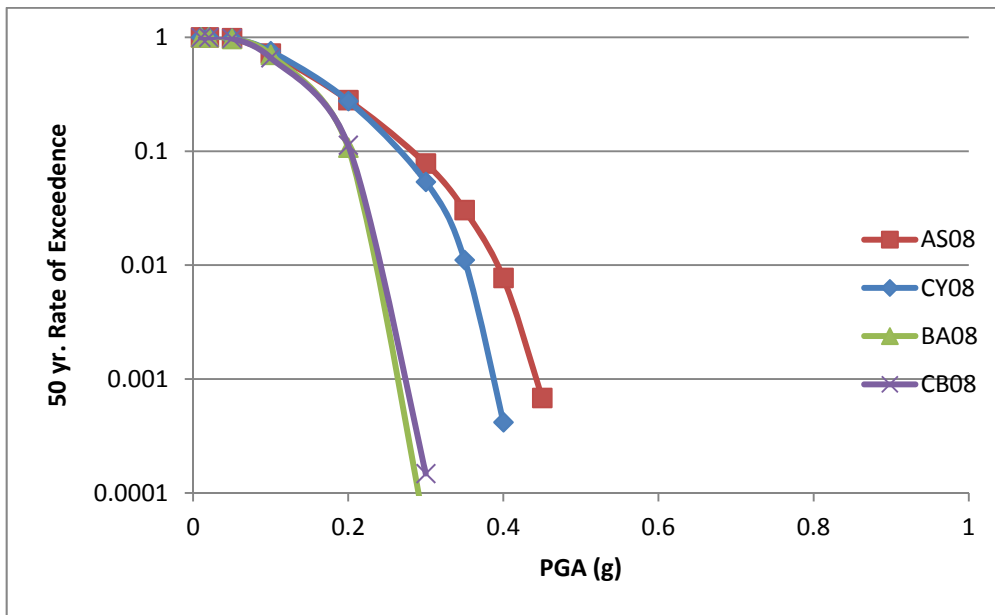
Figure 50. 50 year Rate of exceedence curves for $Vs_{30}=360$ m/s and 0 standard deviation.
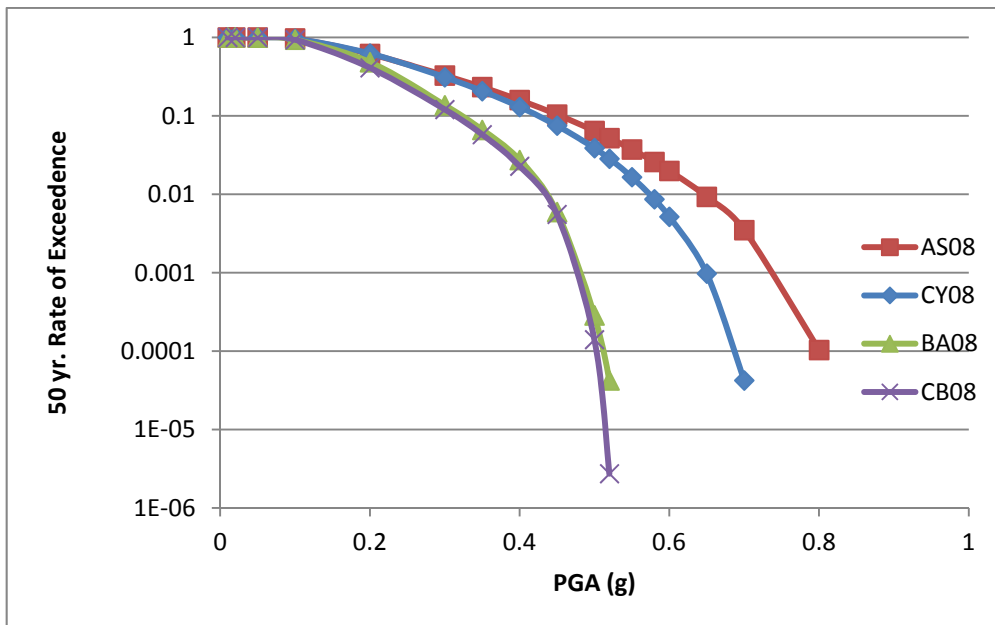
Figure 51. 50 year rate of exceedence curves for $Vs_{30}=360$ m/s and 1 standard deviation.
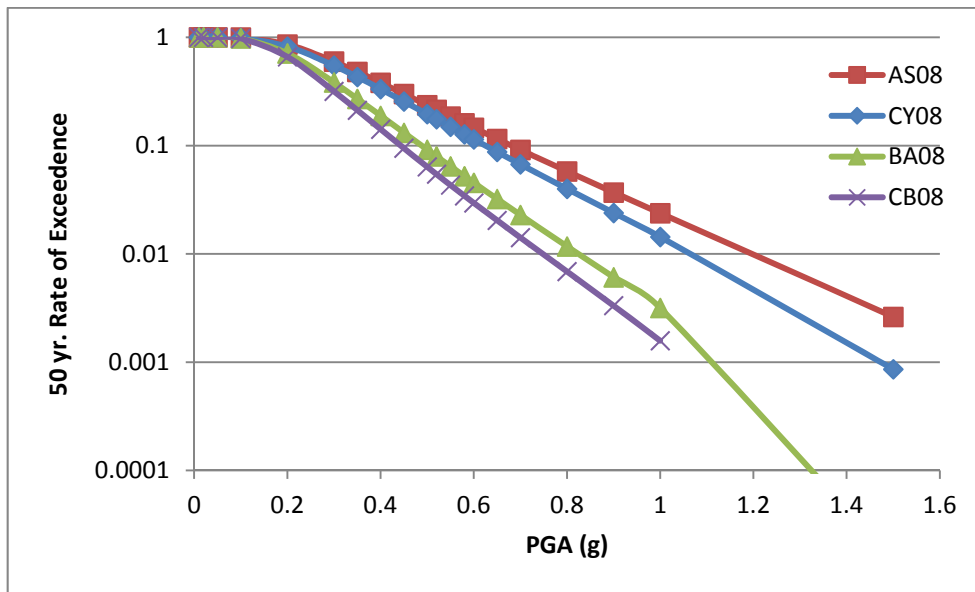
Figure 52. 50 year rate of exceedence curves for Vs_{30}=360 m/s and 3 standard deviation.
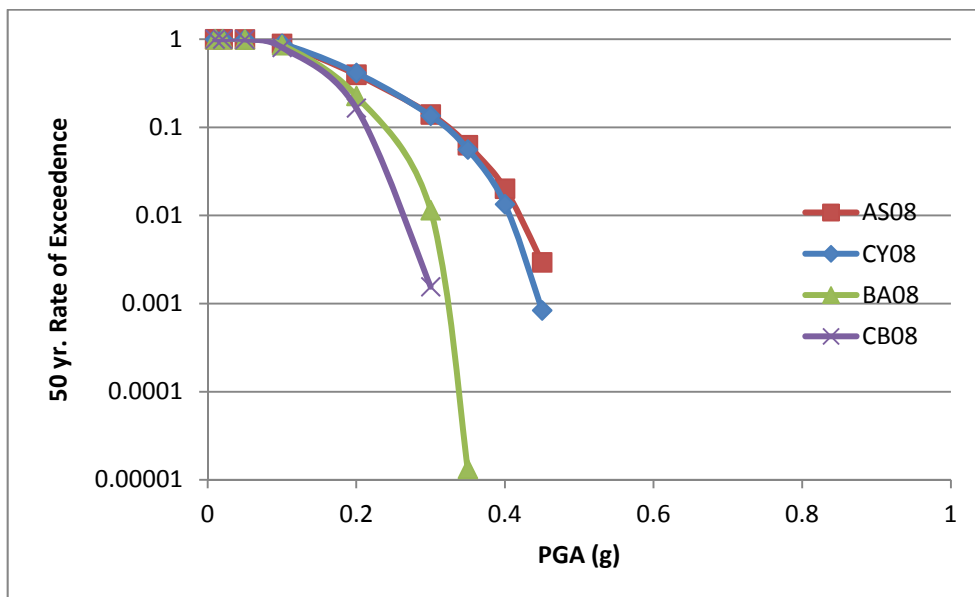
Figure 53. 50 year rate of exceedence curves for Vs_{30}=760 m/s and 0 standard deviation.
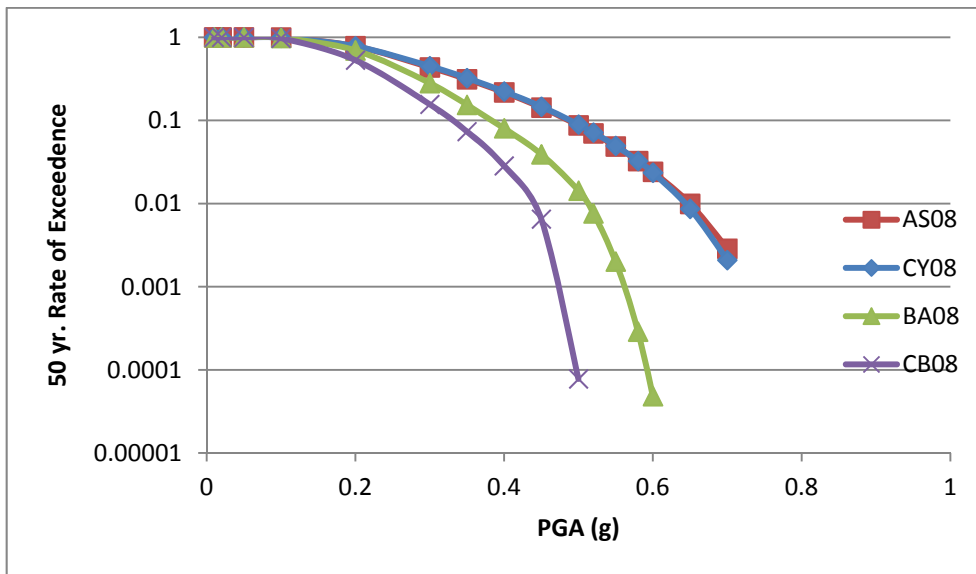
Figure 54. 50 year rate of exceedence curves for Vs_{30}=760 m/s and 1 standard deviation.
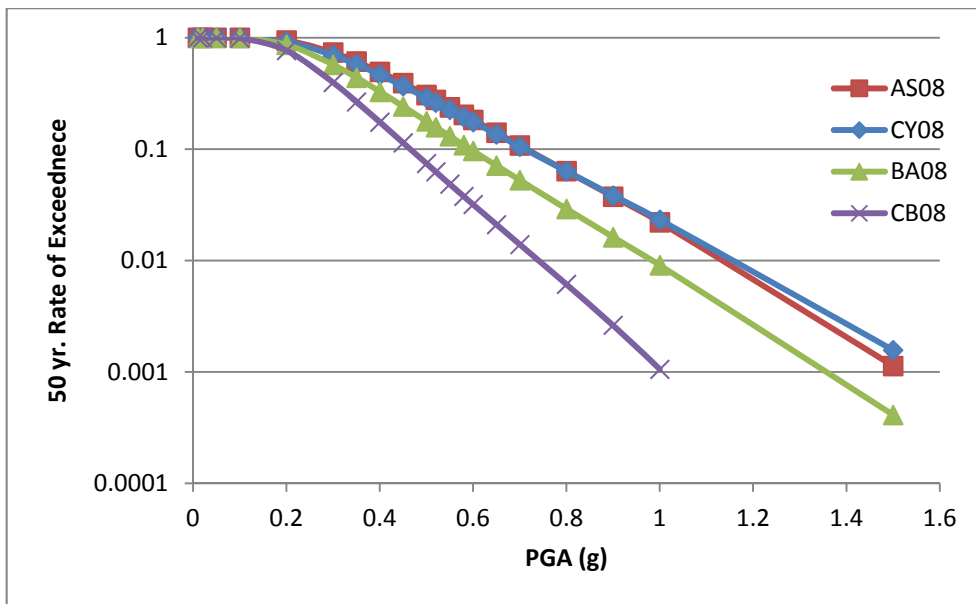
Figure 55. 50 yr rate of exceedence curves for Vs_{30}=760 m/s and 3 standard deviation.

Table 32. Result of analyses in terms of 10% probability of exceedance in 50 years for each GMPE and each standard deviation (std) value.

	CB08	BA08	CY08	AS08	Average
360-0 std.	0.212	0.237	0.319	0.323	**0.273**
360-1 std.	0.33	0.383	0.489	0.487	**0.422**
360-3 std.	0.464	0.593	0.71	0.716	**0.621**
760-0 std.	0.2	0.202	0.267	0.283	**0.238**
760-1 std.	0.313	0.322	0.425	0.455	**0.379**
760-3 std.	0.443	0.489	0.625	0.687	**0.561**

As the above acquired values are compared with the actual strong motion records of the 12 November 1999 Düzce earthquake (Table 33), it was observed that the values acquired from our analysis corresponds well with the actual values as it is known that the minimum distance to rupture in the analysis is 7.8 km; and as we consider the highest value recorded during this event (0.7 g), it can be observed that Abrahamson and Silva (2008) and Chiou and Youngs (2008) with 3 standard deviation are the models that represent our case the best when 10% probability of exceedance in 50 years is considered. As for the record at Düzce city center which indicates an average [(NS+EW/2)] PGA value of 0.47g which has a 9.71 km distance from rupture, again Abrahamson and Silva (2008) and Chiou and Youngs (2008) with 1 standard deviation yields the best results in accordance to the analysis performed for 10% probability of exceedance in 50 years.

These results are deemed consistent when the difference Vs_{30} values and distance to rupture values between the actual cases and our analysis is observed. In other words, when the first record is considered, although Vs_{30} value is lower than our analysis value considered in this study for soil (Vs_{30}=360 m/s), the difference in rupture distance (1.51 km farther) may have caused the decrease in the recorded

PGA value. As for the second record, it is the exact reverse in comparison with the first record, in other words; although the Vs_{30} value is higher and therefore the PGA value is expected to be lower, the difference in rupture distance (4.7 km nearer) can be considered to have caused the rather high PGA value recorded in this station.

These observations where standard deviations play an important part is consistent with the statistical basis for standard deviation value for normally distributed data where +1 standard deviation covers 84% of the total data and +3 standard deviation covers 99% of the data in a normal distribution.

Table 33. PGA values measured during the 12 November 1999, Düzce Earthquake.

Station ID	PGA (NS+EW)/2 (g)	Vs_{30}	Distance to Rupture (km)	Latitude	Longitude	Station Location
8101	**0.47**	282	9.71	40.844	31.149	Düzce City Center, Meteorology Station
9901	**0.70**	481	3.1	40.743	30.876	Sakarya - Karadere Village

As the results acquired from the analyses are compared with the earthquake zonation map prepared by the General Directorate of Disaster Affairs (GDDA) in 1996 (Figure 56), it can be observed that the city of Düzce falls completely within a 1st degree earthquake zone, which means 10% probability of exceedance for 50 years is higher than 0.4g for the entire the area.
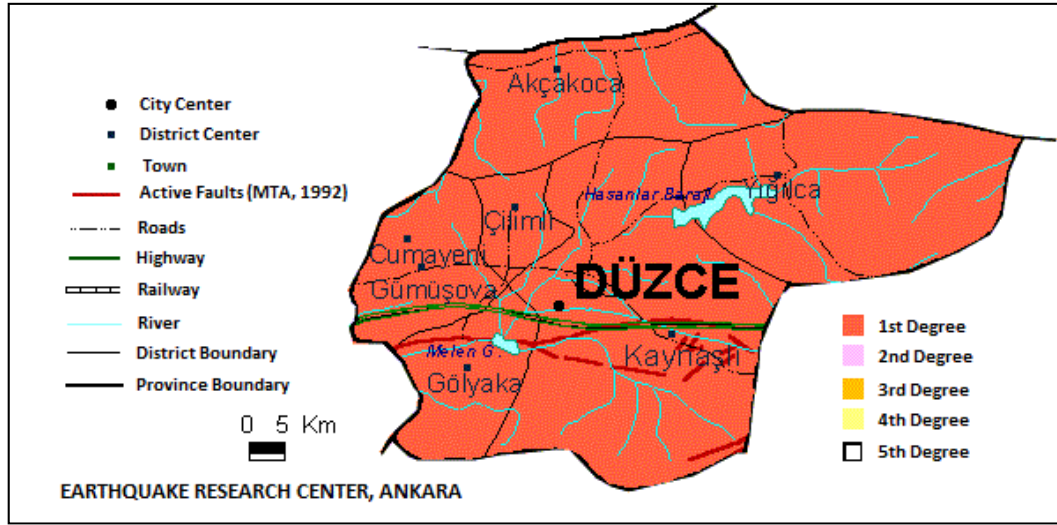
Figure 56. Earthquake Zonning Map of Düzce District (GDDA, 1996).

Along with this, a recent study conducted by Kalkan et al. (2009) by utilizing NGA (Next Generation Attenuation) GMPEs indicate that the area of interest of this study falls within 0.4 – 0.6 g for 10% probability of exceedance in 50 years for Vs_{30}=760 m/s rock site and between 0.44 and 0.72g for Vs_{30}=360 m/s soil site. As these values from the literature to be considered, the previous observation regarding the standard deviation, where the suggestion that utilization of 3 standard deviations should be preferred, is further supported. Therefore the sensitivity analysis which will be discussed in the following section in terms of seismicity (b values) and geometry (alternative models) were performed by considering both Vs_{30} values for each GMPE with 3 standard deviation and the results of these analyses will be compared with the initial findings presented above.

6.2 Sensitivity Analysis in Terms of Seismicity

The seismicity value of 'b' was calculated as 0.71 in the main analysis, and in order to check the sensitivity of the model to this seismicity variable two different values of 'b' were utilized in the model by keeping all the other variables (i.e. geometry) the same. The sensitivity analysis regarding seismicity value of 'b' was performed for 0.6 and 0.8, respectively. These analyses were performed for each four GMPE with Vs_{30} = 360 and 760 m/s and with 3 standard deviations as previously discussed. The comparison of the results with the initial model can be observed in Table 34, and in Figures 57 and 58, respectively, in terms of averages of GMPEs.

As can be clearly seen from either Table 34 and Figures 57 and 58, 'b' value does not have significant effect on the model.

Table 34. Sensitivity analysis results for different 'b' values.

	0.6	**0.71**	**0.8**
360-3 std.	0.621	0.621	0.623
760-3 std.	0.560	0.561	0.562
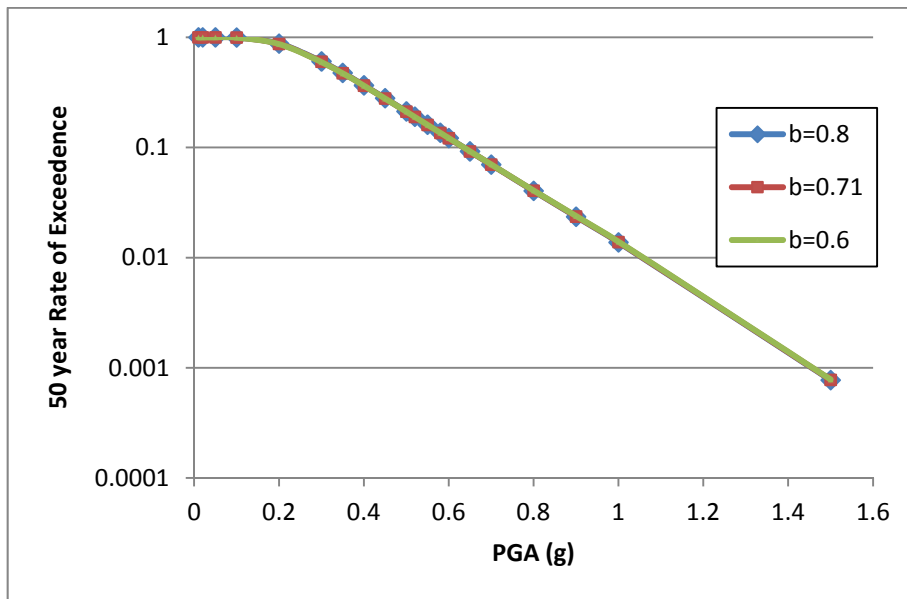
Figure 57. Results of sensitivity analysis in terms of 'b' value variation for Vs_{30}=360 m/sec.
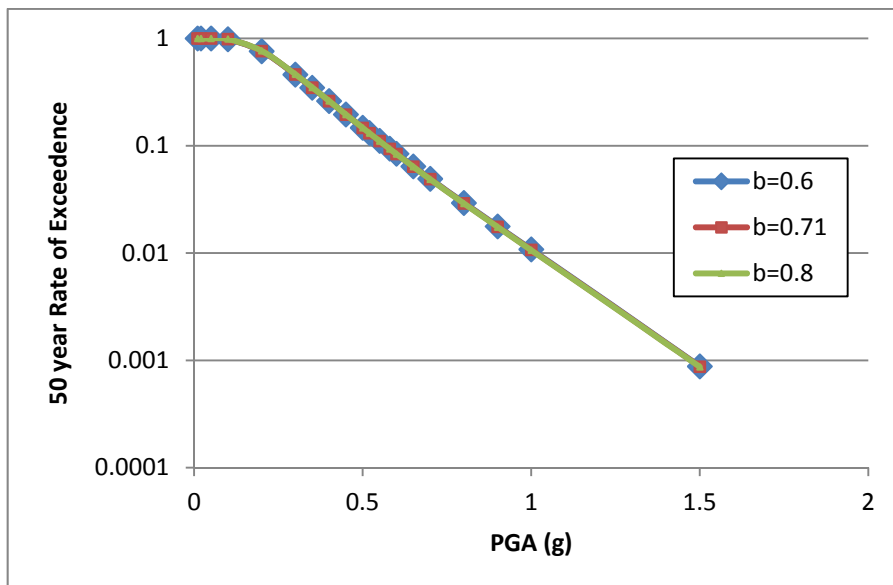
Figure 58. Results of sensitivity analysis in terms of 'b' value variation for Vs_{30}=760 m/sec.

6.3 Sensitivity Analysis in Terms of Model Geometry

As for sensitivity in terms of geometry, two previously mentioned changes were made in the model, namely; the Düzce seismic source was modeled as two segments as proposed by Pucci et al. (2006) and the Bolu seismic source was modeled as proposed by Kondo et al. (2005) as five segments (Figures 59 and 60, respectively). These changes in geometry consequently required changes in segment, source and scenarios and weight values for these scenarios. The fits to seismicity data in Youngs and Coppersmith characteristic model (1985) as well as weight values for scenarios are given below in Figures 61 and 62, for Düzce and Bolu seismic sources, respectively.The weight and scenario relationship for Bolu and Düzce seismic sources can be seen in Tables 35 and 36, respectively.
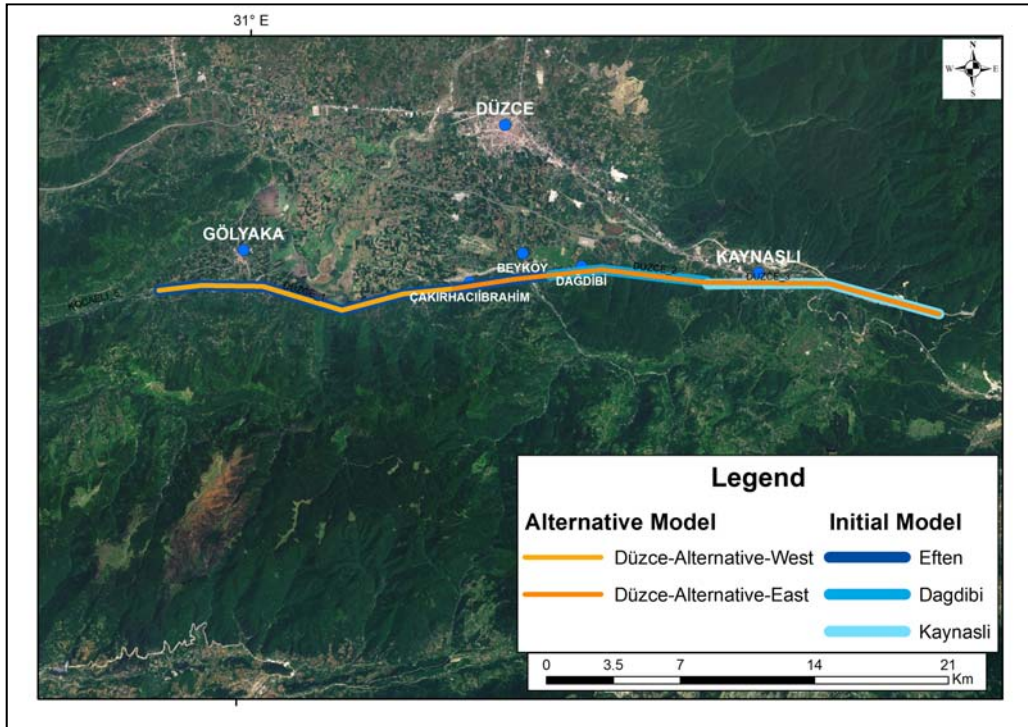
Figure 59. Initial and alternative geometries for Düzce seismic source.
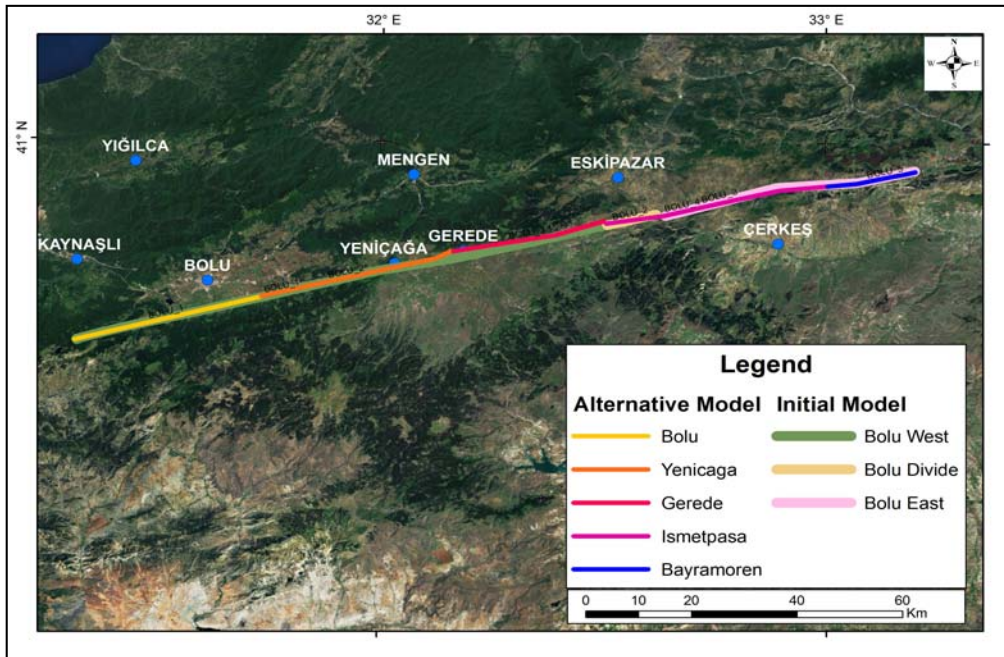
Figure 60. Initial and alternative geometries for Bolu seismic source.
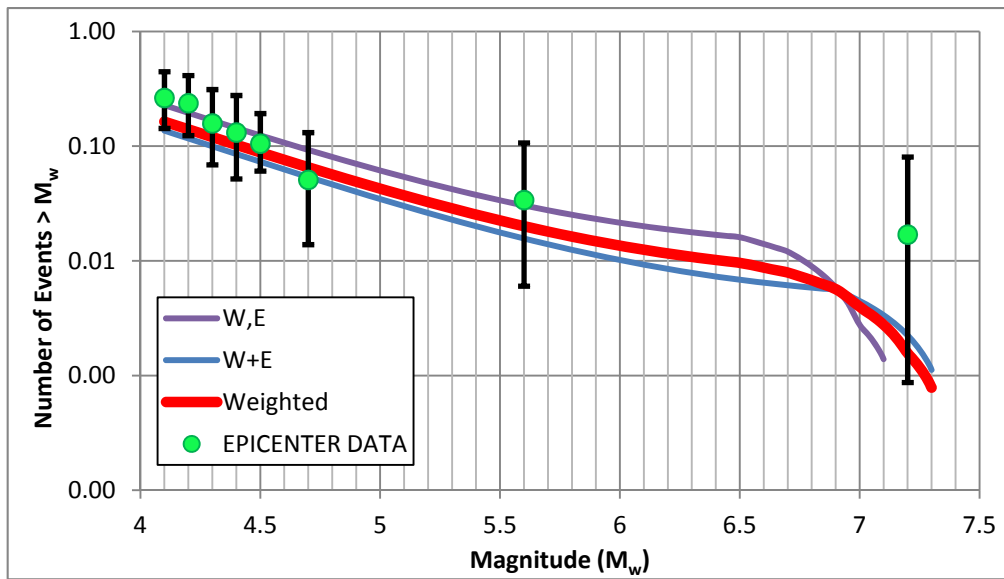
Figure 61. Weighted scenarios for alternative Düzce seismic source.

119
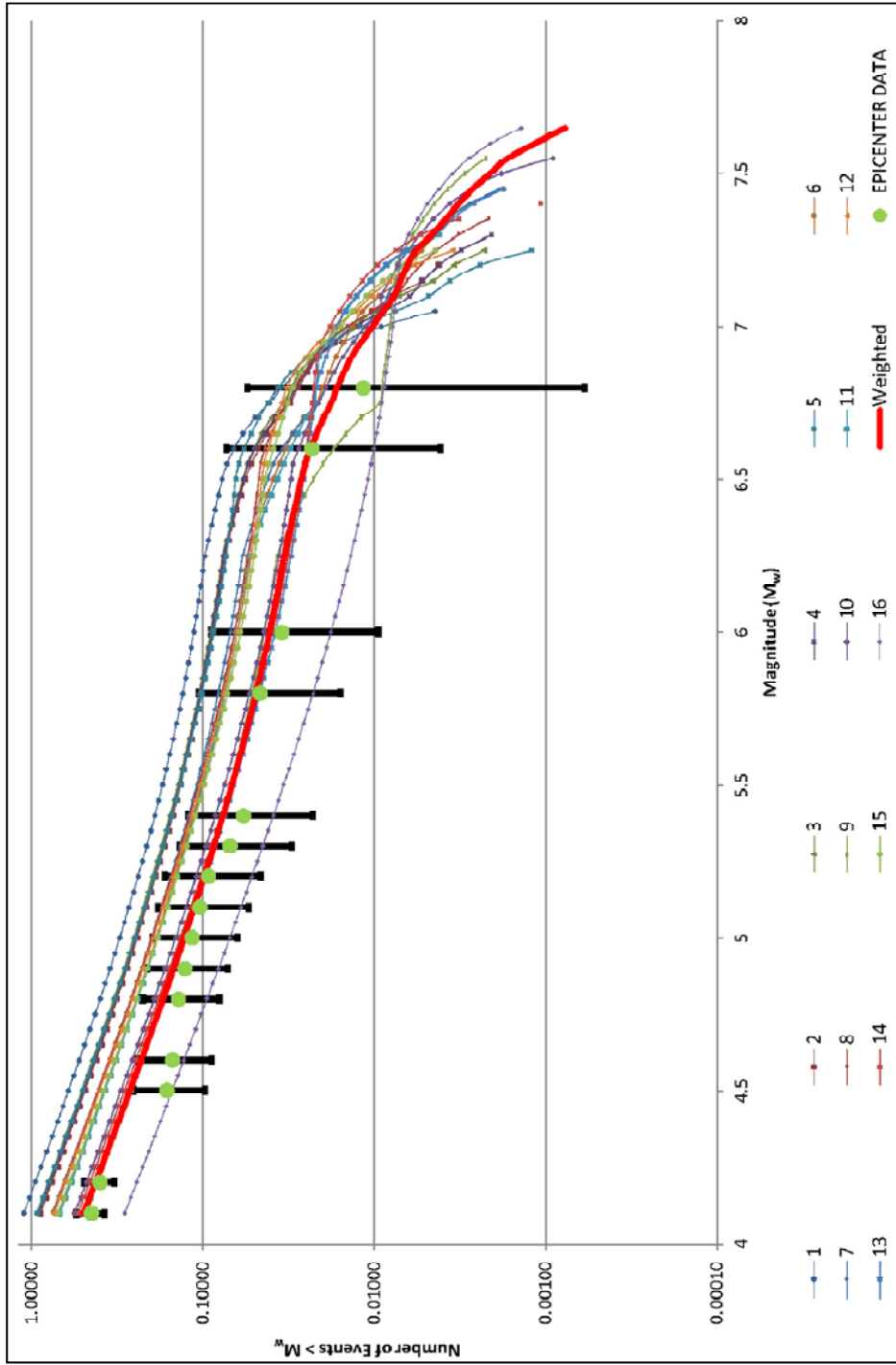
Figure 62. Weighted scenarios for alternative Bolu seismic source.

Table 35. Source and scenarios for the alternative Bolu seismic source.

		Sources															Weights	Scenario Number
		W1	W2	C	E1	E2	W1+W2	W2+C	C+E1	E1+E2	W1+W2+C	W2+C+E1	C+E1+E2	W1+W2+C+E1	W2+C+E1+E2	W1+W2+C+E1+E2		
Scenarios	**W1,W2,C,E1,E2**	1	1	1	1	1	0	0	0	0	0	0	0	0	0	0	0.1	**1**
	W1+W2,C,E1,E2	0	0	1	1	1	1	0	0	0	0	0	0	0	0	0	0.01	**2**
	W1,W2+C,E1,E2	1	0	0	1	1	0	1	0	0	0	0	0	0	0	0	0.01	**3**
	W1,W2,C+E1,E2	1	1	0	0	1	0	0	1	0	0	0	0	0	0	0	0.01	**4**
	W1,W2,C,E1+E2	1	1	1	0	0	0	0	0	1	0	0	0	0	0	0	0.01	**5**
	W1+W2+C,E1,E2	0	0	0	1	1	0	0	0	0	1	0	0	0	0	0	0.01	**6**
	W1,W2+C+E1,E2	1	0	0	0	1	0	0	0	0	0	1	0	0	0	0	0.01	**7**
	W1,W2,C+E1+E2	1	1	0	0	0	0	0	0	0	0	0	1	0	0	0	0.01	**8**
	W1+W2+C+E1,E2	0	0	0	0	1	0	0	0	0	0	0	0	1	0	0	0.04	**9**
	W1,W2+C+E1+E2	1	0	0	0	0	0	0	0	0	0	0	0	0	1	0	0.04	**10**
	W1+W2,C+E1,E2	0	0	0	0	1	1	0	1	0	0	0	0	0	0	0	0.04	**11**
	W1,W2+C,E1+E2	1	0	0	0	0	0	1	0	1	0	0	0	0	0	0	0.04	**12**
	W1+W2+C,E1+E2	0	0	0	0	0	0	0	0	1	1	0	0	0	0	0	0.04	**13**
	W1+W2,C+E1+E2	0	0	0	0	0	1	0	0	0	0	0	1	0	0	0	0.04	**14**
	W1+W2,C,E1+E2	0	0	1	0	0	1	0	0	1	0	0	0	0	0	0	0.04	**15**
	W1+W2+C+E1+E2	0	0	0	0	0	0	0	0	0	0	0	0	0	0	1	0.55	**16**
	Source Number	*1*	*2*	*3*	*4*	*5*	*6*	*7*	*8*	*9*	*10*	*11*	*12*	*13*	*14*	*15*		

Table 36. Source and scenarios for the alternative Düzce seismic source.

		Source			
		W	E	W+E	Weights
Scenario	W , E	1	1	0	0.3
	W+E	0	0	1	0.7

The sensitivity to model geometry was checked in four different models, initial model, changing geometry of only Düzce source, changing geometry of only Bolu source and changing geometries of both Düzce and Bolu seismic sources, and the results for these alternative geometries are presented below as the means of four GMPE with Vs_{30}= 360 and 760 m/s with 3 standard deviation (Table 37, and Figures 63 and 64, respectively).

Table 37. Result of sensitivity in terms of geometry.

	Initial Model	Changing Only Bolu Source	Changing Only Düzce Source	Changing Both Bolu and Düzce Sources
360-3 std.	0.621	0.621	0.598	0.597
760-3 std.	0.561	0.562	0.531	0.530
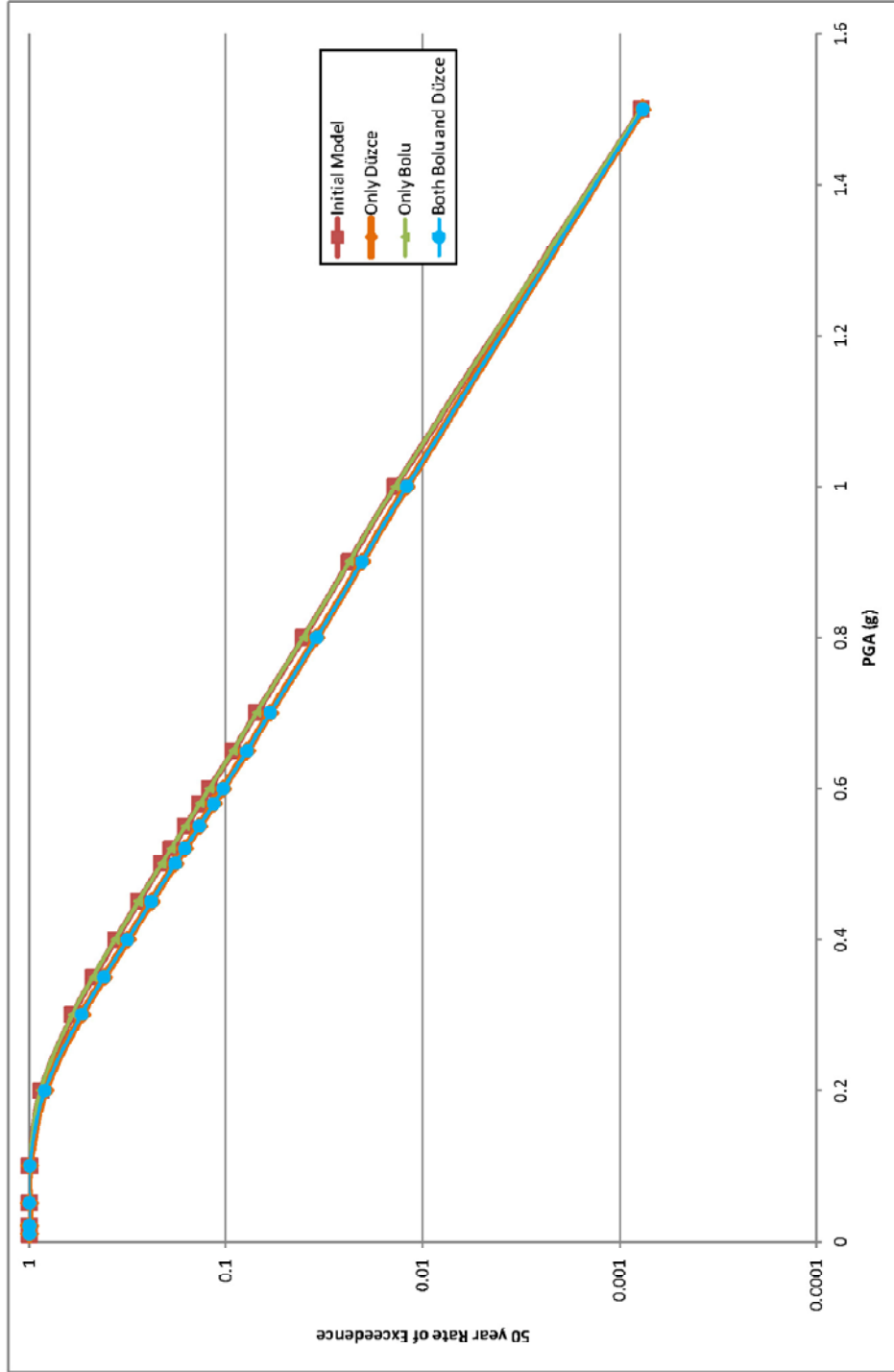
Figure 63. Results of sensitivity analysis in terms of geometry for V_{S30}=360 m/sec.
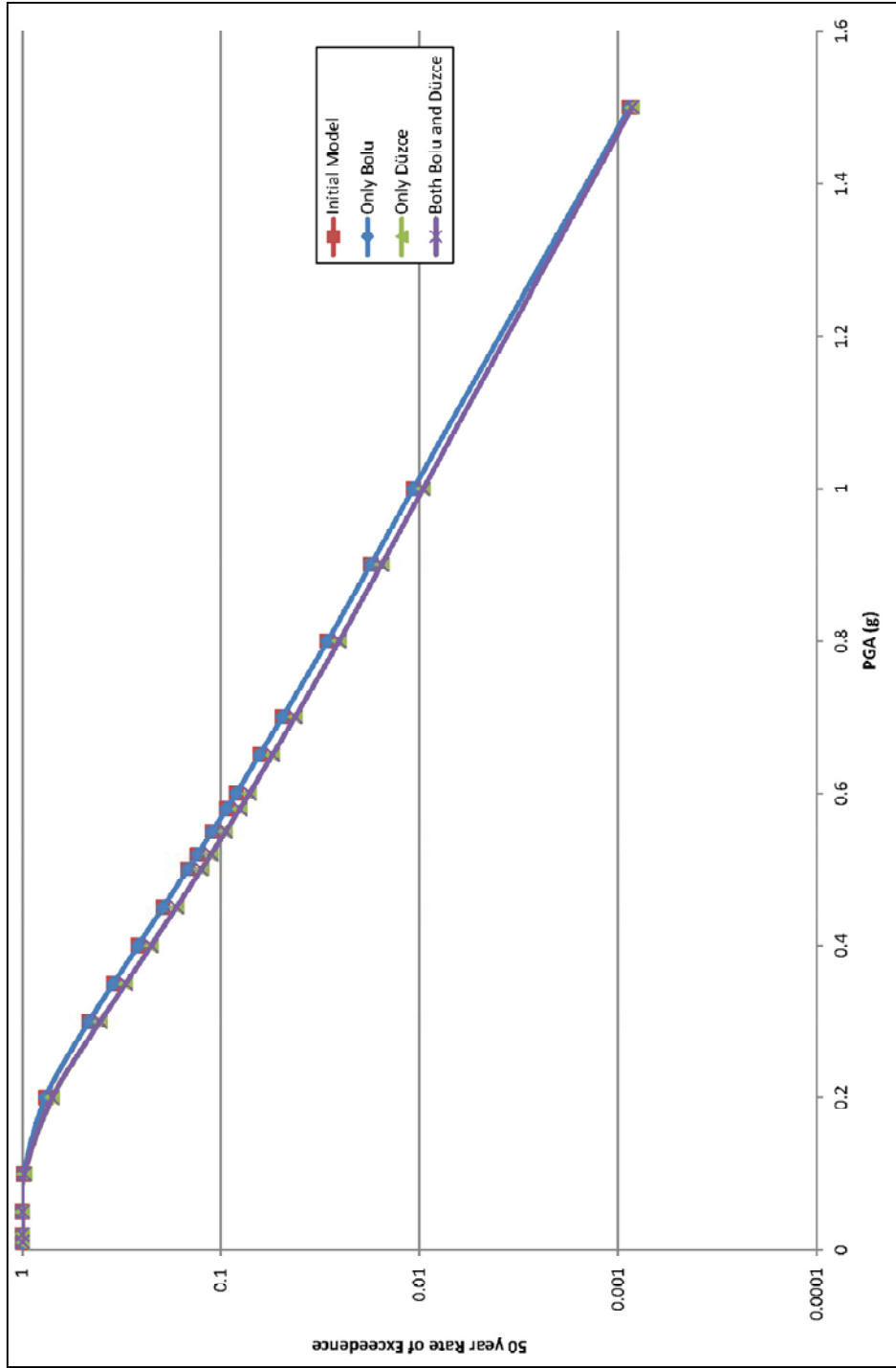
Figure 64. Results of sensitivity analysis in terms of geometry for $Vs_{30}=760$ m/sec.

As can be observed from Table 37 and Figures 63 and 64, change in the model with regards to segmentation of the Bolu seismic source does not affect the results, however the change in the segmentation of the Düzce seismic source from three segments to two segments affects the results with a 5% decrease in the final PGA values.

This change may be caused by the fact that the three segment model may be representing the natural conditions more accurately than the two segment model, or change in the minimum distances to the rupture (Table 38). Another possibility is that better fit of three segment model to the seismicity data (Figure 44) when compared to the two segment model (Figure 61). Although a similar fit for the two segment model could have been acquired, this would have resulted in assigning equal weights for two scenarios where west and east segments rupture individually or together, therefore causing divergence from the actual case where all segments have ruptured during the 12 November 1999, Düzce earthquake. A final possibility is that this decrease might have resulted due to inability of the model to include normal and thrust components of the two segments as discussed by Pucci et al. (2007), and modeling purely strike slip with vertical dip, thus neglecting the hangingwall or footwall effect which might have contributed to the results. This issue will be discussed in the following chapter.

Table 38. Minimum distances to rupture for two alternative Düzce seismic source geometries.

Seismic Source	Segment	Distance (km)
Initial Model with Three Segments	Eften	7.8
	Dağdibi	8
	Kaynaşlı	13.5
Modified Model with Two Segments	West	8.9
	East	7.8

CHAPTER 7

CONCLUSION AND RECOMMENDATIONS

The most recent destructive earthquakes of 17 August 1999, Kocaeli and 12 November 1999, Düzce have resulted numerous researches to be conducted regarding North Anatolian Fault in the Marmara Region and different fault maps from these different studies were generated for the region (Barka, 1997; Akyüz et al., 2002; Barka et al., 2002; MTA, 2003a and 2003b; Duman et al., 2005). These maps have different scales related with the purpose of the relevant study, therefore resulting in fault maps with different concentrations and aspects. Therefore in order to generate a generalized seismic source model for the eastern Marmara and Düzce Region, these studies were incorporated in the GIS environment during this study. As the spatial location of a seismic source is an important parameter in a probabilistic seismic hazard analysis in order to minimize the aleatoric variability, lineament extraction analysis from 10 ASTER images encompassing the study area was performed. As lineaments cannot be readily called as faults, let alone active faults, the previously prepared GIS database from different researchers in terms of active faults of the region was compared with these extracted lineaments and thus the final seismic source model was developed for a probabilistic seismic hazard analysis. Another important aspect of probabilistic seismic hazard assessment, which is the earthquake catalogue to be employed, was also investigated in detail for these records within the study area. Declustering analysis was performed, therefore separation of main events from secondary events and exclusion of these fore- and aftershocks was performed. Therefore, the mutually

exclusiveness of events within the catalogue was ensured. Along with this a magnitude incompleteness range was detected in terms of magnitude and time being M_w=4.5 and 1964, respectively. Due to this incompleteness, the catalogue was divided into two time intervals as 100 year completeness for $M_w > 4.5$ and 41 years for $M_w < 4.6$. If this observation was to be taken as a temporal threshold and only post-1964 records were to be utilized, the equally weighted average 'b' value was found to be 0.706. However, this approach was not utilized in order not to hamper the following seismicity curve fitting analysis. Accordingly, each seismic source zone was assigned their respective earthquake records and curve fitting in terms of source, segment and scenario relationship was utilized by considering Youngs and Coppersmith (1985) characteristic model. Thus weights of each scenario of each seismic source zone were determined.

In order to test the applicability of this source model, a probabilistic seismic hazard analysis for the city of Düzce was performed by considering different magnitudes, ground motion prediction equations, soil types based on IBC-2006; segment and source relations were developed in concordance with the fault rupture mechanisms of the major events in the area as well as known fault zones. The characteristic magnitude of each segment along with the variations related to the scientific approach was also taken into consideration via the standard deviations. Four different Ground Motion Prediction Equations (GMPEs) applicable for Turkey were considered during the probabilistic seismic hazard analysis and a sensitivity analysis in terms of seismicity and geometry of the source model was performed by considering equally weighted results generated by these GMPE via probabilistic seismic hazard assessment for the city of Düzce.

It was observed, as a result of these sensitivity analyses that the Gutenberg and Richter seismicity parameter 'b' have little or no effect over the analysis. Thus

127

utilization of result acquired from either least squares or maximum likelihood estimation approaches would not have affected the results significantly.

On the other hand, the change in the geometry affects the results of approximately 5 percent. In light of this finding, it can be recommended that modeling of fault segments as a 3-D model by incorporating dip amount and dip direction can further enhance the performance of the model by reflecting the natural conditions as well as hanging wall effect when strike-slip fault with normal components are considered. Furthermore, different segmentation models proposed by different researchers can be investigated even further in order to have a more detailed sense regarding the effect of geometry to the final results.

Additionally, characterization of the soft and unconsolidated sedimentary deposits located especially at the city center of Düzce can be implemented to get a spatial variation of the ground motion characteristics. This can be performed via utilizing destructive and/or non-destructive geotechnical and geophysical field testing, or from databases compiled during previous studies and investigations. Thus this newly generated database can be included into the GIS database. This can describe the effects of local geology on the ground motion variations for the city of Düzce in further detail and a seismic zonation map for the city of Düzce can be developed. Inclusion of this data can allow the consideration of local site conditions and site amplification effects can also be included in the final results.

Furthermore, this study can be expanded to Southern Marmara region and Northern Aegean Region, Western Marmara Region and the Sea of Marmara and to the Black Sea coast in order to farther include the area surrounding the study area investigated in this study. Therefore a regional seismic zonation map initially for the Marmara Region and Western Black Sea Region can be completely developed.

Another recommendation can be made regarding Ground Motion Prediction Equations (GMPEs). Although it is known and explained in the text that the utilized NGA-GMPEs are applicable for the study area, event specific GMPEs or GMPEs developed especially for Turkey can be further included in the final result. However this approach was not sought in this study due to limitations of the hazard code in terms of range of GMPEs.

REFERENCES

Abrahamson, N. A., and Silva, W., 2008, *Summary of the Abrahamson & Silva NGA Ground-Motion Relations*, Earthquake Spectra, 24 (1), 67-97.

Abrams, M., 2000, *The Advanced Spaceborne Thermal Emission and Reflection Radiometer (ASTER): Data Products for the High Spatial Resolution Imager on NASA's Terra Platform*, International Journal of Remote Sensing, 21, 847–859.

Aki, K., 1966, *Generation and propagation of G waves from the Niigata earthquake of June 16, 1964,2 , Estimation of earthquake moment, released energy, and stress-strain drop from G-waves spectrum*, Bull. Earthquake Res. Inst. Tokyo Univ., 44, 73-88.

Akman, A.Ü. and Tüfekçi, K., 2004. *Determination and Characterization of Fault Systems and Geomorphological Features by RS and GIS Techniques in the WSW Part of Turkey,* XXth ISPRS Congress, Istanbul.

Akyüz H.S., Hartleb R, Barka A, Altunel E and Sunal G, 2002, *Surface rupture and slip distribution of the 12 November 1999 Düzce earthquake (M 7.1), North Anatolian Fault, Bolu, Turkey*, Bull. Seismol. Soc. Am., 92, 61–66.

Ambraseys, N.N., 1970, *Some characteristic features of the North Anatolian Fault Zone*, Tectonophysics, 9, 143-165.

Ambraseys, N. N., Zapotek, A., Tasdemiroglu, M. and Aytun, A., 1968, *The Mudurnu valley, West Anatolia, Turkey, earthquake of 22 July 1967*, UNESCO Publ. 27.

Ambraseys, N. N. and A. Zatopek, 1969, *The Mudurnu Valley, West Anatolia, Turkey, earthquake of 22 July 1967*, Bull. Seismol. Soc. Am., 59, 521-589.

Armijo, R., Meyer, B., Navarro, S., King, G., and Barka, A., 2002. *Asymmetric slip partitioning in the Sea of Marmara pull-apart: a clue to propagation processes of the North Anatolian Fault?* Terra Nova, 14, 80– 86.

Atakan, K., Ojeda, A., Meghraoui, M., Barka, A., Erdik, M., and Bodare, A., 2002, *Seismic Hazard in Istanbul following the 17 August 1999 Izmit and 12 November 1999 Duzce earthquakes*, Bull. Seismol. Soc. Am., 92 (1), 466-482.

Ayhan, M. E., Bürgmann, R., McClusky, S., Lenk, O., Aktug, B., Herece, E. and Reilinger, R.E., 2001, *Kinematics of the Mw: 7.2, 12 November 1999, Düzce, Turkey earthquake,*, Geophys. Res. Lett., 28, 367– 370.

Ayhan, M. E., and Koçyiğit, A., 2010, *Displacements and Kinematics of the February 1, 1944 Gerede Earthquake (North Anatolian Fault System, Turkey): Geodetic and Geological Constraints*, Turkish J. Earth Sci., 19, 285–311.

Barka, A., 1992, *The North Anatolian Fault Zone*, Ann. Tecton., 6 (1), 64–95

Barka, A., 1996, *Slip distribution along the North Anatolian fault associated with the large earthquakes of the period 1939 to 1967*, Bull. Seismol. Soc. Am., 86, 1238-1254.

Barka, A. and Kadinsky-Cade, K., 1988, *Strike-slip fault geometry in Turkey and its influence on earthquake activity,* Tectonics, 7 (6), 63–84

Barka A., Akyüz, H.S., Altunel, E., Sunal, G. and Çakır Z., 2002, *The surface rupture and slip distribution of the 17 August 1999 Izmit earthquake (M 7.4), North Anatolian Fault*, Bull. Seismol. Soc. Am., 92, 43–60.

Boore, D. M. and Atkinson, G. M., 2008, *Ground-Motion Prediction Equations for the Average Horizontal Component of PGA, PGV, and 5%-Damped PSA at Spectral Periods between 0.01s and 10.0s*, Earthquake Spectra, 24, 99-138.

Bürgmann, R., Ergintav, S., Segall, P., Hearn, E., McClusky, S., Reilinger, R.E., Woith, H. and Zschau, J., 2002, *Time-dependent distributed afterslip on and deep below the Izmit earthquake rupture*, Bull. Seism. Soc. Am., 92, 126-137.

Bürgmann, R., Ayhan, M. E., Fielding, E., Wright, T., McClusky, S., Aktug, B., Demir, C., Lenk, O. and Türkezer, A., 2002, *Deformation during the 12 November 1999, Düzce, Turkey, Earthquake, from GPS and InSAR Data*, Bull. Seismol. Soc. Am., 92 (1), 161–171.

Campbell, K.W. and Bozorgnia, Y., 2008, *NGA ground motion model for the geometric mean horizontal component of PGA, PGV, PGD and 5% damped linear elastic response spectra for periods ranging from 0.01 to 10 s,* Earthquake Spectra, 24, 139-171.

Casas, A. M., Cortes, Angel L., Maestro, A., Soriano, M.A., Riaguas, A. and Bernal, J., 2000, *A program for lineament length and density analysis,* Computers and Geosciences, 26 (9/10), 1011-1022.

Chiou, B.S.-J. and Youngs, R., 2008, *An NGA model for the average horizontal component of peak ground motion and response spectra,* Earthquake Spectra, 24, 173-215.

Cornell, C., 1968, *Engineering seismic risk analysis,* Bull. Seismol. Soc. Am., 58, 1583-1606.

Crowley, H. and Bommer J.J., 2006, *Modeling seismic hazard in earthquake loss models with spatially distributed exposure.* Bull. of Eq. Eng., 4, 249-273.

Cakir, Z., Barka, A.A, Chabalier, J.B, Armijo, R. and Meyer, B., 2003, *Kinematics of the November 12, 1999 (Mw_ 7.2) Duzce earthquake deduced from SAR interferometry,* Turkish J. Earth Sci., 12, 105–118.

Çetin, K.Ö., Yunatçı, A.A., Çağlı, S., Gülkokar, T., Aktaş, R., Altınışık, F., Çelik, S., Arabacı, H.M. and Çekmeceli, M., 2004, *Bursa Şehri için CBS Destekli Olasılıksal Sismik Tehlike Analizi ve Sıvılaşma Risk Haritalarının Oluşturulması,* (In Turkish) ZMTM 10. Ulusal Kongresi, 16-17 Eylül, İTÜ, pp.479-88.

De Louis, B., Giardini, D., Lundgren, P., and Salichon, J., 2002, *Joint inversion of InSAR, GPS, teleseismic, and strong-motion data for the spatial and temporal distribution of earthquake slip: Application to the 1999 Izmit mainshock*, Bull. Seismol. Soc. Am., 92, 278–299.

Demirtaş, R., Erkmen, C., and Yaman, M., 2000, *12 Kasım 1999 Düzce Depremi: Yüzey Kırık Geometrisi, Atım Miktarı Dağılımı ve Gelecek Deprem Potansiyeli*, in '12 November Düzce Earthquake Report' (Özmen B. and Bağcı G., eds.), Earthquake Research Center, General Directorate of Disaster Affairs, Ankara (In Turkish).

Deniz, A., 2006, *Estimation of earthquake insurance premium rates based on stochastic methods*. M.Sc. Thesis, Middle East Technical University, Ankara.

Deniz, A. ve Yücemen, M. S., 2010, *Magnitude conversion problem for the Turkish earthquake data*, Nat. Hazards, 55, 333–352.

Douglas, J., 2011, *Ground-Motion Prediction Equations 1964-2010,* Final report RP-59356-FR. BRGM, Orléans, France.

Duman, T. Y., Emre, O., Doğan, A. and Özalp, S., 2005, *Step-over and bend structures along the 1999 Duzce earthquake surface rupture, North Anatolian fault, Turkey*, Bull. Seismol. Soc. Am., 95, 1250 – 1262.

Emre, O., Erkal, T., Tchepalyga, A., Kazanci, N., Kecer, M. and Unay, E., 1998, *Neogene–Quaternary evolution of Eastern Marmara Region*, Bull. MTA 120, 233–258.

Erdik, M., Demircioglu, M., Sesetyan, K., Durukal, E., Siyahi, B., 2004, *Earthquake hazard in Marmara Region, Turkey*, Soil Dynamics and Earthquake Engineering, 24, 605-631.

Erdik, M., Şeşetyan, K. Demircioğlu, M.B. ve Durukal, E., 2006, *DLH İnşaatı Genel Müdürlüğü Kıyı Yapıları, Demiryolları ve Havameydanları İnşaatları Deprem Teknik Yönetmeliği için Deprem Tehlikesi Belirlemesi*, (In Turkish) BÜ-KRDAE, İstanbul.

Fu, B., and Lin, A., 2002, *Spatial Distribution of the Surface Rupture Zone Associated with the 2001 Ms 8.1 Central Kunlun Earthquake, Northern Tibet, Revealed by Satellite Remote Sensing Data.* International Journal of Remote Sensing. 24 (10), 2191-2198.

Gozzard, J.R., 2006, *Image Processing of ASTER Multispectral Data*, Geological Survey of Western Australia.

Graf, U., Henning, H.J. and Stange, K., 1966, *Forrneln und TabeUen der mathematischen Statistik,* 362 pp., 2nd ed., Springer Verlag, Berlin.

Gupta, I.D., 2002, *The State of the Art in Seismic Hazard Analysis*, ISET Journal of Earthquake Technology, Paper No. 428, 39 (4), 311-346.

Gupta, R. P., 2003, *Remote Sensing Geology*, Berlin, Springer-Verlag.

Gutenberg, B., and Richter, C.F., 1949, *Seismicity of the Earth and Associated Phenomenon,* Princeton University Press, Princeton, New York.

Hanks, T. C., and Kanamori, H., 1979, *A moment magnitude scale*, J. Geophys. Res., 84, 2348–2350.

Harris, R. A., Dolan, J.F., Hartleb, R., and Day, S.M., 2000, *The 1999 Izmit, Turkey earthquake - A test of the dynamic stress transfer model for intra-earthquake triggering*, Bull. Seismol. Soc. Am., 92 (1), 245-255.

Hartleb, R. D., Dolan, J.F., Akyüz, S., Dawson, T.E., Tucker, A.Z., Yerli, B., Rockwell, T.K., Toraman, E., Çakır, Z., Dikbas, A. and Altunel, E., 2002, *Surface rupture and slip distribution along the Karadere segment of the 17 August 1999 Izmit, Turkey, earthquake*, Bull. Seism. Soc. Am. (Special Issue on the 1999 Izmit and Düzce, Turkey, Earthquakes, N. Toksöz [Editor]).

International Code Council, ICC. (2006). International Building Code. Structural and fireand life-safety provisions (seismic, wind, accessibility, egress, occupancy and roof codes), Whittier, CA.

Kahle, H.G., Concord, M., Peter, Y., Geiger, A., Reilinger, R., Barka, A., and Veis G., 2000, *GPS derived strain rate field within the boundary zones of the Eurasian, African, and Arabian plates*, J. Geophys. Res., 105 (23),353-370.

Kalkan, E., Gulkan, P., Yilmaz, N., and Celebi, M., 2009, *Reassessment of Probabilistic Seismic Hazard in the Marmara Region*, Bull. Seismol. Soc. Am., 99 (4), 2127-2146.

Kayabalı, K., 1995, Seismic Hazard Assessment: Theory and Application, JMO Dergisi, 46, 28-43.

Ketin, I., 1948, *Uber die tektonisch-mechanischen Folgerungen aus den grossen anatolischen Erdbeben des letzten Dezenniums*, Geol. Rund. 36, 77–83.

Ketin, I., 1969, *Uber die nordanatolische Horizontalverschiebung*, Bull Mineral Res. Explor. Inst. (MTA) Turkey, 72, 1-28.

Koç, A., 2005, *Remote Sensing Study of Sürgü Fault Zone (Malatya, Turkey)*, M.Sc. Thesis, Middle East Technical University, Ankara.

Koçyiğit, A., Ayhan., M.E., Çetin, H., Aktuğ, B., Aytun, A., Demir, C., Lenk, O., Kılıçoğlu, A., Açıkgöz, M., Deveci, S., Biryol, B., Arca, S., Aktürk, O. and Günaydın, O., 2006, *Earthquake Hazards of the Section Between İsmetpaşa-Gerede and Mengen of the North Anatolian Fault System (NAFS)*. TÜBİTAKYDABAG- 102Y053 project report [in Turkish with English abstract, unpublished].

KOERI, 2007, *A Revised and Extended Earthquake Catalogue for Turkey since 1900 (M≥4)*, Bebek, İstanbul.

Koike, K., Nagano, S. and Kawaba, K., 1998, *Constraction and Analysis of Interpreted Fracture Planes Through Combination of Satellite-Image Derived Lineaments and Digital Elevation Model Data*, Computers and Geosciences, 24 (6), 573-583.

Koike, K., Nagano, S. and Ohmi, M., 1995, *Lineament Analysis of Satellite Images Using A Segment Tracing Algorithm (STA)*, Computers and Geosciences, 21 (9), 1091-1104.

Kondo, H., Awata, Y., Emre, O., Dogan, A., Ozalp, S., Tokay, F., Yildirim, C., Yoshioka, T. and Okumura, K., 2005, *Slip Distribution, Fault Geometry, and Fault Segmentation of the 1944 Bolu-Gerede Earthquake Rupture, North Anatolian Fault, Turkey*, Bull. Seismol. Soc. Am., 95(4), 1234-1249.

Kramer, S.L., 1996, "Geotechinal Earthquake Engineering. ed. William J. H., Prentice-Hall International Series in Civil Engineering and Engineering Mechanics". New Jersey. USA.

Krinitizsky, E. L., 1993, *Earthquake probability in engineering – Part 1: the use and misuse of expert opinion*, Engineering Geology, 33, 257–288.

Langridge, R. M., Stenner, H.D., Fumal, T.E., Christofferson, S.A., Rockwell, T.K., Hartleb, R.D., Bachhuber, J. and Barka, A.A., 2002, *Geometry, slip distribution, and kinematics of surface rupture on the Sakarya fault segment during the 17 August 1999 Izmit, Turkey, earthquake*, Bull. Seismol. Soc. Am. 92 (1), 107–125.

Lettis, W., Bachhuber, J., Witter, R., Brankman, C., Randolph, C. E., Barka, A., Page, W. D. and Kaya, A., 2002, *Influence of Releasing Step-Overs on Surface Fault Rupture and Fault Segmentation: Examples from the 17 August 1999 Izmit Earthquake on the North Anatolian Fault, Turkey*, Bull. Seismol. Soc. Am., 92(1), 19-42.

Lillesand, T.M. and Keifer, R.W., 1999, "Remote Sensing and Image Interpretation", 4th Edition.

McKenzie D.P., 1972, *Active tectonics of the Mediterranean region*, Geophys. J. R. Astron. Soc., 30 (1), 09–85

McClusky, S., Balassanian, S., Barka, A., Demir, C., Ergintav, S., Georgiev, I., Gürkan, O., Hamburger, M., Hurst, K., Kahle, H., Kastens, K., Kekelidze, K., King, R., Kotzev, V., Lenk, O., Mahmoud, S., Mishin, A., Nadariya, M., Ouzounis, A., Paradissis, D., Peter, Y., Prilepin, M., Reilinger, R., Sanlı, I., Seeger, H., Tealeb, A., Toksöz, M.N. and Veis, G., 2000, *Global positioning system constraints on plate kinematics and dynamics in the Eastern Mediterranean and Caucasus*, J. Geophys. Res., 105, 5695-5719.

Meade, B.J., Hager, B.H., McClusky, S., Reilinger, R.E., Ergintav, S., Lenk, O., Barka, A. & Ozener, H., 2002, *Estimates of seismic potential in the Marmara region from block models of secular deformation constrained by Global Positioning System measurements*, Bull. Seismol. Soc. Am., 92, 208–215.

METU and MTA, 1999, *Investigation report on site selection for Sakarya city and surrounding towns after the Gölcük-Arifiye (NW Marmara) earthquake of 17 August 1999*, 148 p (unpublished report, in Turkish).

Ministry of Public Works and Settlement, 2007, *Turkish Seismic Code, Specification for Structures to be Built in Disaster Areas*, Ankara, Turkey.

MTA, 2003a, *Surface Rupture Associated with the Auguts 17, 1999 İzmit Earthquake*, Special Publications Series:1.

MTA, 2003b, *Atlas of North Anatolian Fault*: Special Publications Series:2.

MTA and Ankara University, 1999, *Geological Assessment of Alternative Settlement areas for Düzce Province Following 17 August 1999*, TÜBİTAK, Earth-Sea-Atmosphere Sciences and Environment Research Group Report, ANKARA.

Nakiboğlu, S.M., Ayhan, M.E., Demir, C., Kılıçoğlu, A. and Şanlı, I., 1998, *Crustal Motion Within the Western Section of the North Anatolian Fault: Geodetic Observations and Geophysical Interpretations*. TUBİTAK-Intag 910 [in Turkish with English Abstract, unpublished].

Nama, E.E., 2004, *Lineament detection on Mount Cameroon during the 1999 volcanic eruptions using Landsat ETM*, International Journal of Remote Sensing, 25 (3), 501-510.

Okumura, K., Yoshioka, T., and Kuscu, I., 1993, *Surface faulting on the North Anatolian Fault in these two millennia*, U.S. Geol. Surv. Open-file Rep., 94-568, 143-144.

Özalaybey, S., Ergin, M., Aktar, M., Tapırdamaz, C., Biçmen, F., and Yörük, A., 2002, *The 1999 İzmit earthquake sequence in Turkey: seismological and tectonic aspects*, Bull. Seismol. Soc. Am., 92, 376–386.

Öztürk, A., Inan, S. and Tutlean, Z., 1985, *Abant-Yeniçağa Yöresinin Tektoniği,* Bull. Earth Sci. Cumhuriyet Univ. 2, 35-52 (In Turkish).

Palyvos, N., Pantosti, D., Zabci, C. & D'Addezio, G., 2007, *Paleoseismological Evidence of Recent Earthquakes on the 1967 Mudurnu Valley Earthquake Segment of the North Anatolian Fault Zone*, Bull. Seismol. Soc. Am., 97(5), 1646-1661.

Pucci, S., 2006, *The Duzce segment of the north Anatolian Fault Zone (Turkey): Understanding its seismogenic behavior through earthquake geology, tectonic, geomorphology and paleoseismology*. Unpublished PhD thesis, Universita delgi studi di Perugia.

Pucci S., De Martini, P.M. and Pantosti D., 2007, *Preliminary slip rate estimates for the Duzce segment of the North Anatolian fault Zone from offset geomorphic markers*, Geomorphology, 97 (3-4), 538-554.

Reilinger, R., Ergintav, S., Burgmann, R., McClusky, S., Lenk, O., Barka, A., Gurkan, O., Hearn, L., Feigl, K.L., Cakmak, R., Aktug, B., Ozener, H. and Toksöz, M.N., 2000, *Coseismic and postseismic fault slip for the 17 August 1999, M: 7.5, Izmit, Turkey,* Earthquake, Science, 289, 1519–1524.

Reilinger, R., McClusky, S., Vernant, P., Lawrence, S., Ergintav, S., Cakmak, R., Ozener, H., Kadirov, F., Guliev, I., Stepanyan, R., Nadariya, M., Hahubia, G., Mahmoud, S., Sakr, K., ArRajehi, A., Paradissis, D., Al-Aydrus, A., Prilepin, M., Guseva, T., Evren, E., Dmitrotsa, A., Filikov, S.V., Gomez, F., Al-Ghazzi, R., Karam, G., 2006. *GPS constraints on continental deformation in the Africa–Arabia–Eurasia continental collision zone and implications for the dynamics of plate interactions*, J. Geophys. Res. 111 B05411.

Richards, J. A., 1993, "Remote Sensing Digital Image Analysis: An Introduction", Springer-Verlag, New York, 250 pp.

Rockwell, T. K., Lindvall, S., Dawson, T., Langridge, R., and Lettis, W., 2002, *Lateral offsets on surveyed cultural features resulting from the 1999 Izmit and Düzce Earthquakes, Turkey,* Bull. Seismol. Soc. Am., 92 (1), 79–94.

Rowan, L. C., and Mars, J. C., 2003, *Lithologic mapping in the Mountain Pass, California area using Advanced Spaceborne Thermal Emission and Reflection Radiometer (ASTER) data*, Remote Sensing of Environment, 84, 350–366.

Sarp, G., 2005, Lineament Analysis from Satellite Images, North-East of Ankara, M.Sc. Thesis, Middle East Technical University, Ankara.

Stepp, J. C., 1973, *Analysis of completeness of the earthquake sample in the Puget Sound area,* In Contributions to seismic zoning: U.S. National Oceanic and Atmospheric Administration Technical Report ERL 267-ESL 30 (edited by Harding, S. T.), 16-28.

Stein, R.S., Barka, A.A., and Dieterich, J.H., 1997, *Progressive failure on the North Anatolian fault since 1939 by earthquake stress triggering*, Geophys. J. Int., 128, 594-604.

Straub, C, H., Kahle, G. and Schindler, C., 1997, *GPS and geologic estimates of the tectonic activity in the Marmara sea region, NW Anatolia*, J. Geophys. Res. 102, 27587-27601.

Şaroğlu, F., Emre, Ö., Kuşçu, İ., 1992. *Active Fault Map of Turkey,* General Directorate of the Mineral Research and Exploration, Ankara, Turkey, 2 sheets, 1.2.000.000 scale.

Şengör A.M.C., 1979, *The North Anatolian Transform Fault: its age, offset and tectonic significance*. J. Geol. Soc. London, 136 (2), 69–82.

Şengör, A.M.C., Tüysüz, O., Imren, C., Sakinç, M., Eyidogan, H., Görür, N., Le Pichon, X., and Rangin C., 2004, *The North Anatolian Fault: A new look*, Annu. Rev. Earth Planet. Sci., 33, 1-75.

Tsukuda, T., Satake, K., Honkura, Y., Uçer, S.B. and Işıkara, A.M., 1988, *Low seismicity, low coda-Q, and discontinuities of the upper crust in the vicinity of the Iznik-Mekece fault, the North Anatolian Fault Zone, Turkey,* Bull. Earthquake Res. Inst. Univ. Tokyo, 63, 327–348.

Umutlu, N., Koketsu, K. and Milkereit, C., 2004. *The rupture process during the 1999 Düzce, Turkey, earthquake from joint inversion of teleseismic and strong-motion data*, Tectonophysics, 391, 315–324.

Utkucu, M., Nalbant, S.S., McCloskey, J., Steacy, S., and Alptekin, O., 2003, *Slip distribution and stress changes associated with the 1999 November 12, Düzce (Turkey) earthquake (Mw = 7.1)*, Geophys. J. Int., 153, 229–241.

Wang, J., Howarth, P.J., 1990, *Use of the Hough transform in automated lineament detection*, IEEE Transactions on Geoscience and Remote Sensing, 28 (4), 561– 566.

Weichert, D. H., 1980, *Estimation of earthquake recurrence parameters for unequal observation periods for different magnitudes*, Bull. Seismol. Soc. Am., 70, 1337–1356.

Wells, D.L. and Coppersmith, K.J., 1994, *New empirical relationships among magnitude, rupture length, rupture width, and surface displacement*, Bull. Seismol. Soc. Am., 84, 974-1002.

Wong, H.K., Lüdmann, T.,Ulug, A. and Görür, N., 1995, *The sea of Marmara: A plate boundary sea in an escape tectonic regime*, Tectonophysics, 244, 231-250.

Youngs, R. R., and Coppersmith K.J.,1985, *Implications of fault slip rates and earthquake recurrence models to probabilistic seismic hazard estimates*, Bull. Seismol. Soc. Am., 75, (4), 939–964.

Yücemen M. S., 2008, "Deprem Tehlikesinin Tahmininde Olasılıksal Yöntemler", 14. Bölüm, Binalar için Deprem Mühendisliği Temel İkeleri (In Turkish), ed., E. Canbay, Bizim Büro Basımevi, Ankara.

Zlatopolsky, A. A., 1992, *Program LESSA (Lineament Extraction and Stripe Statistical Analysis) automated linear image features analysis—experimental results*, Computers and Geosciences, 18 (9), 1121-1126.

Zlatopolsky, A. A., 1997, *Description of Texture Orientation in Remote Sensing Data Using Computer Program LESSA*, Computers and Geosciences, 23 (1), 45-62.

Zor, E., Özalaybey, S. and Gürbüz, C., 2006, *The crustal structure of the eastern Marmara region, Turkey by teleseismic receiver functions*, Geophysical Journal International, 167, 213–222.

APPENDIX A: EARTHQUAKE CATALOGUE

Day	Month	Year	Hr	Min	Sec	Latitude	Longitude	Depth	Ms	Mb	Md	Ml	Mw
22	10	1905	3	42	0	41.00	31.00	27.0	5.2	5.1	5.1	5.1	5.4
22	1	1907	2	41	0	41.00	29.00	12.0	4.5	4.6	4.6	4.6	4.7
21	8	1907	0	0	0	40.70	30.10	15.0	5.5	5.4	5.4	5.3	5.6
9	6	1919	7	13	50	41.16	33.20	10.0	5.7	5.5	5.5	5.5	5.8
29	5	1923	11	34	2	41.00	30.00	25.0	5.5	5.4	5.4	5.3	5.6
0	9	1924	0	0	0	40.90	29.20	15.0	4.3	4.5	4.4	4.4	4.6
10	6	1925	4	45	0	41.00	29.00	8.0	4.4	4.6	4.5	4.5	4.6
24	6	1925	0	0	35	40.88	30.39	10.0	4.6	4.7	4.7	4.6	4.8
24	1	1928	7	36	12	40.99	30.86	10.0	5.3	5.2	5.2	5.2	5.5
4	10	1928	11	14	8	40.22	33.67	10.0	5.7	5.5	5.5	5.5	5.8
8	4	1929	1	12	14	41.20	32.20	30.0	4.6	4.7	4.7	4.6	4.8
27	4	1929	22	18	6	40.51	31.43	70.0	4.8	4.9	4.8	4.8	4.9
15	10	1932	22	19	54	40.90	30.60	15.0	4.5	4.6	4.6	4.6	4.7
22	9	1936	11	56	56	40.98	33.26	60.0	4.8	4.9	4.8	4.8	4.9
18	11	1936	15	50	14	41.25	33.33	10.0	5.4	5.3	5.3	5.3	5.5
1	2	1940	5	12	56	41.00	33.00	30.0	4.9	4.9	4.9	4.9	5.2
11	10	1940	1	37	13	40.81	33.30	10.0	4.9	4.9	4.9	4.9	5.2
20	6	1943	16	47	57	40.84	30.73	10.0	5.5	5.4	5.4	5.3	5.6
20	6	1943	15	32	54	40.85	30.51	10.0	6.6	6.1	6.2	6.2	6.4
20	6	1943	15	32	54	40.85	30.51	10.0	6.5	6.1	6.1	6.1	6.3
8	9	1943	13	35	0	40.70	30.40	5.0	4.0	4.3	4.2	4.2	4.4
1	2	1944	6	8	52	40.70	31.27	10.0	5.0	5.0	5.0	4.9	5.3
1	2	1944	21	24	0	41.40	32.70	10.0	5.3	5.2	5.2	5.2	5.5
1	2	1944	3	22	40	41.41	32.69	10.0	7.2	6.6	6.7	6.7	6.8
2	2	1944	3	33	17	40.74	31.44	40.0	5.1	5.1	5.0	5.0	5.3
10	2	1944	12	5	27	41.00	32.30	10.0	5.3	5.2	5.2	5.2	5.5
5	4	1944	4	40	43	40.84	31.12	10.0	5.5	5.4	5.4	5.3	5.6
9	2	1945	2	28	0	40.50	31.20	30.0	4.9	4.9	4.9	4.9	5.2
7	6	1945	1	20	41	41.17	33.25	10.0	5.2	5.1	5.1	5.1	5.4
26	10	1945	13	56	51	41.54	33.29	50.0	5.7	5.5	5.5	5.5	5.8
13	12	1948	2	0	0	41.00	30.00	15.0	4.2	4.4	4.3	4.3	4.5

Day	Month	Year	Hr	Min	Sec	Latitude	Longitude	Depth	Ms	Mb	Md	Ml	Mw
13	5	1949	20	14	7	40.94	32.71	20.0	5.1	5.1	5.0	5.0	5.3
28	11	1949	18	47	18	40.98	30.74	10.0	4.7	4.8	4.7	4.7	4.9
13	8	1951	18	33	34	40.88	32.87	10.0	6.9	6.4	6.5	6.4	6.6
13	8	1951	22	58	52	41.09	33.27	80.0	4.8	4.9	4.8	4.8	4.9
14	8	1951	20	23	12	40.82	33.23	10.0	4.8	4.9	4.8	4.8	4.9
14	8	1951	18	46	8	41.08	33.18	40.0	4.9	4.9	4.9	4.9	5.2
22	1	1952	23	15	0	40.80	30.40	15.0	4.3	4.5	4.4	4.4	4.6
7	9	1953	3	59	4	41.09	33.01	40.0	6.0	5.7	5.8	5.7	6.0
26	6	1955	21	12	35	41.11	33.33	10.0	4.6	4.7	4.7	4.6	4.8
6	1	1956	14	52	59	41.00	30.20	10.0	4.9	4.9	4.9	4.9	5.2
14	7	1956	19	1	7	40.32	30.90	40.0	4.6	4.7	4.7	4.6	4.8
28	8	1956	1	29	51	41.08	29.93	80.0	4.6	4.7	4.7	4.6	4.8
30	8	1956	0	15	0	41.00	30.20	5.0	4.0	4.3	4.2	4.2	4.4
26	5	1957	8	54	51	40.60	30.74	40.0	5.4	5.3	5.3	5.3	5.5
26	5	1957	6	33	35	40.67	31.00	10.0	7.1	6.5	6.6	6.6	6.7
26	5	1957	9	36	39	40.76	30.81	10.0	5.9	5.6	5.7	5.6	5.9
27	5	1957	11	1	35	40.73	30.95	50.0	5.8	5.6	5.6	5.6	5.8
27	5	1957	7	5	15	40.84	31.17	80.0	4.7	4.8	4.7	4.7	4.9
28	5	1957	5	33	49	40.57	31.02	40.0	4.7	4.8	4.7	4.7	4.9
28	5	1957	0	9	54	40.58	30.53	50.0	4.8	4.9	4.8	4.8	4.9
29	5	1957	8	47	53	40.72	31.04	20.0	4.7	4.8	4.7	4.7	4.9
29	5	1957	10	17	48	40.83	30.77	20.0	4.9	4.9	4.9	4.9	5.2
30	5	1957	13	7	57	40.62	31.78	10.0	4.2	4.4	4.3	4.3	4.5
30	5	1957	14	29	52	40.65	31.24	10.0	4.2	4.4	4.3	4.3	4.5
1	6	1957	21	8	20	40.68	30.84	40.0	4.8	4.9	4.8	4.8	4.9
1	6	1957	5	26	60	40.75	30.86	50.0	5.0	5.0	5.0	4.9	5.3
2	6	1957	1	12	1	40.71	30.78	10.0	4.8	4.9	4.8	4.8	4.9
26	12	1957	15	1	45	40.83	29.72	10.0	5.2	5.1	5.1	5.1	5.4
23	11	1958	13	7	38	40.49	30.69	10.0	4.4	4.6	4.5	4.5	4.6
2	4	1959	4	34	29	40.50	29.41	20.0	4.6	4.7	4.7	4.6	4.8
6	8	1959	12	8	0	40.40	29.20	10.0	4.1	4.4	4.3	4.2	4.4
19	4	1962	8	22	19	40.75	28.84	10.0	4.3	4.5	4.4	4.4	4.6
18	9	1963	16	58	15	40.77	29.12	40.0	6.3	5.9	6.0	6.0	6.2
24	9	1963	2	10	44	40.84	28.90	10.0	4.8	4.9	4.8	4.8	4.9
18	4	1964	21	52	54	41.10	29.00	33.0	3.9	4.2	4.1	4.1	4.3
19	10	1964	14	6	50	40.50	29.00	10.0	4.0	4.2	4.2	4.1	4.2
13	12	1964	14	9	2	40.70	31.00	10.0	4.2	4.4	4.3	4.3	4.5

Day	Month	Year	Hr	Min	Sec	Latitude	Longitude	Depth	Ms	Mb	Md	Ml	Mw
30	12	1966	1	57	9	40.74	30.74	31.0	4.2	4.2	4.3	4.3	4.5
1	6	1967	11	31	36	40.93	28.90	10.0	4.0	4.2	4.2	4.1	4.3
22	7	1967	23	41	60	40.64	30.53	30.0	4.7	4.8	4.7	4.8	4.9
22	7	1967	17	48	7	40.66	30.62	26.0	5.0	4.9	5.0	4.9	5.2
22	7	1967	16	56	58	40.67	30.69	33.0	6.8	6.0	6.4	6.3	6.2
22	7	1967	17	14	10	40.70	30.80	6.0	4.6	5.2	4.6	4.7	5.5
22	7	1967	17	18	54	40.70	30.80	10.0	4.2	4.4	4.4	4.4	4.5
22	7	1967	18	8	54	40.70	30.80	10.0	4.2	4.7	4.3	4.3	4.8
22	7	1967	18	14	0	40.70	30.80	10.0	4.2	4.4	4.4	4.4	4.5
22	7	1967	18	9	55	40.72	30.51	35.0	5.0	5.1	5.0	4.9	5.4
22	7	1967	17	30	7	40.73	30.53	10.0	4.8	4.8	4.8	4.8	5.1
22	7	1967	20	35	40	40.79	30.42	4.0	4.7	4.7	4.7	4.7	5.0
22	7	1967	22	8	35	40.80	30.52	40.0	4.4	4.5	4.5	4.5	4.6
22	7	1967	21	21	41	41.00	30.45	49.0	4.6	4.6	4.7	4.6	4.9
22	7	1967	21	27	41	41.00	30.45	49.0	4.6	4.7	4.7	4.6	4.8
22	7	1967	19	47	31	41.07	30.59	59.0	4.6	4.6	4.7	4.6	4.9
23	7	1967	10	3	8	40.40	30.30	33.0	3.9	4.2	4.1	4.1	4.3
23	7	1967	4	3	40	40.61	30.35	21.0	4.5	4.5	4.6	4.6	4.8
23	7	1967	23	19	14	40.61	30.63	15.0	4.3	4.3	4.4	4.4	4.6
23	7	1967	4	48	55	40.63	30.36	33.0	4.7	4.6	4.7	4.7	4.9
23	7	1967	15	57	9	40.63	30.59	23.0	4.4	4.4	4.5	4.5	4.7
23	7	1967	2	25	37	40.70	30.57	33.0	3.7	4.1	4.0	4.0	4.2
23	7	1967	7	42	23	40.74	30.36	11.0	4.4	4.1	4.5	4.5	4.4
23	7	1967	9	39	29	40.98	30.00	33.0	4.0	4.3	4.2	4.2	4.4
24	7	1967	8	7	33	40.58	30.70	10.0	4.0	4.3	4.2	4.2	4.4
24	7	1967	3	40	21	40.64	30.52	4.0	4.0	4.3	4.2	4.2	4.4
25	7	1967	11	22	36	40.70	30.80	10.0	4.0	4.3	4.2	4.2	4.4
26	7	1967	9	16	6	40.61	30.67	21.0	4.4	4.5	4.5	4.5	4.6
26	7	1967	5	59	6	40.70	30.80	10.0	4.0	4.2	4.2	4.1	4.3
30	7	1967	1	57	18	40.70	30.58	7.0	4.2	4.4	4.3	4.3	4.5
30	7	1967	19	5	48	40.70	30.80	10.0	4.2	4.4	4.3	4.3	4.5
30	7	1967	1	19	31	40.71	30.58	23.0	4.6	4.6	4.7	4.6	4.9
30	7	1967	1	31	2	40.72	30.52	18.0	5.4	5.4	5.2	5.5	5.7
30	7	1967	18	58	46	40.75	30.46	27.0	4.5	4.5	4.6	4.6	4.8
30	7	1967	10	25	10	40.77	30.56	22.0	4.2	4.4	4.3	4.3	4.5
1	8	1967	1	5	10	40.40	30.40	46.0	4.3	4.4	4.4	4.4	4.5
1	8	1967	0	13	34	40.72	30.52	26.0	4.6	4.6	4.7	4.6	4.9

Day	Month	Year	Hr	Min	Sec	Latitude	Longitude	Depth	Ms	Mb	Md	Ml	Mw
1	8	1967	0	13	34	40.72	30.52	26.0	4.6	4.7	4.7	4.6	4.8
2	8	1967	15	33	23	40.67	30.46	30.0	4.3	4.4	4.4	4.4	4.5
3	8	1967	7	28	17	41.00	30.30	26.0	4.3	4.0	4.4	4.4	4.3
6	8	1967	14	9	33	41.00	28.80	10.0	4.3	4.4	4.4	4.4	4.5
8	8	1967	4	36	34	40.47	30.61	39.0	4.0	4.2	4.2	4.1	4.3
14	8	1967	11	34	20	40.68	30.27	33.0	4.0	4.4	4.2	4.2	4.5
14	8	1967	20	9	25	40.74	30.37	25.0	4.6	4.7	4.6	4.7	4.8
14	8	1967	1	45	56	40.75	30.38	23.0	4.0	4.4	4.2	4.2	4.5
18	9	1967	23	39	34	40.86	30.30	33.0	4.2	4.4	4.3	4.3	4.5
31	1	1968	13	9	58	40.50	30.75	10.0	4.0	4.2	4.2	4.1	4.3
18	3	1968	5	40	1	40.83	30.53	39.0	4.5	4.4	4.6	4.6	4.7
28	3	1968	17	12	20	40.50	31.34	6.0	4.5	4.5	4.6	4.6	4.8
12	2	1969	8	43	5	40.70	30.29	30.0	4.3	4.5	4.4	4.4	4.6
20	9	1971	8	2	37	41.54	32.66	10.0	3.6	4.0	3.9	3.8	4.1
28	2	1972	2	4	35	40.40	29.00	6.0	3.7	4.1	4.0	4.4	4.2
21	6	1972	5	6	16	40.26	30.04	33.0	3.7	4.1	4.0	4.0	4.2
21	10	1973	22	50	31	40.70	32.41	5.0	3.6	4.0	3.9	4.1	4.1
22	11	1973	14	54	53	40.36	29.88	8.0	3.9	4.2	4.1	4.4	4.3
18	1	1974	10	57	14	40.50	28.94	18.0	3.6	4.0	3.9	4.2	4.1
4	6	1975	2	57	5	41.09	32.31	10.0	3.6	4.0	3.9	3.8	4.1
29	5	1976	22	42	9	40.36	28.89	6.0	3.6	4.0	4.3	4.4	4.1
11	5	1978	16	35	41	40.20	29.58	10.0	3.9	4.2	4.1	4.1	4.3
12	10	1978	6	11	13	41.07	33.21	2.0	3.7	4.1	4.0	4.0	4.2
11	1	1979	20	50	39	40.30	29.26	10.0	4.0	4.3	4.2	4.2	4.4
28	6	1979	21	22	9	40.78	31.85	10.0	4.7	4.7	4.3	4.7	5.0
3	1	1980	13	47	16	40.27	30.83	10.0	3.9	4.2	4.1	4.1	4.3
22	7	1981	22	2	46	40.27	28.90	2.0	3.6	4.0	4.0	3.8	4.1
28	8	1981	7	17	9	40.47	29.21	10.0	3.7	4.1	4.0	4.3	4.2
20	5	1982	2	42	49	40.40	28.98	10.0	3.6	4.0	4.2	4.5	4.1
23	5	1982	16	23	7	40.45	29.04	4.0	3.8	4.1	4.0	4.2	4.2
23	5	1982	22	17	53	40.75	30.55	16.0	3.7	4.1	4.0	4.0	4.2
27	7	1982	10	23	15	40.38	28.95	11.0	4.0	4.3	4.2	4.6	4.4
26	5	1984	8	39	36	40.67	30.27	6.0	3.7	4.1	4.0	4.0	4.2
11	4	1985	13	11	46	40.70	29.01	6.0	4.1	4.3	4.1	4.2	4.4
17	10	1986	10	33	6	41.20	32.39	12.0	4.2	4.4	4.4	4.4	4.5
26	10	1986	4	49	30	40.80	28.99	10.0	3.9	4.2	4.3	4.2	4.3
3	9	1987	16	24	53	40.46	29.24	8.0	3.6	4.0	4.0	4.0	4.1

Day	Month	Year	Hr	Min	Sec	Latitude	Longitude	Depth	Ms	Mb	Md	Ml	Mw
27	1	1989	9	48	36	40.43	29.15	11.0	3.7	4.1	4.0	4.0	4.2
10	6	1990	11	36	44	41.31	29.35	6.0	3.9	4.2	4.3	4.2	4.3
17	12	1990	6	47	30	40.37	31.33	10.0	3.6	4.0	4.1	4.0	4.1
12	2	1991	9	54	59	40.80	28.82	10.0	4.8	4.8	4.5	5.0	5.1
3	3	1991	8	39	26	40.63	29.00	10.0	4.4	4.6	4.4	4.6	4.7
12	12	1993	17	21	27	41.55	28.79	28.0	4.7	4.8	4.6	4.6	4.9
28	3	1994	16	59	1	40.39	29.96	17.0	3.6	4.0	4.0	4.1	4.1
28	5	1994	18	1	19	40.67	29.85	14.0	3.8	4.1	4.0	4.0	4.2
19	8	1995	19	57	13	40.23	29.61	16.0	3.9	4.2	4.2	4.1	4.3
21	10	1997	10	49	34	40.71	30.43	11.0	3.9	4.2	4.1	4.1	4.3
17	8	1999	1	36	38	40.40	30.30	10.0	3.6	4.0	4.1	4.0	4.1
17	8	1999	14	31	11	40.42	28.70	8.0	3.6	4.0	4.1	4.1	4.1
17	8	1999	18	35	22	40.43	28.72	7.0	3.8	4.1	4.0	4.0	4.2
17	8	1999	2	23	12	40.53	29.42	20.0	4.0	4.3	4.3	4.2	4.4
17	8	1999	0	47	2	40.60	30.40	10.0	3.7	4.1	4.2	4.0	4.2
17	8	1999	2	34	53	40.62	30.62	11.0	4.2	4.4	4.4	4.4	4.5
17	8	1999	2	42	55	40.64	30.62	9.0	4.8	4.9	4.8	4.9	5.0
17	8	1999	3	14	2	40.64	30.67	21.0	4.8	4.9	4.6	4.9	5.0
17	8	1999	11	58	9	40.65	30.51	14.0	4.2	4.4	4.1	4.4	4.5
17	8	1999	1	33	7	40.68	29.11	7.0	4.6	4.7	4.6	5.1	4.8
17	8	1999	4	20	18	40.69	30.41	13.0	4.5	4.6	4.6	4.6	4.7
17	8	1999	4	20	18	40.69	30.41	13.0	4.5	4.6	4.6	4.6	4.7
17	8	1999	4	20	18	40.69	30.41	13.0	4.5	4.6	4.6	4.6	4.7
17	8	1999	6	35	2	40.69	30.49	12.0	3.7	4.1	4.2	4.0	4.2
17	8	1999	3	8	17	40.69	30.82	30.0	3.9	4.2	4.0	4.1	4.3
17	8	1999	0	21	6	40.70	30.35	10.0	4.3	4.5	4.5	4.5	4.6
17	8	1999	0	44	24	40.70	30.54	22.0	3.9	4.2	4.2	4.4	4.3
17	8	1999	1	31	56	40.71	29.03	15.0	4.0	4.3	4.5	4.2	4.4
17	8	1999	21	14	14	40.71	30.68	8.0	3.8	4.1	4.0	4.0	4.2
17	8	1999	0	15	24	40.71	30.70	56.0	4.3	4.5	4.5	4.5	4.6
17	8	1999	0	57	44	40.72	29.72	20.0	3.7	4.1	4.2	4.1	4.2
17	8	1999	9	31	55	40.72	30.07	7.0	3.9	4.2	4.2	4.1	4.3
17	8	1999	6	35	20	40.72	30.66	10.0	4.0	4.3	4.3	4.2	4.4
17	8	1999	8	9	19	40.72	30.73	10.0	3.9	4.2	4.2	4.1	4.3
17	8	1999	6	28	0	40.72	31.09	10.0	4.6	4.8	4.1	4.8	4.9
17	8	1999	7	21	2	40.73	30.60	6.0	3.7	4.1	4.2	4.0	4.2
17	8	1999	20	30	41	40.74	29.27	15.0	3.8	4.1	4.0	4.0	4.2

149

Day	Month	Year	Hr	Min	Sec	Latitude	Longitude	Depth	Ms	Mb	Md	Ml	Mw
17	8	1999	5	45	22	40.74	30.02	7.0	4.0	4.3	4.2	4.2	4.4
17	8	1999	5	45	22	40.74	30.02	7.0	4.0	4.3	4.2	4.2	4.4
17	8	1999	5	45	22	40.74	30.02	7.0	4.0	4.3	4.2	4.2	4.4
17	8	1999	3	23	14	40.74	30.25	5.0	3.9	4.2	4.0	4.1	4.3
17	8	1999	3	23	14	40.74	30.25	5.0	3.9	4.2	4.2	4.1	4.3
17	8	1999	3	23	14	40.74	30.25	5.0	3.9	4.2	4.2	4.1	4.3
17	8	1999	5	10	8	40.75	30.20	11.0	4.6	4.7	4.4	4.7	4.8
17	8	1999	5	10	8	40.75	30.20	11.0	4.3	4.7	4.4	4.7	4.8
17	8	1999	5	10	8	40.75	30.20	11.0	4.3	4.7	4.4	4.7	4.8
17	8	1999	4	40	0	40.75	30.26	14.0	4.0	4.3	4.3	4.2	4.4
17	8	1999	4	40	0	40.75	30.26	14.0	4.0	4.3	4.3	4.2	4.4
17	8	1999	4	40	0	40.75	30.26	14.0	4.0	4.3	4.3	4.2	4.4
17	8	1999	4	14	23	40.76	29.15	10.0	4.0	4.3	4.2	4.2	4.4
17	8	1999	4	14	23	40.76	29.15	10.0	4.0	4.3	4.2	4.2	4.4
17	8	1999	4	14	23	40.76	29.15	10.0	4.0	4.3	4.2	4.2	4.4
17	8	1999	0	1	39	40.76	29.95	17.0	7.7	6.1	6.7	7.3	7.5
17	8	1999	1	7	54	40.76	29.95	22.0	4.4	4.6	4.7	4.6	4.7
17	8	1999	2	26	15	40.76	30.75	10.0	3.9	4.2	4.1	4.1	4.3
17	8	1999	15	17	52	40.77	29.80	12.0	3.7	4.1	4.1	4.0	4.2
17	8	1999	6	1	33	40.77	29.91	11.0	3.7	4.1	4.2	4.0	4.2
17	8	1999	22	12	48	40.77	30.61	7.0	3.6	4.0	4.0	4.0	4.1
17	8	1999	5	54	42	40.78	29.05	5.0	3.9	4.2	4.3	4.2	4.3
17	8	1999	0	16	27	40.78	29.93	10.0	5.0	5.0	4.9	5.2	5.3
17	8	1999	2	50	46	40.78	30.06	11.0	4.6	4.9	4.5	4.9	5.0
17	8	1999	1	58	7	40.78	30.91	10.0	3.6	4.0	4.1	4.0	4.1
17	8	1999	17	9	15	40.79	30.25	10.0	3.8	4.1	4.0	4.0	4.2
17	8	1999	1	47	4	40.80	29.32	12.0	3.6	4.0	4.1	4.3	4.1
17	8	1999	3	43	6	40.81	30.35	7.0	3.9	4.2	4.3	4.1	4.3
17	8	1999	3	43	6	40.81	30.35	7.0	3.9	4.2	4.3	4.1	4.3
17	8	1999	3	43	6	40.81	30.35	7.0	3.9	4.2	4.3	4.1	4.3
17	8	1999	9	2	10	40.81	31.14	10.0	4.4	4.6	4.4	4.6	4.7
17	8	1999	8	11	26	40.87	30.59	10.0	3.6	4.0	4.1	4.0	4.1
17	8	1999	9	36	19	40.90	31.09	23.0	3.9	4.2	4.2	4.1	4.3
17	8	1999	4	44	17	40.91	30.80	11.0	3.9	4.2	4.2	4.1	4.3
17	8	1999	4	44	17	40.91	30.80	11.0	3.9	4.2	4.2	4.1	4.3
17	8	1999	4	44	17	40.91	30.80	11.0	3.9	4.2	4.2	4.1	4.3
17	8	1999	8	32	32	40.91	31.11	10.0	3.6	4.0	4.1	4.0	4.1

Day	Month	Year	Hr	Min	Sec	Latitude	Longitude	Depth	Ms	Mb	Md	Ml	Mw
17	8	1999	0	34	52	40.96	30.00	23.0	3.6	4.0	4.1	4.3	4.1
17	8	1999	5	53	5	41.00	31.12	10.0	3.9	4.2	4.2	4.1	4.3
17	8	1999	5	53	5	41.00	31.12	10.0	3.9	4.2	4.2	4.1	4.3
17	8	1999	5	53	5	41.00	31.12	10.0	3.9	4.2	4.2	4.1	4.3
18	8	1999	1	4	26	40.70	30.72	7.0	3.9	4.2	4.1	4.1	4.3
18	8	1999	21	15	54	40.77	30.63	8.0	3.9	4.2	4.0	4.1	4.3
18	8	1999	15	34	17	40.80	30.07	8.0	3.6	4.0	4.0	4.0	4.1
19	8	1999	14	15	58	40.60	29.15	3.0	4.3	4.5	4.5	4.2	4.6
19	8	1999	14	24	34	40.61	29.02	5.0	3.7	4.1	4.0	4.0	4.2
19	8	1999	13	4	13	40.61	30.66	10.0	4.6	4.7	4.6	4.4	4.8
19	8	1999	15	26	21	40.62	29.10	4.0	3.7	4.1	4.0	4.0	4.2
19	8	1999	15	17	45	40.63	29.14	12.0	4.7	4.9	4.7	4.9	5.0
19	8	1999	18	34	56	40.73	30.55	5.0	3.7	4.1	4.2	4.0	4.2
20	8	1999	9	28	56	40.62	29.13	10.0	4.3	4.5	4.2	4.5	4.6
20	8	1999	10	0	20	40.65	30.60	13.0	4.0	4.3	4.0	4.2	4.4
20	8	1999	0	3	2	40.77	29.85	10.0	4.0	4.3	4.1	4.2	4.4
20	8	1999	15	59	2	40.83	30.78	8.0	4.0	4.3	4.0	4.2	4.4
21	8	1999	19	21	24	40.71	30.45	8.0	3.6	4.0	4.0	4.0	4.1
22	8	1999	1	47	30	40.61	29.07	24.0	3.7	4.1	4.3	4.0	4.2
22	8	1999	14	31	0	40.68	30.70	14.0	4.4	4.6	5.0	4.7	4.7
26	8	1999	17	49	39	40.77	30.00	12.0	4.0	4.3	4.4	4.2	4.4
29	8	1999	10	15	4	40.76	31.07	14.0	4.3	4.5	4.0	4.5	4.6
31	8	1999	22	28	34	40.61	29.08	4.0	3.9	4.2	4.2	4.1	4.3
31	8	1999	8	33	23	40.73	29.95	6.0	4.4	4.6	4.6	4.6	4.7
31	8	1999	8	10	49	40.76	29.93	4.0	4.8	5.3	5.0	5.4	5.6
2	9	1999	14	25	20	40.60	30.60	14.0	3.7	4.1	4.0	4.0	4.2
4	9	1999	10	30	53	40.70	29.93	10.0	3.6	4.0	4.2	4.1	4.1
4	9	1999	18	27	44	40.72	30.29	10.0	3.8	4.1	4.0	4.0	4.2
5	9	1999	19	52	48	40.64	30.57	10.0	3.6	4.0	4.2	4.0	4.1
6	9	1999	19	44	30	40.77	31.11	10.0	3.8	4.1	4.0	4.0	4.2
6	9	1999	6	33	27	40.79	29.75	17.0	3.6	4.0	4.0	4.0	4.1
6	9	1999	7	0	1	40.79	31.01	7.0	3.8	4.1	4.0	4.0	4.2
9	9	1999	1	32	8	40.71	29.14	11.0	3.6	4.0	4.2	4.2	4.1
13	9	1999	11	55	28	40.75	30.08	10.0	5.7	5.6	5.5	5.8	5.9
17	9	1999	19	50	5	40.77	30.13	10.0	4.2	4.4	4.5	4.4	4.5
18	9	1999	0	48	25	40.60	29.21	9.0	4.3	4.6	4.4	4.6	4.7
19	9	1999	20	26	36	40.69	30.48	6.0	3.9	4.2	4.1	4.1	4.3

Day	Month	Year	Hr	Min	Sec	Latitude	Longitude	Depth	Ms	Mb	Md	Ml	Mw
29	9	1999	0	13	6	40.74	29.33	12.0	4.7	4.9	4.9	4.9	5.0
20	10	1999	23	8	20	40.83	29.03	7.0	4.6	4.7	4.8	4.7	4.8
7	11	1999	16	54	42	40.70	30.72	7.0	4.7	4.8	4.9	4.8	4.9
7	11	1999	17	6	6	40.75	30.68	5.0	3.9	4.2	4.3	4.1	4.3
11	11	1999	14	41	23	40.75	30.25	7.0	5.5	5.4	5.7	5.5	5.7
11	11	1999	14	55	25	40.80	30.21	3.0	3.6	4.0	4.4	4.0	4.1
12	11	1999	18	24	32	40.50	31.60	10.0	3.6	4.0	4.1	4.0	4.1
12	11	1999	17	54	26	40.61	31.40	24.0	3.6	4.0	4.0	4.0	4.1
12	11	1999	21	24	46	40.65	31.06	8.0	3.8	4.1	4.0	4.0	4.2
12	11	1999	19	5	49	40.68	31.34	9.0	3.7	4.1	4.2	4.0	4.2
12	11	1999	17	29	32	40.70	31.47	11.0	5.0	5.0	5.2	5.0	5.3
12	11	1999	20	4	45	40.74	31.14	10.0	4.3	4.5	4.3	4.5	4.6
12	11	1999	18	14	32	40.74	31.33	10.0	4.4	4.6	4.5	4.6	4.7
12	11	1999	17	26	15	40.74	31.51	10.0	4.2	4.4	4.4	4.4	4.5
12	11	1999	17	17	59	40.75	31.08	28.0	5.3	5.2	5.2	5.3	5.5
12	11	1999	19	6	30	40.77	31.17	10.0	4.0	4.3	4.4	4.2	4.4
12	11	1999	18	7	52	40.77	31.20	10.0	3.6	4.0	4.1	4.0	4.1
12	11	1999	22	49	30	40.78	30.94	10.0	3.7	4.1	4.0	4.0	4.2
12	11	1999	17	46	57	40.78	30.96	13.0	4.3	4.5	4.4	4.5	4.6
12	11	1999	17	22	56	40.78	31.09	19.0	4.4	4.6	4.5	4.6	4.7
12	11	1999	19	15	34	40.78	31.47	10.0	4.0	4.3	4.3	4.2	4.4
12	11	1999	17	6	18	40.79	31.30	10.0	4.2	4.4	4.4	4.4	4.5
12	11	1999	18	23	51	40.80	31.07	10.0	3.6	4.0	4.1	4.0	4.1
12	11	1999	16	57	20	40.81	31.19	10.0	7.4	6.2	6.5	6.8	7.2
12	11	1999	20	53	54	40.81	31.47	5.0	3.7	4.1	4.2	4.0	4.2
12	11	1999	17	16	51	40.82	31.01	9.0	4.6	4.7	4.6	4.7	4.8
12	11	1999	22	1	12	40.82	31.34	10.0	3.6	4.0	4.0	4.0	4.1
12	11	1999	19	9	33	40.83	31.36	12.0	3.8	4.1	4.0	4.0	4.2
12	11	1999	21	38	33	40.84	31.08	11.0	4.2	4.4	4.4	4.4	4.5
12	11	1999	21	42	25	40.84	31.20	7.0	3.6	4.0	4.1	4.0	4.1
12	11	1999	22	20	56	40.84	31.36	25.0	4.4	4.3	4.1	4.2	4.6
12	11	1999	17	13	43	40.86	31.02	10.0	4.0	4.3	4.3	4.2	4.4
12	11	1999	17	57	3	40.86	31.60	10.0	3.7	4.1	4.0	4.0	4.2
12	11	1999	17	52	26	40.88	31.15	10.0	3.6	4.0	4.0	4.0	4.1
12	11	1999	18	59	14	40.89	31.02	11.0	3.9	4.2	4.2	4.1	4.3
12	11	1999	18	10	16	40.89	31.50	10.0	3.6	4.0	4.1	4.0	4.1
12	11	1999	20	44	35	40.90	31.46	9.0	3.6	4.0	4.1	4.0	4.1

Day	Month	Year	Hr	Min	Sec	Latitude	Longitude	Depth	Ms	Mb	Md	Ml	Mw
12	11	1999	20	54	23	41.00	31.40	10.0	3.6	4.0	4.1	4.0	4.1
13	11	1999	3	57	33	40.72	31.44	10.0	3.6	4.0	4.0	4.0	4.1
13	11	1999	0	54	55	40.77	31.02	5.0	4.5	4.9	4.7	4.9	5.0
13	11	1999	9	59	23	40.80	31.00	6.0	3.7	4.1	4.2	4.0	4.2
13	11	1999	8	14	37	40.81	30.95	8.0	3.9	4.2	4.2	4.1	4.3
13	11	1999	8	2	34	40.81	31.05	8.0	3.6	4.0	4.0	4.0	4.1
13	11	1999	8	33	43	40.82	31.39	7.0	3.9	4.2	4.1	4.1	4.3
13	11	1999	0	14	49	40.83	31.41	10.0	3.9	4.2	4.0	4.1	4.3
13	11	1999	4	10	21	40.83	31.45	7.0	3.6	4.0	4.0	4.0	4.1
13	11	1999	18	43	44	40.83	31.50	10.0	3.6	4.0	4.0	4.0	4.1
13	11	1999	10	10	34	40.83	31.51	12.0	3.6	4.0	4.1	4.0	4.1
13	11	1999	1	3	3	40.89	31.40	10.0	3.6	4.0	4.3	4.0	4.1
14	11	1999	22	55	17	40.89	31.48	10.0	3.6	4.0	4.0	4.0	4.1
15	11	1999	16	26	58	40.81	31.07	11.0	3.6	4.0	4.0	4.0	4.1
16	11	1999	17	51	18	40.73	31.59	5.0	4.6	5.0	4.9	5.0	5.3
17	11	1999	3	36	1	40.76	31.35	10.0	3.7	4.1	4.0	4.0	4.2
17	11	1999	8	15	26	40.83	31.49	7.0	4.5	4.7	5.0	4.7	4.8
19	11	1999	19	59	7	40.83	31.02	9.0	4.4	4.8	5.0	5.0	4.9
19	11	1999	14	1	14	40.85	30.85	7.0	3.9	4.2	4.1	4.1	4.3
19	11	1999	10	28	0	40.85	30.99	12.0	4.0	4.3	4.0	4.2	4.4
20	11	1999	8	44	13	40.86	31.46	9.0	3.6	4.0	4.1	4.0	4.1
21	11	1999	22	27	33	40.75	31.50	9.0	4.0	4.3	4.3	4.2	4.4
21	11	1999	4	31	42	40.82	30.91	9.0	3.7	4.1	4.2	4.0	4.2
13	12	1999	19	13	39	40.77	30.72	14.0	4.0	4.3	4.2	4.2	4.4
20	12	1999	3	27	19	40.82	30.96	6.0	3.9	4.2	4.1	4.1	4.3
4	1	2000	16	26	7	40.75	30.69	20.0	3.6	4.0	4.0	4.0	4.1
5	1	2000	14	10	4	40.85	31.24	3.0	3.7	4.1	4.1	4.0	4.2
20	1	2000	10	35	59	40.82	31.32	13.0	4.4	4.6	4.3	4.6	4.7
31	1	2000	14	38	51	40.71	29.25	10.0	3.7	4.1	4.0	4.0	4.2
9	2	2000	16	41	32	40.77	29.94	11.0	3.8	4.1	4.0	4.0	4.2
14	2	2000	6	56	35	41.04	31.74	10.0	4.9	4.8	5.0	4.8	5.1
2	4	2000	18	57	38	40.86	30.29	9.0	4.3	4.5	4.3	4.5	4.6
7	7	2000	0	15	31	40.86	29.29	10.0	4.3	4.5	4.2	4.5	4.6
23	8	2000	13	41	27	40.78	30.76	11.0	4.9	5.1	5.0	5.0	5.4
16	1	2001	3	33	2	40.90	29.07	13.0	3.8	4.1	4.0	4.0	4.2
1	4	2001	1	18	48	40.92	31.08	12.0	3.6	4.0	4.1	4.0	4.1
26	8	2001	0	41	13	40.98	31.54	6.0	5.1	5.1	5.0	4.8	5.4

153

Day	Month	Year	Hr	Min	Sec	Latitude	Longitude	Depth	Ms	Mb	Md	Ml	Mw
23	7	2002	20	6	43	40.96	32.64	5.0	3.8	4.1	4.0	4.0	4.2
17	9	2002	12	5	31	40.72	30.61	6.0	3.8	4.1	4.0	4.0	4.2
9	3	2003	19	1	34	40.71	30.57	9.0	3.6	4.0	4.0	4.0	4.1
1	4	2003	7	51	9	40.74	30.66	9.0	3.7	4.1	4.0	4.1	4.2
21	5	2003	8	21	51	40.78	30.96	14.0	3.9	4.2	4.3	4.5	4.3
25	7	2003	7	21	32	40.89	31.53	8.0	4.0	4.3	4.0	4.1	4.4
13	4	2004	21	47	23	40.75	31.64	10.0	4.3	4.5	4.5	4.6	4.6
16	5	2004	3	30	49	40.70	29.33	10.0	3.9	4.2	4.3	4.3	4.3
29	9	2004	15	42	8	40.79	29.02	13.0	3.8	4.1	4.0	4.0	4.1
28	12	2005	2	11	22	40.98	33.29	6.0	4.2	4.4	4.2	4.2	4.5